Extended sulfo-pillar[6]arenes – a new host family and its application in the binding of direct oral anticoagulants.

Chelsea R. Wilson,[1,2] Austia O. Puckett,[1,2] Allen G. Oliver,[3] Fraser Hof.[1,2*]

[1]Department of Chemistry, University of Victoria, 3800 Finnerty Rd., Victoria, BC V8P 5C2, Canada

[2]Centre for Advanced Materials and Related Technology (CAMTEC), University of Victoria, 3800 Finnerty Rd., Victoria, BC V8W 2Y2, Canada

[3]Department of Chemistry and Biochemistry, University of Notre Dame, 251 Nieuwland Science Hall, Notre Dame, IN, 46556 USA

ABSTRACT: Herein we report the synthesis of extended sulfo-pillar[6]arenes, a new supramolecular host class with a pedigree in salt tolerance and ultra-high binding affinity towards multiple drug classes. The parent sulfo-pillar[6]arene (**sP6**) is a high affinity host with the potential to act as a supramolecular reversal agent. However, it lacks synthetic diversification of the core scaffold. The new extended sulfo-pillar[6]arenes have either a mono-directional (**A1sP6**) or bi-directional (**A1A2sP6**) extension of the hydrophobic cavity. This new functionality enables more non-covalent interactions and strong affinity towards guests, which we demonstrate using the direct oral anticoagulants (DOACs) dabigatran, betrixaban, and edoxaban. DOACs are highly prescribed therapeutics that are underexplored in host-guest chemistry. These agents prevent the formation of blood clots and reversing their action during emergencies is paramount. We show that the new hosts have ultra-high affinity towards dabigatran (K_d = 27 nM, **A1A2sP6**) in salty solutions. Their increased functionality resulted in a 6- and 2.5-fold increase in affinity towards betrixaban (K_d = 230 nM, **A1A2sP6**) and edoxaban (K_d = 800 nM, **A1sP6**), relative to the unfunctionalized sulfo-pillar[6]arene.

INTRODUCTION

Antidotes, reversal agents or rescue drugs are a class of therapeutics that can nullify the effects of another drug by sequestering it or by competing for the target receptor. Naloxone is a notable example of the latter; by directly outcompeting opioids for the opioid receptor and thus blocking binding, it reverses their action *in vivo*.[1] Sequestration is an attractive approach to drug reversal. Instead of the rescue drug creating competition at the biological receptor, the synthetic agent binds the drug directly and, in principle, can have fewer unintended side effects.[2,3] For example in the reversal of neuromuscular blocking agents, cholinesterase inhibitors have off-target parasympathetic effects requiring the co-administration of additional therapeutics.[4] A sequestration agent, Sugammadex,[5] leads to a 40% reduction in harmful side effects and >6 times faster reversal compared with small-molecule inhibitors.[6]

Supramolecular hosts are synthetic concave macrocycles that use non-covalent interactions to recognize and bind a target drug or analyte. These hosts have found many promising applications in healthcare, where they are primarily used to increase drug solubility or to deliver drugs.[7-10] When a supramolecular host encapsulates a drug *in vivo*, the host-guest complex is most often removed from general circulation by excretion.[3,4,11] A high binding affinity, salt tolerance and low dissociation rate are required for supramolecular reversal agents to be effective. Supramolecular hosts can be improved by synthetic functionalization.[12,13] For example, the aforementioned Sugammadex is a synthetically modified cyclodextrin, and is currently the only FDA-approved supramolecular reversal agent. There are other non-clinical examples of macrocycle functionalization leading to introduction of key properties. A sulfonatocalix[4]arene was imbued with the ability to detoxify V-type nerve agents.[14] Additionally, the methylation of cucurbit[8]uril drastically improved water solubility enabling the reversal of PCP-induced hyperlocomotion in mice.[15] These examples highlight the promise of developing new host functionalization methods.

Direct oral anticoagulants (DOACs) are a class of drug in need of reversal agents. In recent years DOACs have gained popularity for prevention of blood clotting, as evidenced by their increased prescription rates over classic vitamin K antagonists (VKAs) such as warfarin.[16] Relative to VKAs, DOACs have a larger therapeutic window, do not require routine monitoring, have fewer adverse interactions, and have more predictability which allows for better dosing.[17] DOACs are now commonly prescribed for the prevention of deep vein thrombosis, stroke and pulmonary embolism.[18] There are two major groups of DOACs, direct thrombin (Factor IIa) inhibitors such as dabigatran; and direct factor Xa inhibitors such as apixaban, rivaroxaban, betrixaban, and edoxaban (Figure 1). Even though DOACs have many advantages over VKAs there are still serious concerns around the ability to reverse their action during emergency care.[19] Protein-based biologics are the only DOAC reversal agents used clinically. The modified recombinant factor Xa andexanet alfa is currently used as a reversal agent for apixaban and rivaroxaban. However, the drug itself has significant and life-threat-

ening side effects.[20] Idarucizumab, an antibody-based treatment for the reversal of dabigatran, comes with a high price tag of >$3500 per dose.[21] Cheaper and safer alternatives to DOAC reversal are needed. The cyclodextrin OKL-1111 was recently reported as a broad-spectrum experimental reversal agent for DOACs.[22] While this report illustrated the potential of a supramolecular reversal agent, the affinity (K_d of 25 μM – 6.7 mM) of OKL-1111 towards DOACs is weaker than would be expected to lead to success in the clinic. A stronger binding host class is needed.

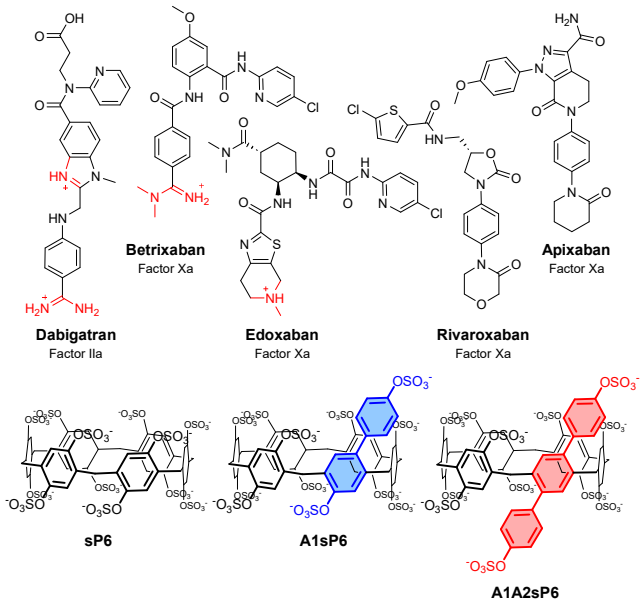

Figure 1. Chemical structure of select direct oral anticoagulants in charge state present at pH 3.0; and pillar[6]MaxQ (**sP6**) previously reported by Isaacs and co-workers,[23] with functionalized analogs **A1sP6** and **A1A2sP6** (this work).

Sulfo-pillar[6]arene (**sP6**) is an ultra-high (pM-nM) affinity host. First reported in 2020, **sP6** has become an attractive candidate for use in therapeutic applications due to its high affinity to biologically-relevant analytes,[23, 24] and was recently shown to act as a broad spectrum reversal agent for opioid-related overdose.[25] In addition to its high affinity, sulfo-pillar[6]arene has also been shown to be salt tolerant. The binding affinity of the opioid fentanyl for **sP6** only decreased from a K_d of 9.8 nM to 78 nM when excessive salt was present.[25] Additionally, **sP6** showed 16 nM affinity towards the peptidic biomarker H3K4Me3 in a salty media (137 mM NaCl).[26] With its good biocompatibility, salt tolerance and high affinity to multiple drug classes like amino acids,[26] steroids,[27] opioids,[25] and neuromuscular blocking agents,[23] **sP6** has a bright future in medicinal applications. However, the ability to modify the host scaffold is paramount to manipulating the binding affinity, selectivity, and pharmacological properties of the host. Functionalization methods for pillar[6]arenes are very limited and the functionalization of sulfo-pillar[6]arenes have been non-existent until now.

RESULTS

We prepared **sP6** derivatives with an elongated hydrophobic surface area to complement the rod-like structure of the DOACs. We predicted that by extending the hydrophobic surface and cavity depth of sulfo-pillar[6]arene we would create an increase in binding strength, as well as a tuning of guest selectivity through modification of host-guest contacts. We targeted mono- and di-functionalization to create new analogs with an extended aromatic pendent arm on either one face (**A1sP6**) or both faces (**A1A2sP6**) of the macrocycle, while maintaining the twelve negatively charged sulfate groups (Figure 1).

The high symmetry of pillar[6]arene renders mono-functionalization a challenging endeavor. The key starting material in functionalized derivatives is an alkoxy-protected pillar[6]arene, most commonly ethoxypillar[6]arene (**EtOP6**). We recently reported a protocol that allows for access to *ca.* 20 grams of pure **EtOP6** in one day without chromatography.[28] With ample starting material in hand, the functionalization of **EtOP6** can be achieved through two main desymmetrisation arteries, deprotection and oxidation.

A multi-step synthetic pathway was developed for the **A1** and **A1A2** functionalization of ethoxypillar[6]arene (Figure 2). The mono-functionalization of one of the twelve ethoxy groups is achieved by removing the stated protecting group in the presence of BBr_3, exposing one reactive phenol, **1**.[29] Di-functionalization is done by oxidizing one of the six diethoxybenzenes to a quinone.[30-32] Once oxidized the quinone can be reduced to a hydroquinone to provide two reactive alcohols.[30] The now available mono- and di-reactive sites in the ethoxypillar[6]arene scaffold allow for more elaborate modifications leading to functionalized water sulfo-pillar[6]arenes.

The mono-oxidation product can be prepared with $(NH_4)_2[Ce(NO_3)_6]$ following the literature protocol.[31] However, like Zuilhof and coworkers[32] we also obtained notably lower yields than reported.[31] Through optimization we arrived at an alternative method for the mono-oxidization of ethoxypillar[6]arene. Over the course of 1.5 hours, 0.9 M $(NH_4)_2[Ce(NO_3)_6]$ (aq) was added via syringe pump to a solution of **EtOP6** in degassed DCM at –20°C; reliably obtaining **5** in a 24% yield after flash chromatography. The quinone in **5** was reduced with $NaBH_4$ as in literature[30] to obtain the hydroquinone **6**. It is important to note that **6** displayed stability issues when stored for more than a few days, so we carried this intermediate forward promptly. Triflation of **1** gave the monotriflated analog **2** in a 91% yield. Compound **6** was triflated in a similar manner to obtain ditriflate **7** in an 83% yield. The Suzuki–Miyaura coupling protocol was inspired by Zuilhof and coworkers[33] work on rim-differentiated pillar[5]arenes. For the **A1** coupling, triflate **2** was coupled with 4-methoxyphenylboronic acid using XPhos Pd G3, providing **3** in 73% yield. Compound **8** was similarly obtained from **7** in a 69% yield, the nature of the **A1A2** extended hydrophobic surface of **8** was confirmed by crystallography (Figure S27-28).

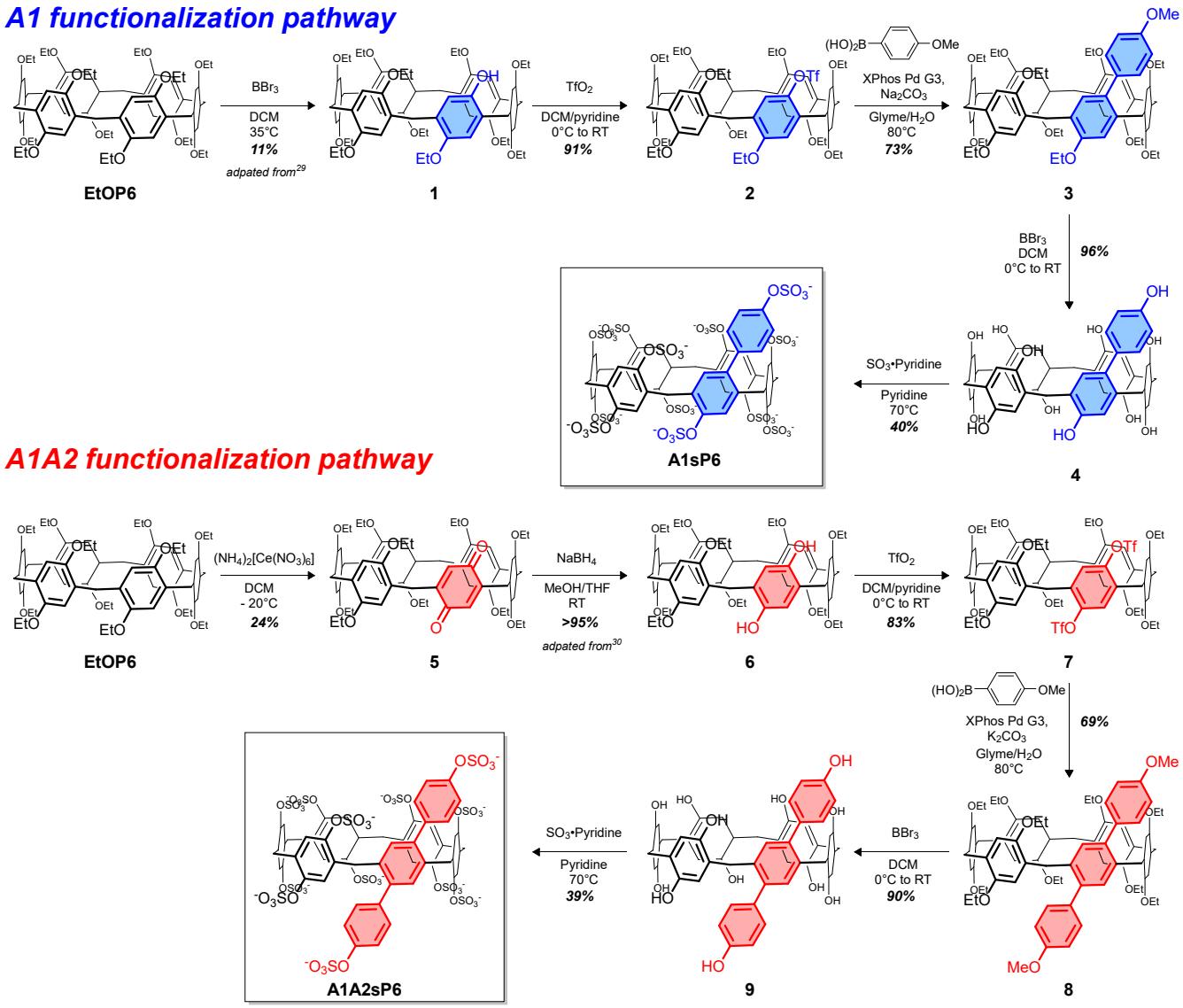

Figure 2. Synthetic scheme for the **A1** and **A1A2** functionalization pathway of **sP6**.

Water soluble **A1-** and **A1A2**-functionalized pillar[6]arenes were obtained via sulfation. The remaining ethoxy protecting groups of **3** and **8** were removed through treatment with BBr_3 in dry dichloromethane at 0°C, thus providing **4** (96% yield) and **9** (90% yield). Again, the unprotected phenols created stability problems and it is recommended to carry these intermediates forward immediately after deprotection. The sulfation protocol of **4** and **9** was adapted from Isaacs and coworkers[23] work on **sP6** with some noted modifications, including rigorous drying of reagents and most notably the achievement of post-workup desalting by dialysis rather than by host precipitation.[25] The revised method reliably yields products that meet our standard of ≤50 % salt content to allow for subsequent characterization and binding studies. In a typical set of outcomes for this new sulfation protocol, we obtained the novel extended sulfo-pillar[6]arenes **A1A2sP6** in 39% yield (49% salt content, yield corrected for salt) and **A1sP6** in 40% yield (36% salt content, yield corrected for salt).

We first examined the binding affinity towards DAPI,[26] which is a rod-like dicationic guest. Due to the insolubility of the DOACs at pH 7.4, we studied the binding of DAPI with the extended sulfo-pillar[6]arenes at both pH 3.0 and 7.4. The pH and buffer showed minimal effect on the emission and excitation of the host-dye complexes (Figure 3a.). When complexed with the hosts, DAPI showed an increase in emission at 450 nm (λ_{ex} = 360 nm) at both pH 7.4 and pH 3.0, while the hosts by themselves showed no emission at these wavelengths (Figure S29). Through the direct titration of host into DAPI the dissociation constant (K_d) for the host-dye complex was determined at both pH values (Figure 3b, Figure S30-31). The change in pH and buffer had no effect on the K_d values of the respective host-dye complex, which is consistent with the hosts' highly acidic sulfate groups remaining anionic even at pH 3.0 (Table 1.). All three

hosts showed nanomolar affinity to DAPI with the **A1A2sP6** displaying the strongest binding of 15 ± 4 nM. The parent host (**sP6**) and **A1sP6** showed comparable strength to each other. The increase in affinity of DAPI to **A1A2sP6** over the other hosts demonstrates the effect of host extension on guest affinity.

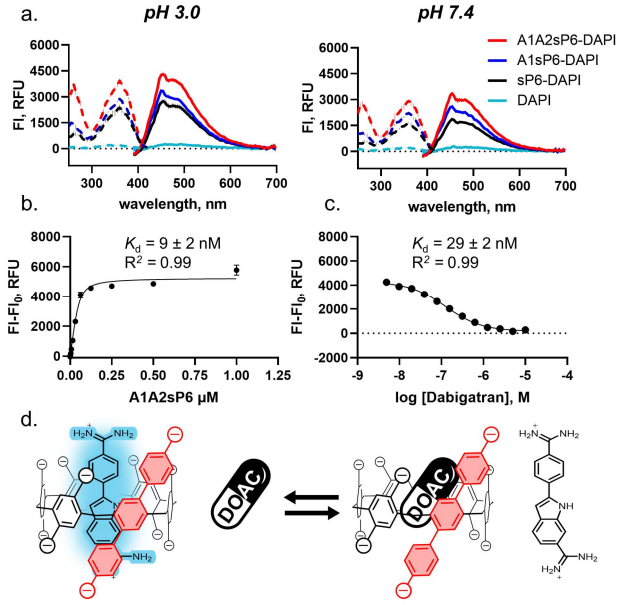

Figure 3. Fluorescence assays determine dissociation constants for DAPI and DOACs. a. Emission (λ_{ex} = 360 nm, solid lines) and excitation (λ_{em} = 450 nm, dashed lines) of DAPI (100 nM), **sP6**-DAPI (1µM; 100 nM), **A1sP6**-DAPI (1µM; 100 nM) and **A1A2sP6**-DAPI (1µM; 100 nM) at pH 3.0 (10 mM CBS) and pH 7.4 (10 mM PBS). b. Exemplary direct binding titration of DAPI (50 nM) into **A1A2sP6** (1 µM – 0.5 nM) at pH 3.0 (10 mM CBS), λ_{ex} = 360 nm, λ_{em} = 450 nm. Reported dissociation constants and R^2 are for the exemplary set of triplicates. c. Exemplary indicator displacement titration of dabigatran (10 µM – 5 nM) into **A1A2sP6**-DAPI (62.5 nM; 50 nM) at pH 3 (10 mM CBS), λ_{ex} = 360 nm, λ_{em} = 450 nm. Reported dissociation constants and R^2 are for the exemplary set of triplicates. d. Representation of the displacement of DAPI from the host-DAPI complex by a DOAC guest, leading to a decrease in emission; negative charges represent sulfate groups.

The dissociation constants of DOACs were determined via an indicator displacement assay using DAPI (Table 1, Figure 3c-d). Due to previously stated solubility issues, the DOAC competition experiments were conducted at pH 3.0 in 10 mM CBS buffer with ≤2.5 % DMSO (Figure S32-34). Out of the 5 DOACs studied, sulfo-pillar[6]arene and its extended analogs showed low micromolar to nanomolar affinity towards dabigatran, betrixaban and edoxaban. Apixaban showed no binding at the tested concentration range (K_d > 500 µM) and rivaroxaban was not soluble in the assay conditions. Based off the similar chemical structures of apixaban and rivaroxaban it is unlikely rivaroxaban would be a strong binder. The strongest affinity was observed for dabigatran which displayed comparable nanomolar binding to the three hosts. The increasing hydrophobic area altered the binding to betrixaban and edoxaban. Betrixaban had the strongest binding to the **A1A2** extended cavity with a K_d = 230 ± 40 nM, a 6- and 4-fold increase over the parent host and the **A1** extension, respectively. The **A1** extension led to a greater than 2.5-fold increase in affinity towards edoxaban, relative to the parent sulfo-pillar[6]arene.

Table 1. Dissociation constants (K_d, nM) determined by fluorescence-based assay.[a]

	sP6	A1sP6	A1A2sP6
DAPI[b]	40 ± 10	50 ± 10	17 ± 5
DAPI[c]	40 ± 8	35 ± 7	15 ± 4
Dabigatran[c]	21 ± 2	32 ± 4	27 ± 3
Apixaban[c,d,e]	n.b.	n.b.	n.b.
Betrixaban[c,d]	1400 ± 200	1000 ± 300	230 ± 40
Edoxaban[c,d]	2000 ± 300	800 ± 200	1300 ± 200

[a] Binding constants were determined assuming a 1:1 stoichiometry. All values reported are the average of six measurements with propagated standard error, unless stated otherwise. [b] Assays performed at pH 7.4 in phosphate buffer saline (10 mM). [c] Assays performed at pH 3.0 in citrate buffer saline (10 mM). [d] ≤2.5 % DMSO used. [e] No binding observed at 500 µM guest concentration, triplicate measurement.

The recognition of DOACs by extended sulfo-pillar[6]arenes is enthalpically driven. The thermodynamic parameters of pillararene-DOAC binding were determined using isothermal titration calorimetry (ITC). Each sulfo-pillar[6]arene was titrated into the DOAC in 10 mM CBS buffer (pH 3.0); to aid in solubility 0.5% DMSO was used for edoxaban and betrixaban, in these instances a control for the DMSO was run and subtracted from the respective thermograms (Figure S35). Apixaban and rivaroxaban were excluded from this study as they either showed no binding (Table 1) or solubility issues in the competitive displacement assay. Sulfo-pillar[6]arene and its extended analogs showed low micromolar to high nanomolar affinity for all three DOACs tested (Table 2, Figure 4a-b, S36-38).

Compared to the dissociation constants obtained from the competitive displacement assays, the values from the ITC experiments are between 1–7-fold weaker, however the general trend in host-DOAC preference is the same. This decrease in affinity might be in part due to the increased concentration of the host during ITC vs. fluorescence experiments (250–500 µM vs 60–100 nM), which may lead to aggregation of the titrant. Overall, all pillararene-DOAC complexes were enthalpically driven with minor entropic contributions.

The **A1** extension and the parent **sP6** had identical affinity for dabigatran but different entropic and enthalpic contributions. The parent **sP6** had an unfavourable entropic contribution of 2.2 ± 0.2 kcal·mol^{-1}; the **A1** analog reduced this unfavourability to 0.77 ± 0.08 kcal·mol^{-1}. The increased hydrophobic surface area increased the entropic favourability by 1.4 kcal·mol^{-1}, equally decreasing the enthalpic contribution. This apparent enthalpy-entropy compensation might be due to the increased depth of the **A1** host, which prevents optimal alignment for cation-anion interactions between the benzimidazole moiety of dabigatran and the sulfates on the upper rim of **A1sP6** (Figure 4c). The

Table 2. Thermodynamic parameters of DOACs and sulfo-pillar[6]arene recognition determined by isothermal calorimetry.[a]

	Host	K_d (nM)	ΔG (kcal/mol)	ΔH (kcal/mol)	−TΔS (kcal/mol)
Betrixaban[b]	**sP6**	3000 ± 400	−7.7 ± 0.1	−7.5 ± 0.1	−0.2 ± 0.2
	A1sP6	2000 ± 100	−7.90 ± 0.06	−7.73 ± 0.06	−0.17 ± 0.09
	A1A2sP6	1500 ± 100	−8.08 ± 0.09	−7.7 ± 0.1	−0.3 ± 0.1
Edoxaban[b]	**sP6**	2900 ± 200	−7.67 ± 0.07	−7.39 ± 0.07	−0.3 ± 0.2
	A1sP6	1370 ± 70	−8.14 ± 0.05	−8.82 ± 0.05	0.69 ± 0.07
	A1A2sP6	3800 ± 300	−7.52 ± 0.08	−5.78 ± 0.07	−1.7 ± 0.1
Dabigatran	**sP6**	150 ± 20	−9.5 ± 0.1	−11.67 ± 0.09	2.2 ± 0.2
	A1sP6	150 ± 10	−9.47 ± 0.07	−10.24 ± 0.05	0.77 ± 0.08
	A1A2sP6	370 ± 40	−8.93 ± 0.09	−9.96 ± 0.08	1 ± 0.1

[a] All assays performed in citrate buffer saline solution (10 mM, pH 3.0) at 303 K. One site binding model was used to fit the data. All values reported as the average of two replicates with propagated standard error [b] Guest contains 0.5% DMSO.

A1A2 extension had over 2-fold weaker binding to dabigatran, with an enthalpic loss of 1.7 kcal·mol^{-1} and an entropic gain of 1.2 kcal·mol^{-1} with respect to the parent **sP6**. Similar to **A1sP6**, the enthalpic loss maybe due to the less-than-optimal alignment of cation-anion interactions (Figure 4c).

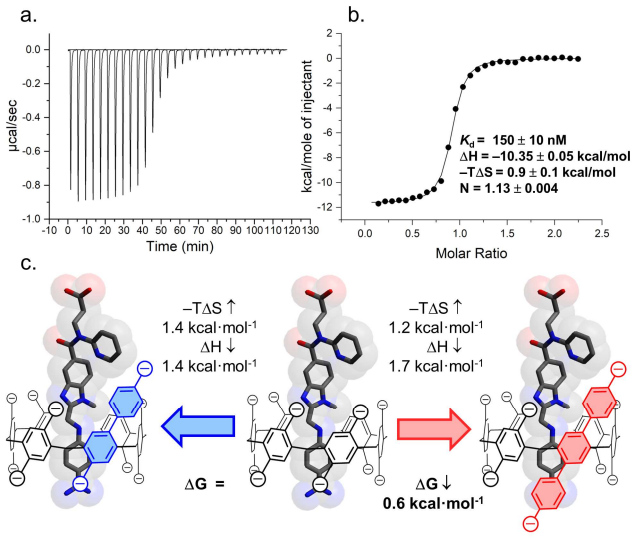

Figure 4. Thermodynamic parameters of sulfo-pillar[6]arene-DOAC binding determined by isothermal calorimeter. a. Plot of DP versus time from the titration of a **A1sP6** (250 µm) into dabigatran (25 µm) in CBS (10 mM, pH 3.0) at 30°C. b. Plot of DH versus molar ratio of **A1sP6** to dabigatran, thermodynamic parameters of respective replicate. c. Cartoon representation of the interaction of extended sulfo-pillar[6]arenes and dabigatran; negative charges represent sulfate groups.

As observed in the indicator displacement assay, edoxaban and betrixaban showed preferential binding to **A1sP6** and **A1A2sP6**, respectfully. The binding of edoxaban to sulfo-pillar[6]arene (K_d = 2900 ± 200 nM) increased 2-fold with the **A1** increased surface area (K_d = 1370 ± 70 nM), but decreased with the **A1A2** (K_d = 3800 ± 300 nM). This increase in affinity towards **A1sP6** is due to the increased enthalpic contribution of −8.82 ± 0.05 kcal·mol^{-1}, which is 1.43 and 3.04 kcal·mol^{-1} greater than **sP6** and **A1A2sP6**, respectively. While the **A1sP6** host had the most enthalpic contribution, it also had the most unfavourable entropy (0.69 ± 0.07 kcal·mol^{-1}). Betrixaban favoured **A1A2sP6** (K_d = 1500 ± 100 nM), with the **A1** and **A1A2** functionalization leading to a subtle increase in enthalpy relative to the parent **sP6** and no notable change in entropy with the reported values being within error. These subtle changes in betrixaban binding indicate that the DOAC is binding the three hosts in a similar fashion.

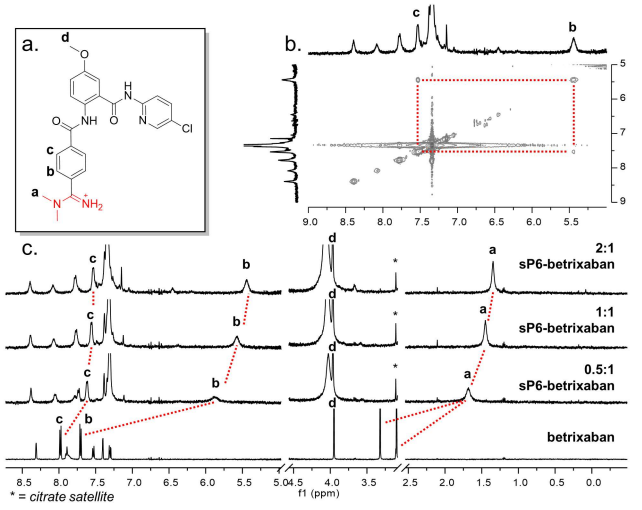

Figure 5. a. Chemical structure of betrixaban with key residues labeled. b. COSY data of 1.0 mM **sP6** 0.5 mM Betrixaban in 20 mM deuterated CBS buffer (pH 3.0) with 1% DMSO. Red box indicates correlation between aromatic protons b and c of betrixaban. c. ^{1}H-NMR titration of **sP6** (0-1 mM) into betrixaban (0.5 mM) in 20 mM deuterated CBS buffer (pH 3.0) with 1% DMSO. Citrate and D_2O signals removed for clarity, see Figure S42 for full spectrum.

Extended sulfo-pillar[6]arenes form a complex with the benzamidinium moiety of betrixaban. The binding orientation of betrixaban and the extended sulfo-pillar[6]arenes was determined using ^{1}H-NMR by titrating the host into 0.5 mM betrixaban in deuterated CBS buffer at pH 3.0 with 1% DMSO; monitoring the chemical shift change of betrixaban (Figure 5). The NMR signals were assigned from 2D correlation spectroscopy (COSY) (Figures 5a-b, S39, S40). When 0.5 equivalent (0.25 mM) **sP6** is added the two singlets of the benzamidinium methyl resonances at 3.32 and 3.10 ppm converge and move upfield to 1.68 ppm, indicating the inclusion of amidinium moiety in the hydrophobic cavity of sulfo-pillar[6]arene (Figures 5c, S41, S42). In addition to the shielding effect observed with the methyl protons, the signals of the aromatic doublet (b) move upfield from 7.70 ppm to 5.88 ppm, further confirming the inclusion in the cavity of **sP6**. However, the aromatic doublet (c) only moves 0.36 ppm upfield showing a much smaller shielding effect relative to (b) (1.82 ppm shift). When 1 equivalent (0.5 mM) **sP6** is added, the amidinium methyl resonances move further upfield by 0.23 ppm. While the aromatic protons (b) adjacent to the amidinium move an additional 0.30 ppm, the more distant aromatic protons (c) move only 0.06 ppm upfield. Minor downfield shifts are noted in the remaining protons of betrixaban, but their assignment is ambiguous in the pillararene complex, except for the methoxy singlet at 3.95 ppm which has a very minor downfield shift (0.02 ppm) in the presence of **sP6**. From the chemical shift changes, it is clear that **sP6** encapsulates the cationic benzamidinium moiety of betrixaban and that it forms a 1:1 complex.

Increasing the aromatic surface area increases the host guest interactions. In the ^{1}H-NMR titrations, **A1sP6** and **A1A2sP6** overall have more broadening of the host and guest signals upon complexation. This causes chemical shift tracking to be more obscure (Figures 6a, S43-S45). However, it is clear from the upfield shift of an aromatic proton (b) and the methyl groups of the amidinium (a) that all three hosts bind in a similar fashion. In the case of **A1sP6** the singlet from the amidinium methyl moieties (a) is shifted less upfield than with **sP6** (Figure 6a) this would indicate that the amidinium is not as shielded by the **A1sP6** cavity. The aromatic proton (b) moves very minorly upfield, likely experiencing a similar environment between the **A1sP6** and the **sP6**. This is also seen with **A1A2sP6**; where with respect to **sP6** the amidinium methyl resonances (a) are less upfield, but the aromatic proton (b) is only minorly affected (Figure 6a). From this we propose that the amidinium moiety of betrixaban is inside the cavity and is interacting with the sulfates on the bottom rim of the host (Figure 6b). This would cause the remaining aromatic residues of betrixaban to have more interaction with the hosts. Due to broadening these signals could not be assigned. However, there is an overall upfield movement in the functionalized host relative to **sP6** (Figure 6a, gold stars), possibly due to increased interactions. This proposed binding motif is supported by the general trend observed in binding affinity between the three hosts, where increasing surface area (**A1A2sP6**) increased affinity 6-fold (Table 1). Rudimentary molecular modeling was used to visualize the sulfo-pillar[6]arene complexes with betrixaban. Betrixaban was oriented in the host cavity based off the respective NMR titration data and the complex was minimized in Maestro 13.8 using OPLS-2005 (Figures 6c, S46). The minimized structures show increased interaction between the pendant arm of **A1sP6** and **A1A2sP6** and betrixaban as proposed.

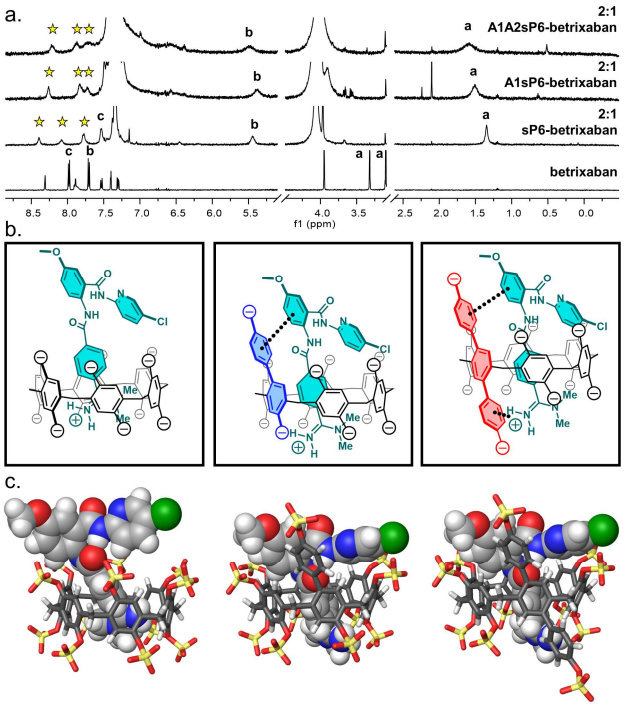

Figure 6. Functionalized analogs have more interactions with betrixaban. a. ^{1}H-NMR (bottom to top); betrixaban (0.5 mM), betrixaban (0.5 mM) with **sP6** (1 mM), betrixaban (0.5 mM) with **A1sP6** (1 mM), betrixaban (0.5 mM) with **A1A2sP6** (1 mM) in 20 mM deuterated CBS buffer (pH 3.0) with 1% DMSO. Citrate and D_2O signals removed for clarity, see Figure S45 for full spectrum. b. Perspective drawing of potential increased interactions between betrixaban and functionalized sulfo-pillar[6]arene; negative charges represent sulfate groups. c. Molecular models of (left to right) **sP6**-betrixaban, **A1sP6**-betrixaban, **A1A2sP6**-betrixaban. Models made in Maestro 13.8, structures minimized with OPLS-2005.

DISCUSSION

Herein we report the first functionalized derivatives of **sP6** and their molecular recognition properties towards DOACs. **A1sP6** and **A1A2sP6** are the first reported mono- or di-functionalized water-soluble pillar[6]arenes. Different water-solubilizing groups have been utilized to functionalize pillar[6]arene in a global way such that all twelve positions are modified uniformly.[34] However, there are no reports of a water-soluble pillar[6]arene that is not symmetrical (i.e. contains a mono- or di-functionalization in its core scaffold). This vacancy in the field is also present in water-soluble pillar[5]arene research where examples of mono- or di-functionalization is limited.[35-40] A water-soluble *meso*-TPE-functionalized pillar[5]arene diversified the core scaffold through a McMurray coupling at the methylene bridge.[35] Additionally, a water-soluble pillar[4]arene[1]quinone had a dissymmetrical scaffold.[36] The remaining reported functionalized water-soluble pillar[5]arenes have

the diversifying element on an elongated alkyl-based appendage, removed from the core structure.[37-40] With these novel extended sulfo-pillar[6]arenes we sought to explore the change in the molecular recognition properties relative to the unfunctionalized sulfo-pillar[6]arene.

The elongated hydrophobic surface of the extended sulfo-pillar[6]arenes resulted in stronger affinity towards the DOACs edoxaban and betrixaban. Betrixaban bound **A1A2sP6** with a 6-fold stronger binding affinity than the unfunctionalized parent **sP6**, and similarly edoxaban bound **A1sP6** 2.5-fold stronger than **sP6**. The preferential binding of edoxaban to **A1sP6** was due to a more favourable enthalpy, likely due to improve size complementarity with the **A1** extension. All host-guest complexes were enthalpically driven with minor entropic contributions. The high binding affinities we observed (Tables 1 and 2) demonstrate that the collapsed state seen in the crystal structure for intermediate **8** (Figures S27, S28) is unlikely to exist in solution for **A1A2sP6**; this makes sense since the finished host is decorated with twelve mutually repulsive anionic sulfates in a way that would prevent host collapse.

There is limited literature precedent on the direct binding affinity of a DOAC to a supramolecular host. Researchers have looked at the effect β-cyclodextrin has on the binding between human serum albumin and the pro-drug dabigatran etexilate.[41] In the presence of β-cyclodextrin the affinity for human serum albumin towards dabigatran etexilate decrease from 5.95 x 10^3 M^{-1} (K_d ~ 0.2 mM) to 1.02 x 10^3 M^{-1} (K_d ~ 1 mM), indicating that β-cyclodextrin was competing in the binding event. However, the equilibrium constant for the β-cyclodextrin – dabigatran etexilate complex was not reported.[41] In 2023 the modified procoagulant β-cyclodextrin , OKL-1111, was reported as a potential reversal agents for DOACs.[22] The mechanism of the reversal is unclear and as stated by the researchers it is unlikely that it acts through the sequestration of circulating DOAC in the blood stream. This is based on the low affinity of the DOACs for OKL-1111 which binds with dissociation constants (K_d) of >6 mM for dabigatran, >2 mM for apixaban, >50 μM for rivaroxaban, and 25 μM for exodaban. Betrixaban was not included in this study. Our extended sulfo-pillar[6]arene hosts range from 25–200,000 times stronger than OKL-1111 at binding DOAC targets. Additionally, the affinities we determined for extended sulfo-pillar[6]arene are in the presence of 137 mM NaCl which closely resemble the concentration of salt circulating in the blood stream; the reported OKL-1111 affinities were obtained in the absence of physiological salt concentrations.

CONCLUSION

Sulfo-pillar[6]arene was an ultra-high affinity, salt tolerant, supramolecular host that previously lacked synthetic functionalizability – an important factor in tuning affinities and in pursuing applications. Through the development of an **A1** and **A1A2** synthetic pathway we modified the host cavity in ways that directly impact guest binding and selectivity. The **A1sP6** and **A1A2sP6** offer a larger surface area allowing more host-guest interactions for guests with complementary shapes and functionality. The **A1A2** functionalization had a 6-fold improved potency for betrixaban, which had been previously unexplored in host-guest chemistry. Previous work has highlighted the potential for sulfo-pillar[6]arene as a supramolecular reversal agent for neuromuscular blocking agents and opioids.[23, 25] We have shown that these hosts have high affinity towards an underexplored drug class, DOACs, in biologically relevant salty media. We believe the functionalized sulfo-pillar[6]arenes have the potential as a supramolecular reversal agent for direct oral anticoagulants. Additionally, the developed synthetic methods can easily be adapted in future endeavours to diversify the parent host and allow researchers to explore the full potential of sulfo-pillar[6]arenes.

ASSOCIATED CONTENT

The Supporting Information is available free of charge at http://pubs.acs.org.
Synthesis and characterization data, crystallography, fluorescence experiments, isothermal titration calorimetry, NMR titrations and molecular modeling (PDF).

AUTHOR INFORMATION

Corresponding Author

Fraser Hof – Department of Chemistry, University of Victoria, 3800 Finnerty Rd., Victoria, BC V8P 5C2, Canada; Centre for Advanced Materials and Related Technology (CAMTEC), University of Victoria, Victoria, BC V8W 2Y2, Canada; orcid.org/0000-0003-4658-9132; Email: fhof@uvic.ca

Authors

Chelsea R. Wilson – Department of Chemistry, University of Victoria, 3800 Finnerty Rd., Victoria, BC V8P 5C2, Canada; Centre for Advanced Materials and Related Technology (CAMTEC), University of Victoria, 3800 Finnerty Rd., Victoria, BC V8W 2Y2, Canada; orcid.org/0000-0001-6743-715X
Austia O. Puckett – Department of Chemistry, University of Victoria, 3800 Finnerty Rd., Victoria, BC V8P 5C2, Canada; Centre for Advanced Materials and Related Technology (CAMTEC), University of Victoria, 3800 Finnerty Rd., Victoria, BC V8W 2Y2, Canada; orcid.org/0000-0001-7797-1970
Allen G. Oliver – Department of Chemistry and Biochemistry, University of Notre Dame, 251 Nieuwland Science Hall, Notre Dame, IN, 46556 USA orcid.org/0000-0002-0511-1127

Author Contributions

All authors have given approval to the final version of the manuscript.

Notes

The authors declare no competing financial interest.

ACKNOWLEDGMENT

The authors thank the Natural Sciences and Engineering Research Council of Canada (NSERC, RGPIN-2019-04806) for financial support. C.R.W. thanks NSERC for the Postgraduate Scholarship – Doctoral (PGS D). We thank Dr. Alisdair Boraston for providing access to an isothermal titration calorimeter. We thank Christopher Barr for helpful discussion on NMR. We also thank CAMTEC for the use of shared facilities. Funding for the Bruker Venture was supported by NSF MRI Award CHE-2214606

REFERENCES

(1) Kim, H. K.; Nelson, L. S. Reducing the harm of opioid overdose with the safe use of naloxone: a pharmacologic review. *Expert Opin. Drug Saf.* **2015**, *14* (7), 1137-1146. DOI: 10.1517/14740338.2015.1037274.

(2) Yin, H.; Zhang, X.; Wei, J.; Lu, S.; Bardelang, D.; Wang, R. Recent advances in supramolecular antidotes. *Theranostics.* **2021**, *11* (3), 1513-1526. DOI: 10.7150/thno.53459.

(3) Deng, C.-L.; Murkli, S. L.; Isaacs, L. D. Supramolecular hosts as *in vivo* sequestration agents for pharmaceuticals and toxins. *Chem. Soc. Rev.* **2020**, *49* (21), 7516-7532. DOI: 10.1039/d0cs00454e.

(4) Welliver, M.; McDonough, J.; Kalynych, N.; Redfern, R. Discovery, development, and clinical application of sugammadex sodium, a selective relaxant binding agent. *Drug Des. Dev. Ther.* **2009**, *2*, 49-59. DOI: 10.2147/dddt.s2757.

(5) Bom, A.; Bradley, M.; Cameron, K.; Clark, J. K.; Van Egmond, J.; Feilden, H.; Maclean, E. J.; Muir, A. W.; Palin, R.; Rees, D. C.; et al. A Novel Concept of Reversing Neuromuscular Block: Chemical Encapsulation of Rocuronium Bromide by a Cyclodextrin-Based Synthetic Host *Angew. Chem. Int. Ed.* **2002**, *41* (2), 266-270. DOI: 10.1002/1521-3773(20020118)41:2<265::aid-anie265>3.0.co;2-q.

(6) Hristovska, A.-M.; Duch, P.; Allingstrup, M.; Afshari, A. Efficacy and safety of sugammadex versus neostigmine in reversing neuromuscular blockade in adults. *Cochrane Database Syst. Rev.* **2017**, *2017* (9). DOI: 10.1002/14651858.cd012763.

(7) Geng, W.-C.; Sessler, J. L.; Guo, D.-S. Supramolecular prodrugs based on host–guest interactions. *Chem. Soc. Rev.* **2020**, *49* (8), 2303-2315. DOI: 10.1039/c9cs00622b.

(8) Yu, G.; Chen, X. Host-Guest Chemistry in Supramolecular Theranostics. *Theranostics.* **2019**, *9* (11), 3041-3074. DOI: 10.7150/thno.31653.

(9) Webber, M. J.; Langer, R. Drug delivery by supramolecular design. *Chem. Soc. Rev.* **2017**, *46* (21), 6600-6620. DOI: 10.1039/c7cs00391a.

(10) Ma, X.; Zhao, Y. L. Biomedical Applications of Supramolecular Systems Based on Host-Guest Interactions. *Chem. Rev.* **2015**, *115* (15), 7794-7839. DOI: 10.1021/cr500392w.

(11) Haerter, F.; Simons, J. C. P.; Foerster, U.; Moreno Duarte, I.; Diaz-Gil, D.; Ganapati, S.; Eikermann-Haerter, K.; Ayata, C.; Zhang, B.; Blobner, M.; et al. Comparative Effectiveness of Calabadion and Sugammadex to Reverse Non-depolarizing Neuromuscular-blocking Agents. *Anesthesiology.* **2015**, *123* (6), 1337-1349. DOI: 10.1097/aln.0000000000000868.

(12) Yin, H.; Cheng, Q.; Bardelang, D.; Wang, R. Challenges and Opportunities of Functionalized Cucurbiturils for Biomedical Applications. *J. Am. Chem. Soc. - Au.* **2023**, *3* (9), 2356-2377. DOI: 10.1021/jacsau.3c00273.

(13) Nimse, S. B.; Kim, T. Biological applications of functionalized calixarenes. *Chem. Soc. Rev.* **2013**, *42* (1), 366-386. DOI: 10.1039/c2cs35233h.

(14) Schneider, C.; Bierwisch, A.; Koller, M.; Worek, F.; Kubik, S. Detoxification of VX and Other V-Type Nerve Agents in Water at 37 °C and pH 7.4 by Substituted Sulfonatocalix[4]arenes. *Angew. Chem. Int. Ed.* **2016**, *55* (41), 12668-12672. DOI: 10.1002/anie.201606881.

(15) Murkli, S.; Klemm, J.; Brockett, A. T.; Shuster, M.; Briken, V.; Roesch, M. R.; Isaacs, L. In Vitro and In Vivo Sequestration of Phencyclidine by Me4Cucurbit[8]uril**. *Chem. Eur. J.* **2021**, *27* (9), 3098-3105. DOI: 10.1002/chem.202004380.

(16) Ho, K. H.; Van Hove, M.; Leng, G. Trends in anticoagulant prescribing: a review of local policies in English primary care. *BMC Health Serv. Res.* **2020**, *20* (1). DOI: 10.1186/s12913-020-5058-1.

(17) Shaw, J. R.; Siegal, D. M. Pharmacological reversal of the direct oral anticoagulants—A comprehensive review of the literature. *Res. Pract. Thromb. Haemostasis.* **2018**, *2* (2), 251-265. DOI: 10.1002/rth2.12089.

(18) Chen, A.; Stecker, E.; A. Warden, B. Direct Oral Anticoagulant Use: A Practical Guide to Common Clinical Challenges. *J. Am. Heart Assoc.* **2020**, *9* (13). DOI: 10.1161/jaha.120.017559.

(19) Rose, D. K.; Bar, B. Direct Oral Anticoagulant Agents: Pharmacologic Profile, Indications, Coagulation Monitoring, and Reversal Agents. *J. Stroke Cerebrovasc. Dis.* **2018**, *27* (8), 2049-2058. DOI: 10.1016/j.jstrokecerebrovasdis.2018.04.004.

(20) Cuker, A.; Burnett, A.; Triller, D.; Crowther, M.; Ansell, J.; Van Cott, E. M.; Wirth, D.; Kaatz, S. Reversal of direct oral anticoagulants: Guidance from the Anticoagulation Forum. *Am. J. Hematol.* **2019**, *94* (6), 697-709. DOI: 10.1002/ajh.25475.

(21) Tangedal, K.; Semchuk, W.; Bolt, J. How Should Canadian Pharmacy Departments Utilize Idarucizumab? *Can. J. Hosp. Pharm.* **2016**, *69* (5). DOI: 10.4212/cjhp.v69i5.1601.

(22) Meijers, J. C. M.; Bakhtiari, K.; Zwiers, A.; Peters, S. L. M. OKL-1111, A modified cyclodextrin as a potential universal reversal agent for anticoagulants. *Thromb. Res.* **2023**, *227*, 17-24. DOI: 10.1016/j.thromres.2023.05.003.

(23) Xue, W.; Zavalij, P. Y.; Isaacs, L. Pillar[*n*]MaxQ: A New High Affinity Host Family for Sequestration in Water. *Angew. Chem. Int. Ed.* **2020**, *59* (32), 13313-13319. DOI: 10.1002/anie.202005902.

(24) Isaacs, L. D., Xue, W. Sulfated pillararenes, methods of making same, and uses thereof. U.S. Patent App. 17/822,863., 2023.

(25) Brockett, A. T.; Xue, W.; King, D.; Deng, C. L.; Zhai, C.; Shuster, M.; Rastogi, S.; Briken, V.; Roesch, M. R.; Isaacs, L. Pillar[6]MaxQ: A Potent Supramolecular Host for In Vivo Sequestration of Methamphetamine and Fentanyl. *Chem.* **2023**, *9* (4), 881-900. DOI: 10.1016/j.chempr.2022.11.019.

(26) King, D.; Wilson, C. R.; Herron, L.; Deng, C.-L.; Mehdi, S.; Tiwary, P.; Hof, F.; Isaacs, L. Molecular recognition of methylated amino acids and peptides by Pillar[6]MaxQ. *Org. Biomol. Chem.* **2022**, *20* (37), 7429-7438. DOI: 10.1039/d2ob01487d.

(27) King, D. D., C. L.; Issacs, L. Pillar[n]MaxQ sensing ensemble: Application to world anti-doping agency banned substances. *Tetrahedron.* **2023**, *145*, 133607. DOI: 10.1016/j.tet.2023.133607.

(28) Wilson, C. R.; Chen, E. F. W.; Puckett, A. O.; Hof, F. Ethoxypillar[6]arene. *Org. Synth.* **2022**, *99*, 125-138. DOI: 10.15227/orgsyn.99.0125.

(29) Ogoshi, T.; Kayama, H.; Yamafuji, D.; Aoki, T.; Yamagishi, T.-A. Supramolecular polymers with alternating pillar[5]arene and pillar[6]arene units from a highly selective multiple host–guest complexation system and monofunctionalized pillar[6]arene. *Chem. Sci.* **2012**, *3* (11), 3221. DOI: 10.1039/c2sc20982a.

(30) Ogoshi, T.; Yamafuji, D.; Kotera, D.; Aoki, T.; Fujinami, S.; Yamagishi, T. A. Clickable di- and tetrafunctionalized pillar[n]arenes (n = 5, 6) by oxidation-reduction of pillar[n]arene units. *J. Org. Chem.* **2012**, *77* (24), 11146-11152. DOI: 10.1021/jo302283n.

(31) Rashvand Avei, M.; Etezadi, S.; Captain, B.; Kaifer, A. E. Visualization and quantitation of electronic communication pathways in a series of redox-active pillar[6]arene-based macrocycles. *Commun. Chem.* **2020**, *3* (1), 117. DOI: 10.1038/s42004-020-00363-4.

(32) Zhu, Y.; Escorihuela, J.; Wang, H.; Sue, A. C. H.; Zuilhof, H. Tunable Supramolecular Ag+-Host Interactions in Pillar[n]arene[m]quinones and Ensuing Specific Binding to 1-Alkynes. *Molecules.* **2023**, *28* (20), 7009. DOI: 10.3390/molecules28207009.

(33) Demay-Drouhard, P.; Du, K.; Samanta, K.; Wan, X.; Yang, W.; Srinivasan, R.; Sue, A. C. H.; Zuilhof, H. Functionalization at Will of Rim-Differentiated Pillar[5]arenes. *Org. Lett.* **2019**, *21* (11), 3976-3980. DOI: 10.1021/acs.orglett.9b01123.

(34) Tang, R.; Ye, Y.; Zhu, S.; Wang, Y.; Lu, B.; Yao, Y. Pillar[6]arenes: From preparation, host-guest property to self-assembly and applications. *Chin. Chem. Lett.* **2023**, *34* (3), 107734. DOI: 10.1016/j.cclet.2022.08.014.

(35) Tian, X.; Zuo, M.; Niu, P.; Velmurugan, K.; Wang, K.; Zhao, Y.; Wang, L.; Hu, X.-Y. Orthogonal Design of a Water-Soluble meso-Tetraphenylethene-Functionalized Pillar[5]arene with Aggregation-Induced Emission Property and Its Therapeutic Application. *ACS Appl. Mater. Interfaces.* **2021**, *13* (31), 37466-37474. DOI: 10.1021/acsami.1c07106.

(36) Wang, J.; Cen, M.; Wang, J.; Wang, D.; Ding, Y.; Zhu, G.; Lu, B.; Yuan, X.; Wang, Y.; Yao, Y. Water-soluble pillar[4]arene[1]quinone: Synthesis, host-guest property and application in the fluorescence turn-on sensing of ethylenediamine in aqueous solution, organic solvent and air. *Chin. Chem. Lett.* **2022**, *33* (3), 1475-1478. DOI: 10.1016/j.cclet.2021.08.044.

(37) Zhang, Y.; Chen, L.; Du, X.; Yu, X.; Zhang, H.; Meng, Z.; Zheng, Z.; Chen, J.; Meng, Q. Selective Fluorescent Sensing for Iron in Aqueous Solution by A Novel Functionalized Pillar[5]arene. *ChemistryOpen.* **2023**, *12* (10). DOI: 10.1002/open.202300109.

(38) Sun, J.; Shao, L.; Zhou, J.; Hua, B.; Zhang, Z.; Li, Q.; Yang, J. Efficient enhancement of fluorescence emission via TPE functionalized cationic pillar[5]arene-based host–guest recognition-mediated supramolecular self-assembly. *Tetrahedron Lett.* **2018**, *59* (2), 147-150. DOI: 10.1016/j.tetlet.2017.12.009.

(39) Shurpik, D. N.; Aleksandrova, Y. I.; Mostovaya, O. A.; Nazmutdinova, V. A.; Zelenikhin, P. V.; Subakaeva, E. V.; Mukhametzyanov, T. A.; Cragg, P. J.; Stoikov, I. I. Water-soluble pillar[5]arene sulfo-derivatives self-assemble into biocompatible nanosystems to stabilize therapeutic proteins. *Bioorg. Chem.* **2021**, *117*, 105415. DOI: 10.1016/j.bioorg.2021.105415.

(40) Wu, X.; Ni, M.; Xia, W.; Hu, X.-Y.; Wang, L. A novel dynamic pseudo[1]rotaxane based on a mono-biotin-functionalized pillar[5]arene. *Org. Chem. Front.* **2015**, *2* (9), 1013-1017, 10.1039/C5QO00159E. DOI: 10.1039/C5QO00159E.

(41) Naik, R. S.; Pawar, S. K.; Tandel, R. D.; J, S. Insights in to the mechanism of interaction of a thrombin inhibitor, dabigatran etexilate with human serum albumin and influence of β-cyclodextrin on binding: Spectroscopic and computational approach. *J. Mol. Liq.* **2018**, *251*, 119-127. DOI: 10.1016/j.molliq.2017.12.056.

TOC Graphic

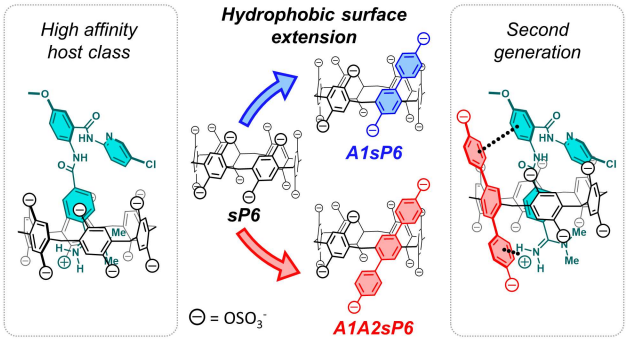

Supporting Information:

Extended sulfo-pillar[6]arenes – a new host family and its application in the binding of direct oral anticoagulants.

1. Synthesis

1.1 General remarks

Materials. Boron tribromide, cerium ammonium nitrate, sodium borohydride, trifluoromethanesulfonic anhydride solution (1 M in methylene chloride), 4-methoxyphenyl boronic acid and XPhos Pd G3 were obtained from Sigma-Aldrich. Sulfur trioxide pyridium complex (48-50% active SO_3) was obtained from ThermoScientific. Sulfur trioxide pyridium complex (48-50% active SO_3) was further dried under vacuum (60°C, 0.3 mmHg) for 48 hours and pyridine was freshly distilled over CaH_2 prior to sulfation reactions. All other reagents were used as received.

NMR. Deuterated solvents were purchased from Sigma Aldrich or Tokyo Chemical Industry (TCI). Spectra were collected on a Bruker Avance Neo 500 MHz spectrometer or 300 MHz spectrometer (^{19}F NMR). ^{1}H, ^{13}C, ^{19}F NMR spectra were processed using MestReNova by Mestrelab Research S.L. ^{1}H NMR data was referenced as follows; $CDCl_3$ (δ 7.26), $(CD_3)_2CO$ (δ 2.05) and D_2O (δ 4.79). ^{13}C NMR data was referenced as follows; $CDCl_3$ (δ 77.2), CD_3OD (δ 49.0).

Dialysis. Excess salt was removed from **sP6**, **A1sP6** and **A1A2sP6** via dialysis. Float-A-Lyzer® (MWCO 0.1 – 0.5 kD), 5 mL tubes were used (Repligen). The salt content was determined by quantitative NMR (see below), and a cutoff of ≤ 50% salt content was applied as a quality control standard.

Quantitative NMR. The ratio of host to salt was determined by quantitative NMR using 2,2,3,3-d(4)-3-(trimethylsilyl)propionic acid sodium salt, 98+ atom % D (Alfar Aesar) as a standard. Deuterium oxide was purchased from Tokyo Chemical Industry (TCI). Quantitative NMR spectrum was collected on a Bruker Avance Neo 500 MHz spectrometer with a D1 set to 60 seconds. Spectra were processed using TopSpin 4.0.7. For **A1sP6** and **A1A2sP6** the salt content percent was calculated by determining the host concentration independently using the integrations of the aromatic region, the methylene region and the upfield aromatic singlet. The average of these three measurements was taken and used to determine the % salt content of the host solid, where all mass that is not host is assumed to be the NMR-invisible salts that arise from the reaction workup. For **sP6** the salt content percent was calculated for the aromatic region and the methylene region, the average of these two measurements was taken and used to determine the % salt content of the host solid.

Mass spectrum. Accurate mass was obtained by electrospray ionization using a Thermo Scientific™ Exactive™ Plus Orbitrap Ultimate 3000 LC-MS system, using an eluent of 50:50 Mili-Q™ water and Optima™ Acetonitrile.

EtOP6[1], and **sP6**[2] were synthesized as described in literature. Excess salt from **sP6** was removed via dialysis, a cutoff of ≤ 50% salt content was applied as a quality control standard. **sP6** was obtained with 18% salt content.

1.2 A1 functionalization pathway

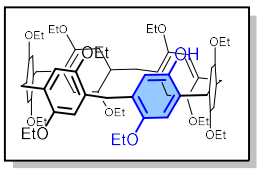

1: This method was adapted from literature.[3] A oven-dry 100 mL round-bottom equipped with a stir bar was charged with **EtOP6** (5.0 g, 1 equiv, 4.69 mmol) the vessel was purged and backfilled with argon 3 times. Anhydrous DCM (250 mL) was added with a syringe and the round-bottom was placed in 35°C oil bath. BBr_3 (1.3 mL, 13.4 mmol, 2.85 eq) was added via syringe using a disposable 2" long needle all at once. The reaction was stirred for 1.5 minutes then was quenched by adding H_2O. The organic layer was washed with H_2O (x2), the combined aqueous layer was washed with DCM (1x). The combined organic layer was dried over $MgSO_4$ and concentrated to dryness on a rotary evaporator. Unreacted **EtOP6** (800mg) was recovered by washing the crude solid with acetone and vacuum filtering. The filtrate was crude product and the remaining solid was **EtOP6**. The filtrate was then concentrated to dryness on a rotary evaporator and purified on a Biotage® Selekt Flash Purification System using Biotage Sfar Silica HC D (25g) columns and dry loaded with a 2.5 g samplet. Load capacity for separation was ~500 mg of crude using a gradient of ethyl acetate:pentane, 3%-100%. **2** was obtained (530 mg, 11% yield). ^{1}H NMR (500 MHz, $CDCl_3$) δ 6.83 (s, 1H), 6.80 (s, 1H), 6.76 (s, 1H), 6.75 (s, 1H), 6.69 (s, 1H), 6.68 (s, 1H), 6.66 – 6.65 (m, 4H), 6.63 (s, 1H), 6.59 – 6.58 (m, 2H), 4.01 (q, *J* = 7.0 Hz, 2H), 3.95 (q, *J* = 7.0 Hz, 2H), 3.92 – 3.72 (m, 30H), 1.44 (t, *J* = 7.0 Hz, 3H), 1.41 – 1.36 (m, 6H), 1.32 – 1.20 (m, 24H). ^{13}C NMR (126 MHz, $CDCl_3$) δ 151.5, 150.7, 150.6, 150.6, 150.6, 150.5, 150.5, 150.4, 148.2, 148.0, 130.3, 129.4, 128.6, 128.4, 128.3, 128.1, 128.0, 127.8, 127.8, 127.4, 126.7, 124.6, 118.8, 115.6, 115.6, 115.5, 115.5, 115.3, 115.2, 115.1, 115.0, 114.6, 114.3, 65.0, 64.4, 64.4, 64.4, 64.3, 64.2, 64.2, 64.1, 64.0, 31.5, 31.3, 30.9, 30.6, 30.5, 29.8, 15.3, 15.3, 15.3, 15.2, 15.2, 15.2, 15.1, 14.8. HR-ESI-MS: m/z $[M+Na]^{1+}$ calculated for $C_{64}H_{80}O_{12}Na$: 1063.55475; found: 1063.55432.

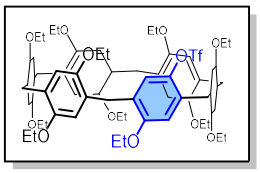

2: A oven-dry round-bottom flask equipped with a stir bar was charged with **1** (440 mg, 0.42 mmol, 1 eq.) and the vessel was purged and backfilled with argon 3 times. Under argon, anhydrous DCM (75 mL) was added. The reaction was placed in an ice bath and dry pyridine (170 µL, 2.11 mmol, 5 eq.) was added. Triflic anhydride (1.3 mL, 7.82 mmol, 18.5 eq.) was slowly added dropwise. The reaction was left to stir overnight (18 hours), 0°C to room temperature. The reaction was quenched with H_2O and the organic layer was washed with H_2O (3x), brine (3x). The organic layer was dried over $MgSO_4$ and vacuum filtered. The filtrate was concentrated to dryness on a rotary evaporator. **2** was obtained (450 mg, 91% yield) as a white solid and carried forward without purification. ^{1}H NMR (500 MHz, $CDCl_3$) δ 7.11 (s, 1H), 6.77 (s, 1H), 6.75 (s, 1H), 6.71 – 6.69 (m, 7H), 6.64 (s, 1H), 6.60 (s, 1H), 3.94 – 3.75 (m, 32H), 3.72 (q, *J* = 7.0 Hz, 2H), 1.39 – 1.22 (m, 30H), 1.18 (t, *J* = 7.0 Hz, 3H). ^{13}C NMR (126 MHz, $CDCl_3$) δ 155.9, 150.7, 150.7, 150.6, 150.6, 150.6, 150.5, 150.5, 150.5, 150.4, 141.1, 132.3, 129.2, 129.0, 128.5, 128.3, 128.1, 128.1, 127.9, 127.7, 127.6, 126.1, 125.2, 123.6, 115.6, 115.5, 115.5, 115.4, 115.3, 115.2, 115.2, 115.0, 114.8, 114.8, 113.8, 64.3, 64.2, 64.2, 64.1, 64.1, 64.1, 64.0, 63.8, 63.8, 63.6, 31.8, 31.3, 31.1, 31.1, 30.7, 15.4, 15.4, 15.3, 15.3, 15.3, 15.3, 15.0, 15.0.^{19}F NMR (283 MHz, $CDCl_3$) δ -73.9. HR-ESI-MS: m/z $[M+Na]^{1+}$ calculated for $C_{65}H_{79}F_3O_{14}SNa$: 1195.50404; found: 1195.50359.

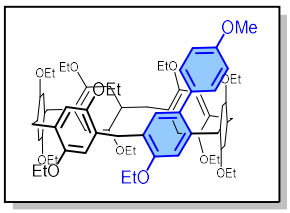

3: Under a flow of argon an oven-dry microwave vial equipped with a stir bar was charged with **2** (400 mg, 0.34 mmol, 1 eq.), Na_2CO_3 (283 mg, 2.05 mmol, 6 eq.), 4-methoxyphenylboronic acid (467 mg, 3.07 mmol, 9 eq.) and XPhos Pd G3 (87 mg, 0.10 mmol, 0.3 eq.). Glyme (degassed via sparging with argon for 30 minutes, 12 mL) was added, the microwave vial was cap and placed in a pre-heated 80°C oil bath. An argon balloon was added. Water (degassed via sparging with argon for 30 minutes, 3 mL) was added via syringe and the reaction was stirred under argon at 80°C for 18 hours. The vessel was removed from heat and let cool to room temperature. Water and DCM were added, and the organic layer was extracted and washed with water (x2) and brine (x1). The organic layer was dried over $MgSO_4$ and vacuum filtered. The filtrate was concentrated to dryness on a rotary evaporator. Crude **3** was purified on a Biotage® Selekt Flash Purification System using Biotage Sfar Silica HC D (50 g) columns and a 5 g samplet using a gradient of ethyl acetate:pentante, 3%-100%. **3** was obtained (280 mg, 73% yield) as a white solid. ^{1}H NMR (500 MHz, $CDCl_3$) δ 7.14 (d, *J* = 8.6 Hz, 2H), 7.10 (s, 1H), 6.84 (d, *J* = 8.6 Hz, 2H), 6.78 (s, 1H), 6.77 (s, 1H), 6.76 – 6.75 (m, 3H), 6.74 (s, 1H), 6.71 (s, 1H), 6.67 (s, 1H), 6.62 (s, 1H), 6.59 (s, 1H), 6.10 (s, 1H), 3.89 – 3.78 (m, 33H), 3.71 (q, *J* = 7.0 Hz, 2H), 3.63 (q, *J* = 7.0 Hz, 2H), 1.34 – 1.26 (m, 27H), 1.21 (t, *J* = 7.0 Hz, 3H), 1.17 (t, *J* = 7.0 Hz, 3H). ^{13}C NMR (126 MHz, $CDCl_3$) δ 158.2, 156.0, 150.6, 150.6, 150.6, 150.5, 150.5, 150.5, 150.3, 137.5, 135.0, 133.2, 133.2, 130.9, 128.1, 128.1, 128.1, 128.0, 128.0, 127.9, 127.8, 127.8, 126.9, 115.7, 115.6, 115.5, 115.5, 115.2, 115.2, 115.1, 115.1, 114.9, 113.3, 113.1, 64.3, 64.2, 64.2, 64.1, 64.1, 64.1, 64.1, 64.0, 64.0, 63.2, 55.3, 55.3, 34.0, 31.3, 31.2, 31.1, 31.0, 15.4, 15.4, 15.3, 15.3, 15.3, 15.2, 15.1. HR-ESI-MS: m/z $[M+Na]^{1+}$ calculated for $C_{71}H_{86}O_{12}Na$: 1153.60170; found: 1153.60117.

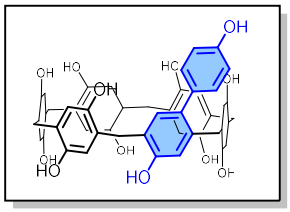

4: An oven-dry reaction vessel with a stir bar was charged with **3** (100 mg, 0.9 mmol, 1 eq.). The vessel was evacuated and backfilled with argon 3 times. A septum and argon balloon were added to close the vessel under an inert atmosphere. Dry dichloromethane (10 mL) was added via syringe and the round-bottom was placed in an ice bath. BBr_3 (180 µL, 1.95 mmol, 22 eq.) was added via syringe using a disposable 2" long needle dropwise (waiting until the green color disappears before adding more). Once all BBr_3 was added, the reaction was stirred for 24 hours. The reaction was quenched by adding water (10 mL). The precipitate was collected via vacuum filtration and was washed with 1 M (aq) HCl and chloroform. **4** was obtained (69 mg, 96% yield) as a white solid and carried forward without purification. ^{1}H NMR (500 MHz, $(CD_3)_2CO$) δ 7.14 (d, *J* = 8.5 Hz, 2H), 7.03 (s, 1H), 6.83 (d, *J* = 8.5 Hz, 2H), 6.63 – 6.62 (m, 2H), 6.61 (s, 1H), 6.59 (s, 1H), 6.57 (s, 1H), 6.56 (s, 1H), 6.55 (s, 1H), 6.50 (s, 1H), 6.46 (s, 1H), 6.44 (s, 1H), 6.32 (s, 1H), 3.76 (s, 2H), 3.71 (s, 2H), 3.68 – 3.67 (m, 8H). ^{13}C NMR (126 MHz, MeOD) δ 156.9, 154.2, 149.0, 148.6, 148.6, 148.5, 148.3, 148.3, 148.2, 148.0, 139.6, 135.3, 134.7, 133.3, 131.7, 128.4, 128.0, 127.8, 127.7, 127.7, 127.6, 127.6, 127.4, 127.3, 126.1, 118.9, 118.4, 118.4, 118.3, 118.2, 118.2, 118.1, 117.9, 117.7, 117.4, 115.7, 33.6, 31.1, 30.9, 30.8, 30.5, 30.2. HR-ESI-MS: m/z $[M+Na]^{1+}$ calculated for $C_{48}H_{40}O_{12}Na$: 831.24175; found: 831.24178.

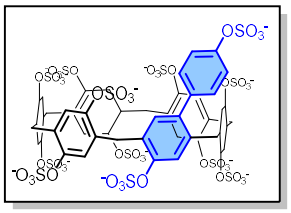

A1sP6: Sulfur trioxide pyridium complex (48-50% active SO_3) and **4** were dried under vacuum (60°C, 0.3 mmHg) for 48 hours prior to sulfation. Under a flow of argon an oven-dry microwave vial equipped with a stir bar was charged with **4** (65 mg, 0.08 mmol, 1 eq) and sulfur trioxide pyridinium complex (600 mg, 3.77 mmol, 48 eq). The vial was flushed with argon 3 times, then capped. The solids were mixed till homogeneous. Freshly distilled pyridine (4 mL) was added via syringe. The vial was placed in a pre-heated 70°C oil bath. The reaction was stirred at 70°C for 48 hours. The vial was removed from the heat. The clear supernatant was pipetted out leaving a brown residue in the vial. The residue was dissolved in H_2O (1 mL) and the pH (pH = 5.6) was adjusted to 8.4 with sat. aq. $NaHCO_3$. The resulting solution was filtered, and the filtrate was concentrated to dryness on a rotary evaporator, the **A1sP6** salt (380 mg) was isolated. Excess salt was removed via dialysis (see above). The solution was concentrated to dryness on a rotary evaporator to obtain **A1sP6** as a white solid (100 mg, 36% salt content, 40% yield corrected for salt). ^{1}H NMR (500 MHz, D_2O) δ 7.42 – 7.19 (m, 15H), 6.73 (s, 1H), 4.15 – 4.02 (m, 12H). ^{13}C NMR (126 MHz, D_2O+MeOD) δ 165.7, 151.5, 149.8, 147.9, 140.1, 139.2, 138.2, 134.7, 134.2, 133.9, 133.5, 132.0, 132.0, 131.7, 130.7, 130.7, 126.2, 125.9, 125.9, 125.2, 124.9, 124.6, 123.9, 122.7, 121.4, 33.9, 32.5, 31.5, 30.4. HR-ESI-MS: m/z $[M+7Na]^{5-}$ calculated for $C_{48}H_{28}O_{48}S_{12}Na_7$: 383.31420; found: 383.31380.

1.3 A1A2 functionalization pathway

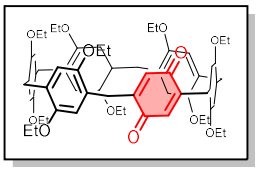

5: For alternative preparations see references.[4-6] A three-neck 250-mL round-bottom flask was equipped with a stir bar and charged with **EtOP6** (2.0 g, 1.87 mmol, 1 eq), the vessel was purged and backfilled with argon three times. 150 mL of DCM was degasssed via freeze-pump thaw (3 cycles) than transferred via cannula to the vessel. The solution was left to stir under argon for 5 minutes. The round-bottom was cooled to -20° C and 0.9 M cerium ammonium nitrate solution (Cerium ammonium nitrate (3.1 g, 5.65 mmol, 3 eq) dissolved in water (10 mL)) was added dropwise over 1.5 hours using a syringe pump. After 1.5 hours the reaction vessel was removed from the ice bath and let stir at room temperature for 5 minutes. The reaction was quenched by adding water and the organic layer was extracted and washed with H_2O (x3). The organic layer was dried over $MgSO_4$ and concentrated to dryness on a rotary evaporator. Crude **5** was obtained and purified on a Biotage® Selekt Flash Purification System using Biotage Sfar Silica HC D (25 g) columns and dry loaded with a 2.5 g samplet. Load capacity for separation was ~500 mg of crude using a gradient of ethyl acetate:pentane, 3%-100%. **5** was obtained (450 mg, 24% yield) as a red solid. ^{1}H NMR (500 MHz, $CDCl_3$) δ 6.77 (s, 2H), 6.71 – 6.71 (m, 4H), 6.69 (s, 2H), 6.63 (s, 2H), 6.45 (s, 2H), 3.94 – 3.76 (m, 28H), 3.58 (s, 4H), 1.40 – 1.32 (m, 18H), 1.28 (t, *J* = 7.0 Hz, 6H), 1.23 (t, *J* = 7.0 Hz, 6H). ^{13}C NMR (126 MHz, $CDCl_3$) δ 188.4, 150.7, 150.7, 150.6, 150.6, 150.5, 146.7, 133.7, 129.4, 128.3, 128.1, 127.4, 122.8, 115.6, 115.4, 115.4, 115.2, 114.6, 64.3, 64.3, 64.2, 64.1, 63.7, 31.2, 30.7, 30.5, 15.3, 15.3, 15.3, 15.1. HR-ESI-MS: m/z $[M+Na]^{1+}$ calculated for $C_{62}H_{74}O_{12}Na$: 1033.50780; found: 1033.50775.

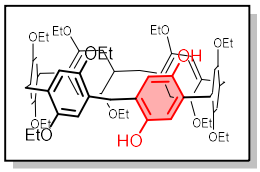

6: This method was adapted from literature.[6] In a 50 mL round-bottom flask equipped with a stir bar, **5** (350 mg, 0.35 mmol, 1eq) was dissolved in a 1:4 solution of MeOH (7 mL) and THF (28 mL). $NaBH_4$ (105 mg, 2.78 mmol, 8 eq) was added and the solution was stirred at room temperature for 30 minutes. The reaction was quenched by adding 1M HCl (10 mL). DCM/H_2O was added, and the organic layer was extracted and washed with H_2O (x2) and brine (x1). The organic layer was dried over $MgSO_4$ and vacuum filtered. The filtrate was concentrated to dryness on a rotary evaporator. Crude **6** was obtained (345 mg, >95% yield) as a white solid and carried forward without purification. ^{1}H NMR (500 MHz, $CDCl_3$) δ 7.23 (s, 2H), 6.86 (s, 2H), 6.76 (s, 2H), 6.69 (s, 2H), 6.68 (s, 2H), 6.62 (s, 2H), 6.61 (s, 2H), 4.06 (q, *J* = 7.0 Hz, 4H), 3.91 – 3.68 (m, 18H), 1.47 (t, *J* = 7.0 Hz, 6H), 1.38 – 1.20 (m, 24H). ^{13}C NMR (126 MHz, $CDCl_3$) δ 151.9, 150.6, 150.5, 150.5, 147.8, 147.6, 129.0, 128.4, 128.1, 127.2, 126.8, 126.4, 117.9, 115.9, 115.8, 114.9, 114.1, 65.1, 64.5, 64.3, 64.2, 63.9, 31.4, 31.3, 31.0, 30.5, 15.3, 15.3, 15.3, 15.3, 15.2, 14.8. HR-ESI-MS: m/z $[M+Na]^{1+}$ calculated for $C_{62}H_{76}O_{12}Na$: 1035.52345; found: 1035.52286.

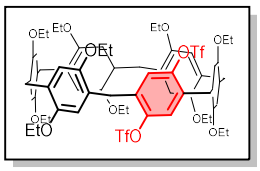

7: An oven-dry round-bottom flask equipped with a stir bar was charged with **6** (300 mg, 0.30 mmol, 1 eq) the vessel was purged and backfilled with argon 3 times. Under argon, anhydrous DCM (50 mL) was added. The reaction was placed in an ice bath and dry pyridine (140 uL, 1.70 mmol, 5.8 eq) was added. Triflic anhydride was slowly added dropwise (1.3 mL, 7.7 mmol, 26 eq). The reaction was left to stir overnight, 0°C to room temperature. The reaction was quenched with H_2O (20 mL). The organic layer was washed with H_2O (x3), brine (x2). The organic layer was dried over $MgSO_4$ and vacuum filtered. The filtrate was concentrated to dryness on a rotary evaporator. **7** was obtained (315 mg, 83% yield) as a light brown solid and carried forward without purification. ^{1}H NMR (500 MHz, Chloroform-*d*) δ 7.22 (s, 2H), 6.75 (s, 2H), 6.71 – 6.70 (m, 4H), 6.69 (s, 2H), 6.64 (s, 2H), 3.93 – 3.79 (m, 28H), 3.75 (q, *J* = 7.0 Hz, 4H), 1.39 – 1.30 (m, 18H), 1.27 (t, *J* = 7.0 Hz, 6H), 1.20 (t, *J* = 7.0 Hz, 6H). ^{13}C NMR (126 MHz, $CDCl_3$) δ 150.7, 150.5, 150.3, 146.6, 134.0, 129.7, 128.3, 128.0, 127.3, 124.9, 123.3, 115.5, 115.4, 115.3, 114.7, 114.5, 64.2, 64.2, 64.2, 64.1, 63.5, 31.8, 31.1, 30.8, 30.5, 15.3, 15.3, 15.3, 14.8. ^{19}F NMR (283 MHz, $CDCl_3$) δ -73.7. HR-ESI-MS: m/z $[M+Na]^{1+}$ calculated for $C_{64}H_{74}F_6O_{16}S_2Na$: 1299.42202; found: 1299.42183.

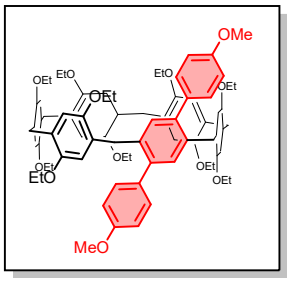

8: Under a flow of argon an oven-dry 50 mL three-neck round-bottom was equipped with a stir bar and charged with **7** (320 mg, 0.25 mmol, 1 eq.), K_2CO_3 (208 mg, 1.50 mmol, 6 eq.), 4-methoxyboronic acid (343 mg, 2.25 mmol, 9 eq.) and XPhos Pd G3 (64 mg, 0.08 mmol, 0.30 eq.). Glyme (degassed via sparging with argon for 30 minutes, 22 mL) was added and vessel was sealed with a septum and argon balloon. The vessel was then placed in a pre-heated 80°C oil bath and water (degassed via sparging with argon for 30 minutes, 5.5 mL) was added via syringe. The reaction was stirred under argon at 80°C for 5 hours. The vessel was removed from heat and let cool to room temperature. Water and DCM were added, and the organic layer was extracted and washed with water (x2) and brine (x1). The organic layer was dried over $MgSO_4$, the filtrate was concentrated to dryness on a rotary evaporator. Crude **8** was purified on a Biotage® Selekt Flash Purification System using Biotage Sfar Silica HC D (25 g) columns and a 2.5 g samplet using a gradient of ethyl acetate:pentante, 3%-100%. **3** was obtained (205 mg, 69% yield) as a pink solid. ^{1}H NMR (500 MHz, $CDCl_3$) δ 7.13 – 7.11 (m, 6H), 6.82 – 6.79 (m, 8H), 6.65 (s, 2H), 6.63 (s, 2H), 6.09 (s, 2H), 4.00 – 3.62 (m, 38H), 1.36 – 1.29 (m, 18H), 1.24 (t, *J* = 7.0 Hz, 6H), 1.14 (t, *J* = 7.0 Hz, 6H). ^{13}C NMR (126 MHz, $CDCl_3$) δ 158.4, 150.6, 150.5, 150.5, 150.4, 150.2, 140.1, 136.2, 134.8, 132.6, 130.7, 128.1, 128.1, 128.0, 127.9, 115.8, 115.4, 115.2, 115.0, 114.6, 113.2, 64.3, 64.1, 64.0, 64.0, 63.9, 55.3, 33.6, 31.2, 30.9, 15.4, 15.3, 15.3, 15.2, 15.1. HR-ESI-MS: m/z $[M+Na]^{1+}$ calculated for $C_{76}H_{88}O_{12}Na$: 1215.61735; found: 1215.61724.

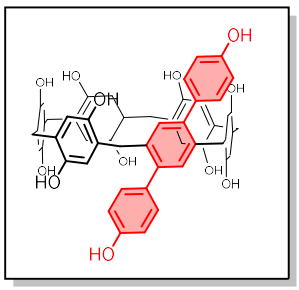

9: An oven-dry reaction vessel vial with a stir bar was charged with **8** (100 mg, 0.8 mmol, 1 eq.). The vessel was evacuated and backfilled with argon 3 times. A septum and argon balloon were added to close the vessel under an inert atmosphere. Dry dichloromethane (10 mL) was added via syringe and the round-bottom was placed in an ice bath. BBr_3 (170 µL, 1.84 mmol, 22 eq.) was added via syringe using a disposable 2" long needle dropwise (waiting until the green color disappears before adding more). Once all BBr_3 is added, the reaction was stirred for 24 hours. The reaction was quenched by adding water. The precipitate was collected via vacuum filtration and was washed with 0.5 M (aq) HCl and chloroform. **9** was obtained (60 mg, 90% yield) and carried forward without purification.^{1}H NMR (500 MHz, $(CD_3)_2CO$) δ 7.07 (s, 2H), 7.04 (d, *J* = 8.5 Hz, 4H), 6.78 (d, *J* = 8.5 Hz, 4H), 6.65 (s, 2H), 6.63 (s, 2H), 6.58 (s, 2H), 6.41 (s, 2H), 6.20 (s, 2H), 3.86 (s, 4H), 3.67 (s, 4H), 3.62 (s, 4H). ^{13}C NMR (126 MHz, MeOD) δ 156.9, 148.9, 148.3, 148.3, 148.2, 147.8, 142.1, 137.3, 134.5, 133.5, 131.3, 128.7, 127.9, 127.9, 127.6, 127.1, 118.6, 118.4, 118.1, 118.0, 117.9, 115.7, 33.4, 31.2, 30.3. HR-ESI-MS: m/z $[M+Na]^{1+}$ calculated for $C_{54}H_{44}O_{12}Na$: 907.27305 found: 907.27282.

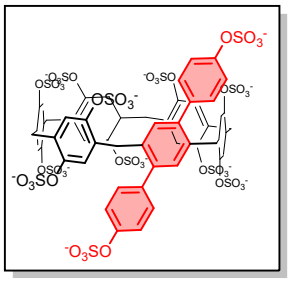

A1A2sP6: Sulfur trioxide pyridium complex (48-50% active SO_3) and **9** were dried under vacuum (60°C, 0.3 mmHg) for 48 hours prior to sulfation. Under a flow of argon an oven-dry microwave vial equipped with a stir bar was charged with **9** (50 mg, 0.06 mmol, 1 eq) and sulfur trioxide pyridinium complex (432 mg, 2.71 mmol, 48 eq). The vial was flushed with argon 3 times, then capped. The solids were mixed till homogeneous. The vial was placed in a pre-heated 70°C oil bath. Distilled (over CaH_2) pyridine (3 mL) was added via syringe. The reaction was stirred at 70°C for 48 hours. The vial was removed from the heat. The clear solution was pipetted out leaving a brown residue in the vial. The residue was dissolved in H_2O (1 mL) and the pH (pH = 5.6) was adjusted to 8.4 with sat. aq. $NaHCO_3$. The resulting solution was concentrated to dryness on a rotary evaporator, the **A1A2sP6** salt (360 mg) was isolated. Excess salt was removed via dialysis. The solution was concentrated to dryness on a rotary evaporator to obtain **A1A2sP6** as a white solid (90 mg, 49% salt content, 39% yield corrected for salt). ^{1}H NMR (500 MHz, D_2O+MeOD) δ 7.45 – 7.17 (m, 18H), 6.71 (s, 2H), 4.10 – 4.01 (m, 12H). ^{13}C NMR (126 MHz, D_2O+MeOD) δ 167.7, 151.3, 147.8, 147.4, 141.2, 139.2, 136.1, 136.0, 134.4, 134.4, 133.6, 133.6, 133.6, 133.4, 133.4, 133.2, 133.2, 133.1, 133.1, 132.8, 132.8, 132.4, 131.6, 131.5, 130.3, 130.3, 126.1, 126.0, 125.6, 125.4, 124.7, 124.3, 124.1, 122.4, 122.4, 121.1, 34.4, 33.3, 32.6, 32.3, 31.5, 31.2, 30.6, 30.2. HR-ESI-MS: m/z $[M+7Na]^{5-}$ calculated for $C_{54}H_{32}O_{48}S_{12}Na_7$: 398.52046; found: 398.52014.

1.4 NMR Characterization data:

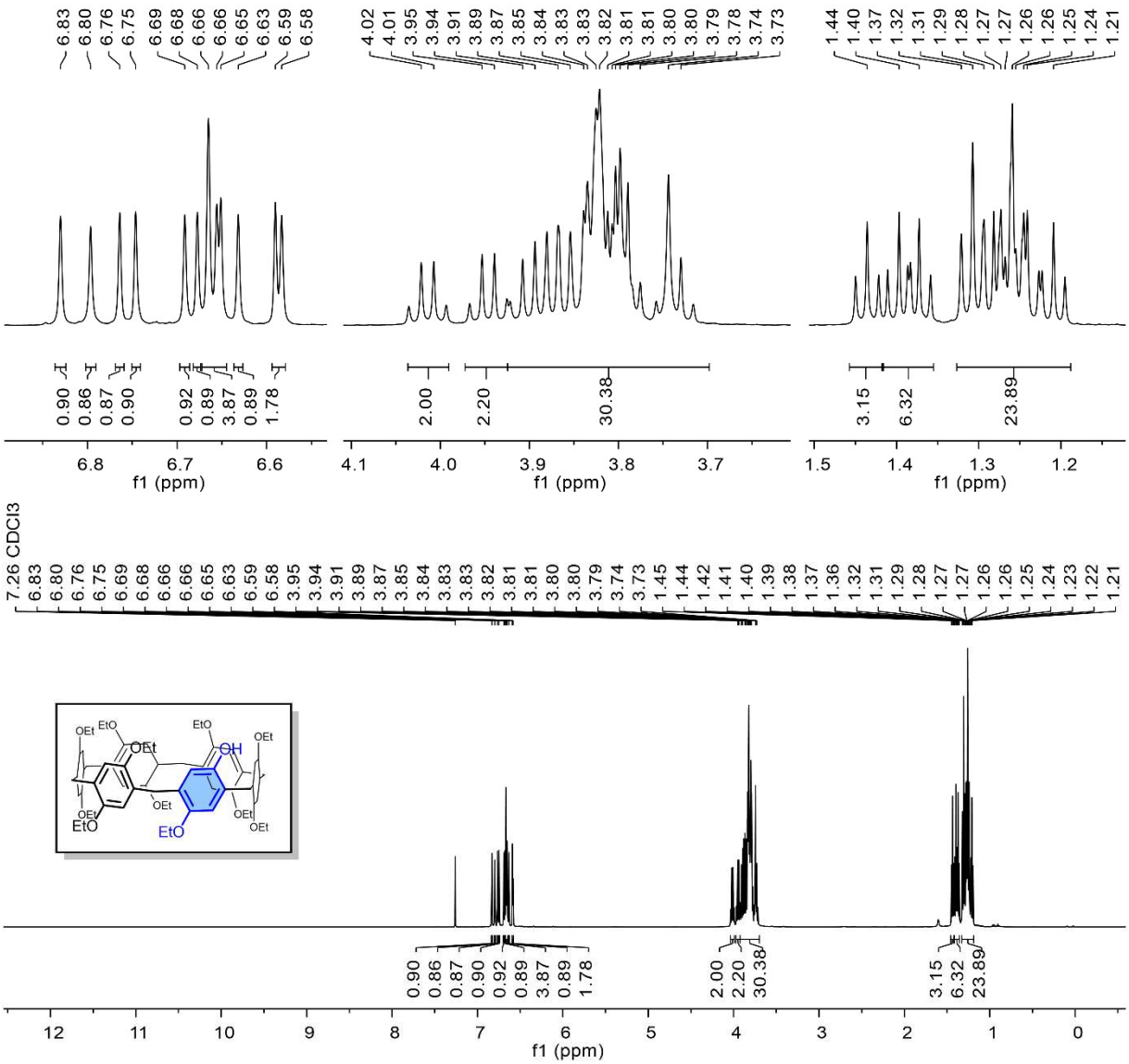

Figure S1: ^{1}H-NMR characterization of **1** (500 MHz, $CDCl_3$, 298 K), expansion in top panel.

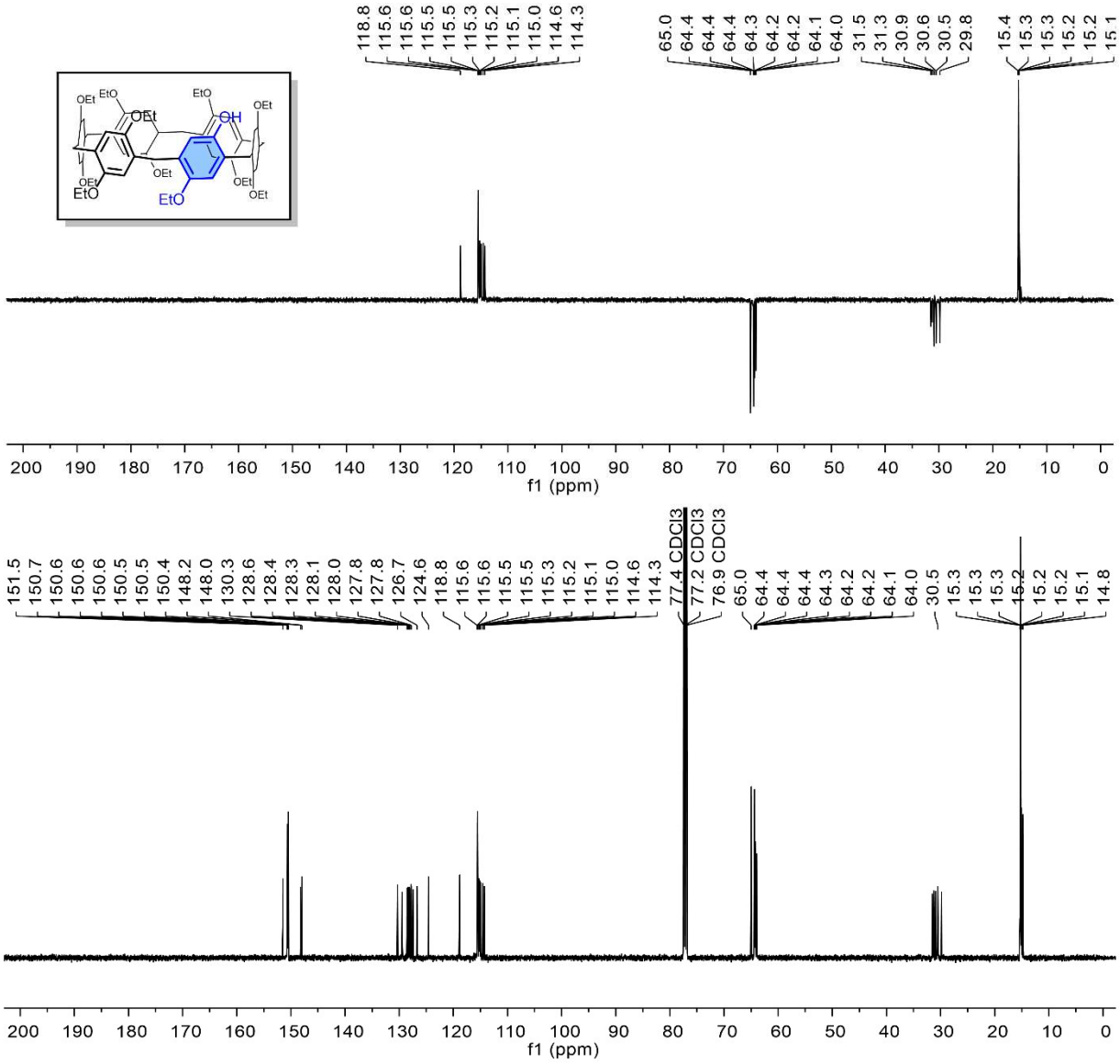

Figure S2: ^{13}C-NMR characterization of **1** (126 MHz, $CDCl_3$, 298 K), DEPT-135 ^{13}C-NMR top panel.

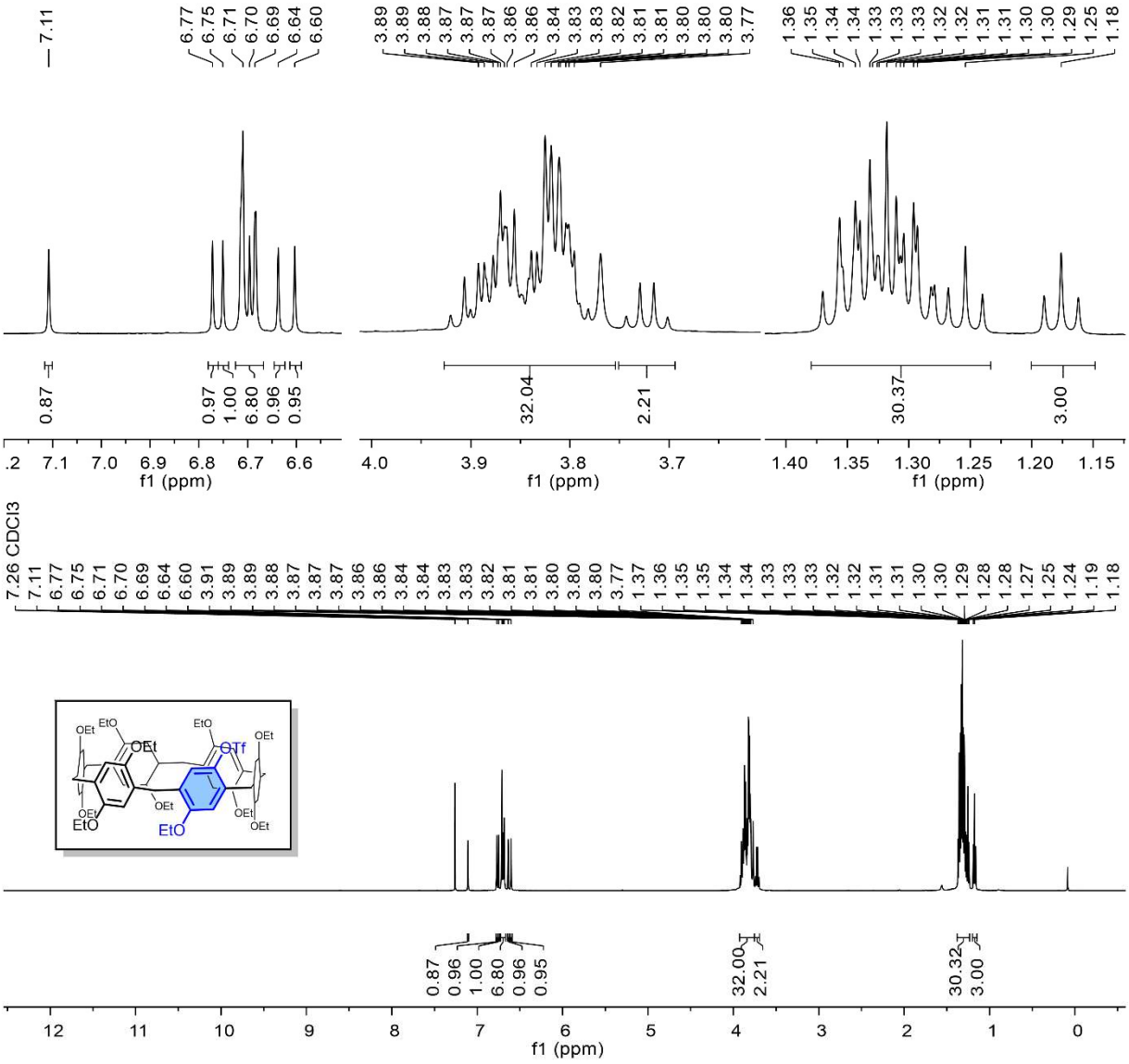

Figure S3: ^{1}H-NMR characterization of **2** (500 MHz, $CDCl_3$, 298 K), expansion in top panel.

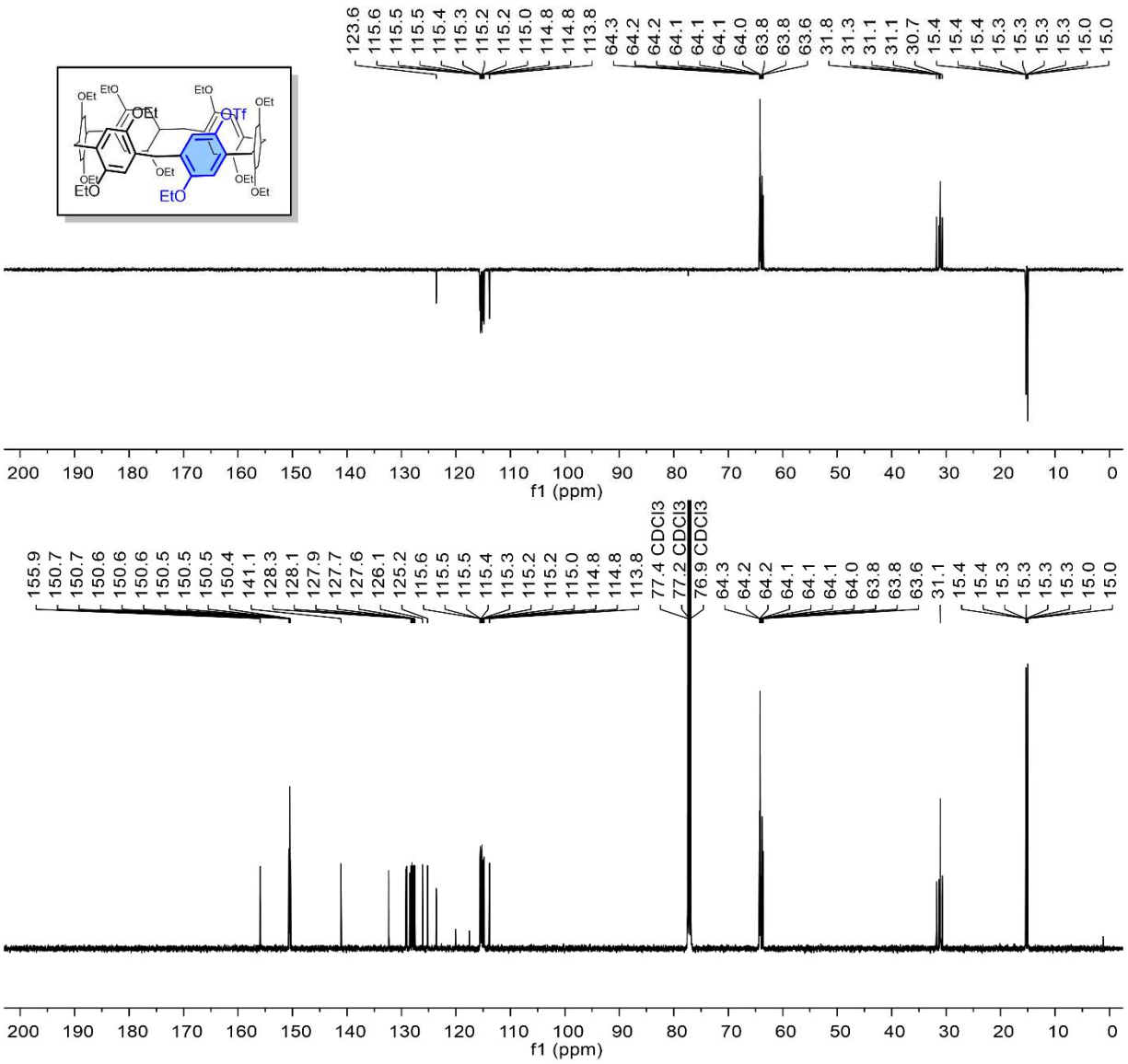

Figure S4: ^{13}C-NMR characterization of **2** (126 MHz, $CDCl_3$, 298 K), DEPT-135 ^{13}C-NMR top panel.

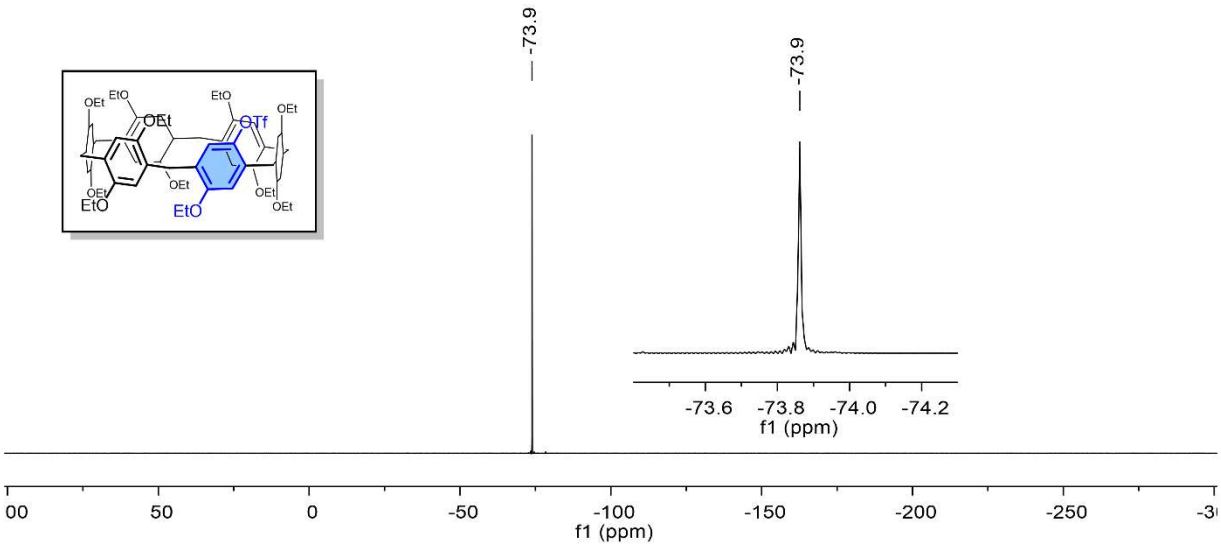

Figure S5: ^{19}F-NMR characterization of **2** (283 MHz, $CDCl_3$, 298 K).

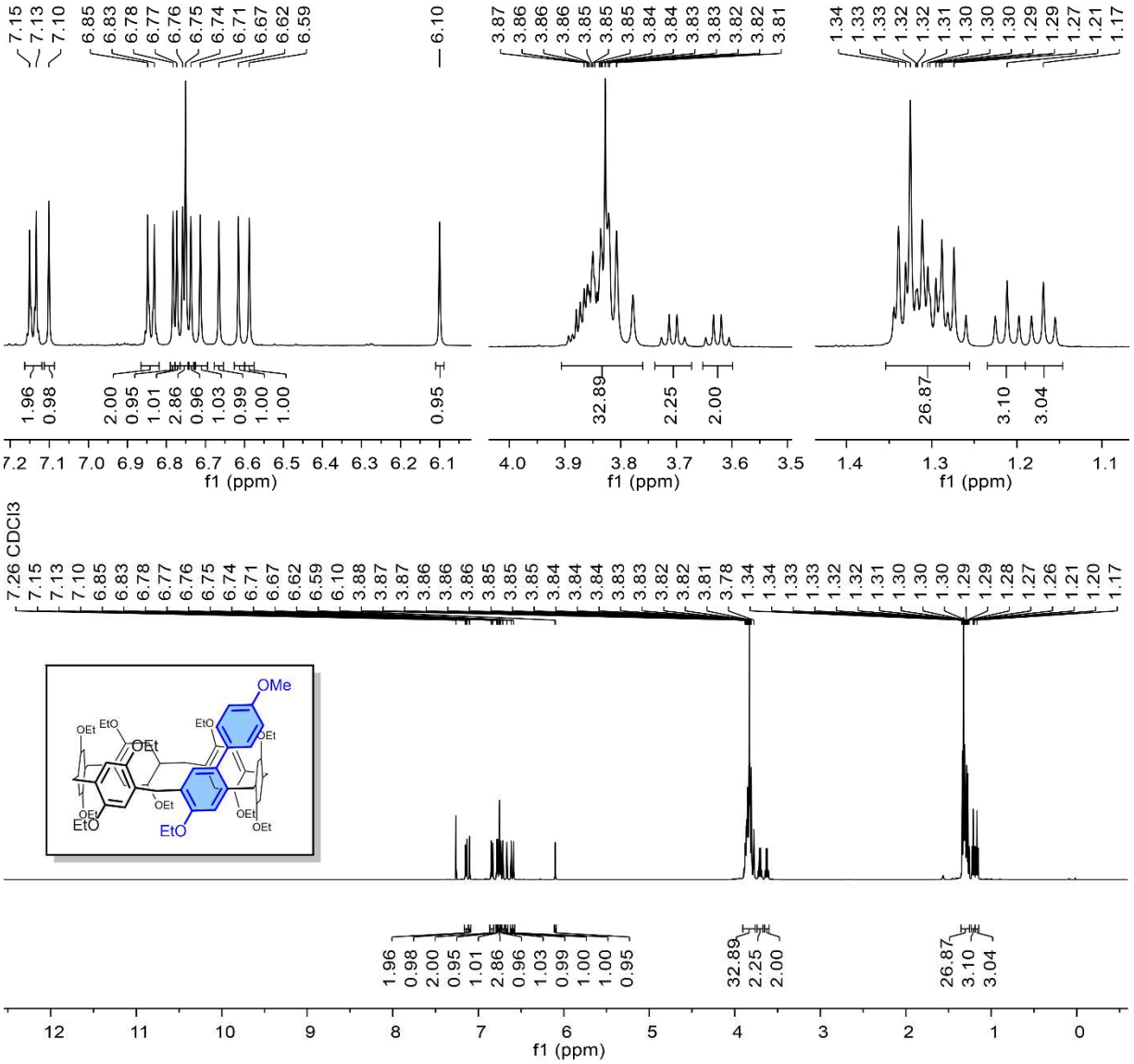

Figure S6: ^{1}H-NMR characterization of **3** (500 MHz, $CDCl_3$, 298 K), expansion in top panel.

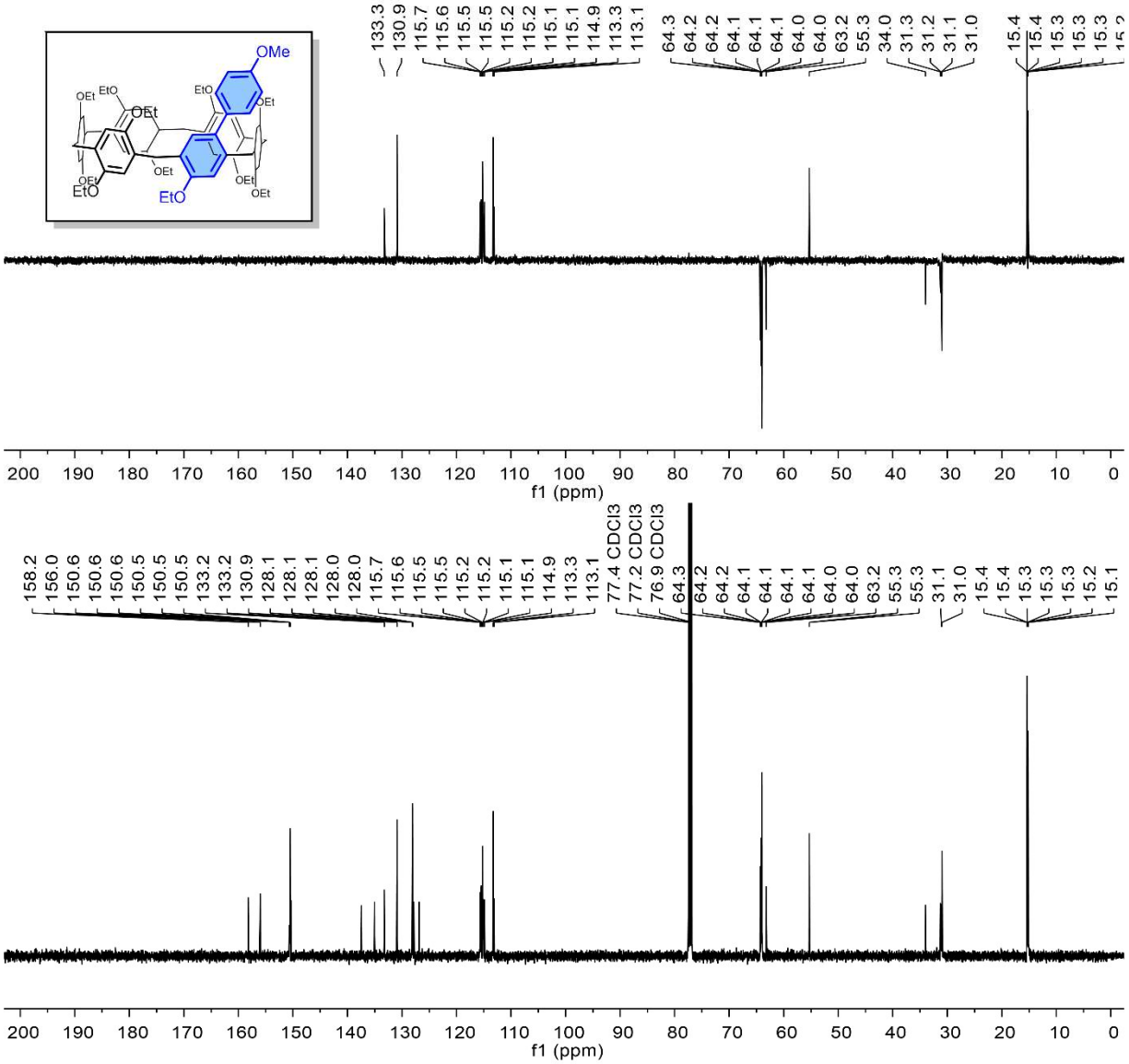

Figure S7: ^{13}C-NMR characterization of **3** (126 MHz, $CDCl_3$, 298 K), DEPT-135 ^{13}C-NMR top panel.

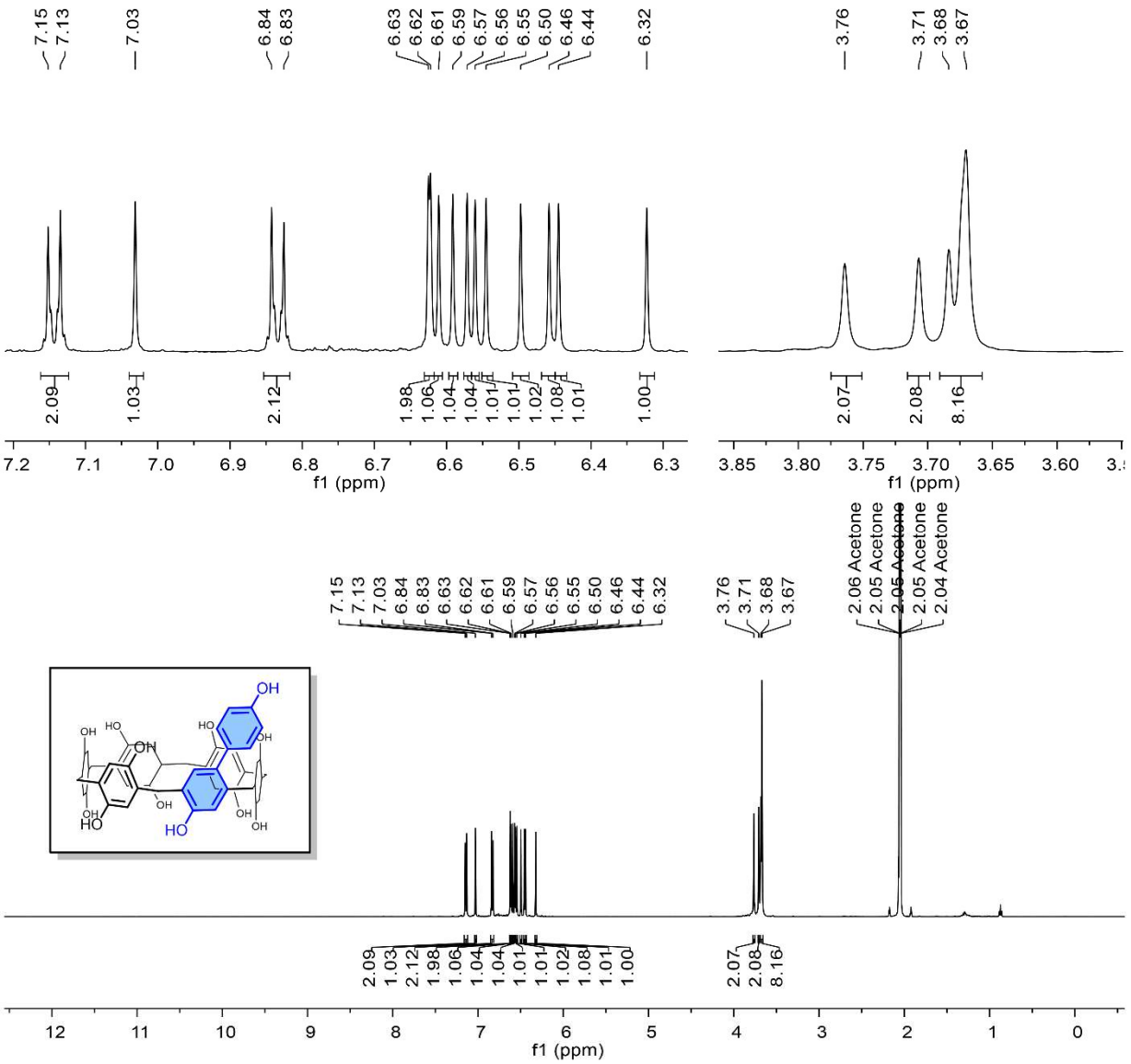

Figure S8: ^{1}H-NMR characterization of **4** (500 MHz, $(CD_3)_2CO$, 298 K), expansion in top panel.

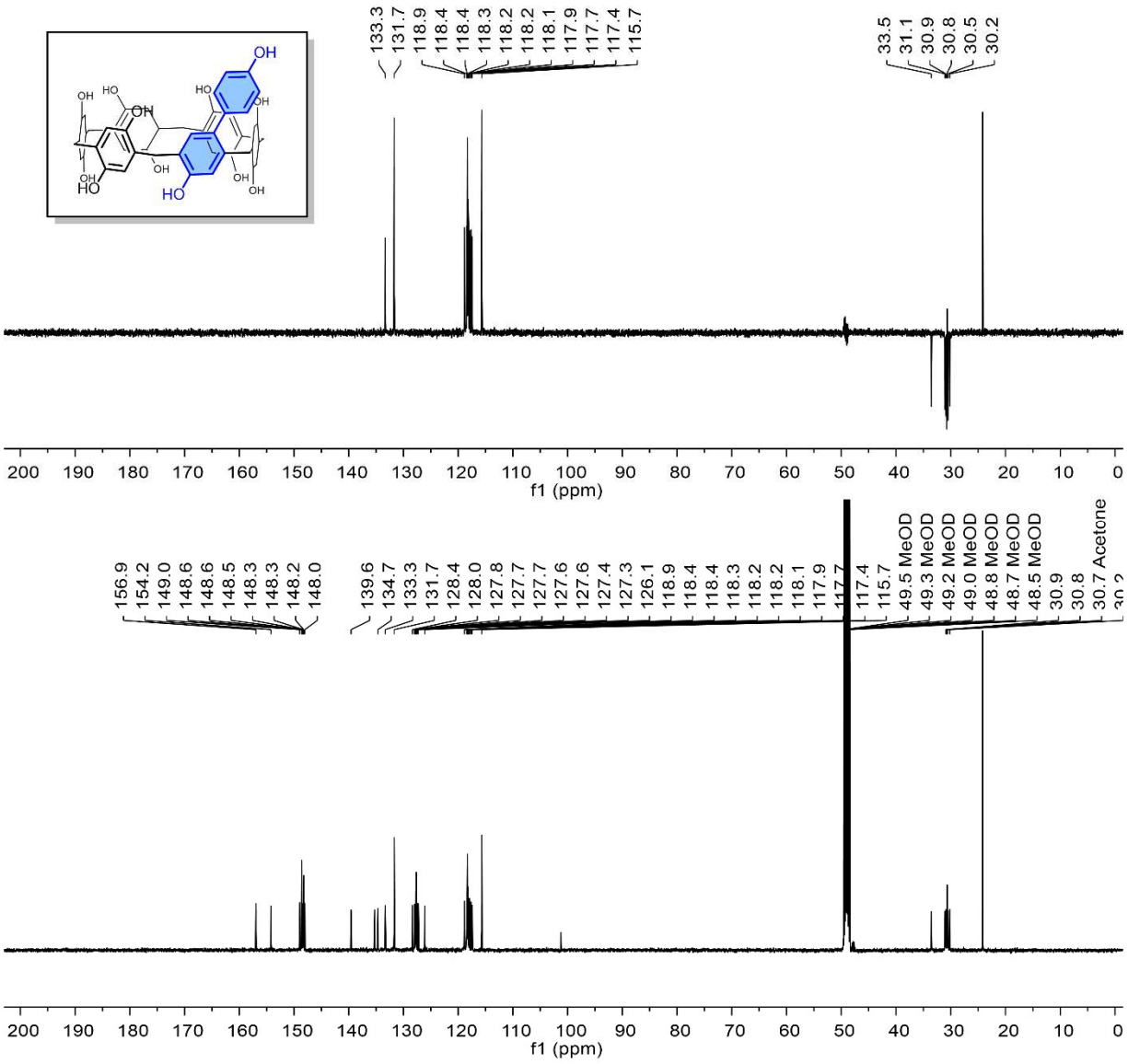

Figure S9: ^{13}C-NMR characterization of **4** (126 MHz, CD_3OD, 298 K), DEPT-135 ^{13}C-NMR top panel.

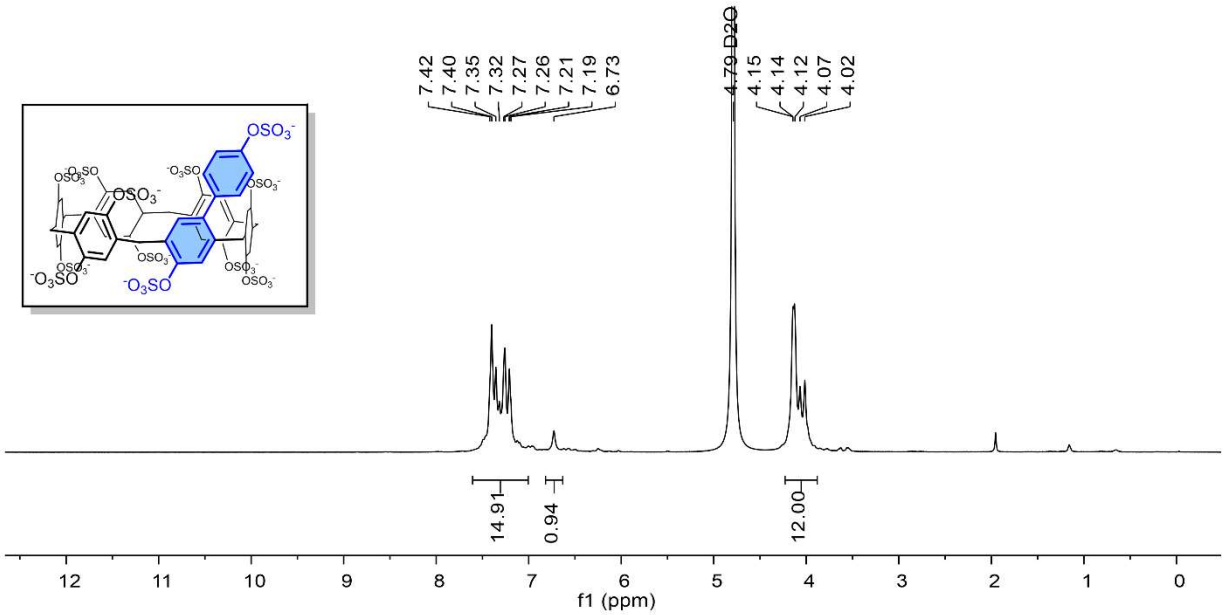

Figure S10: ^{1}H-NMR characterization of **A1sP6** (500 MHz, D_2O, 298 K).

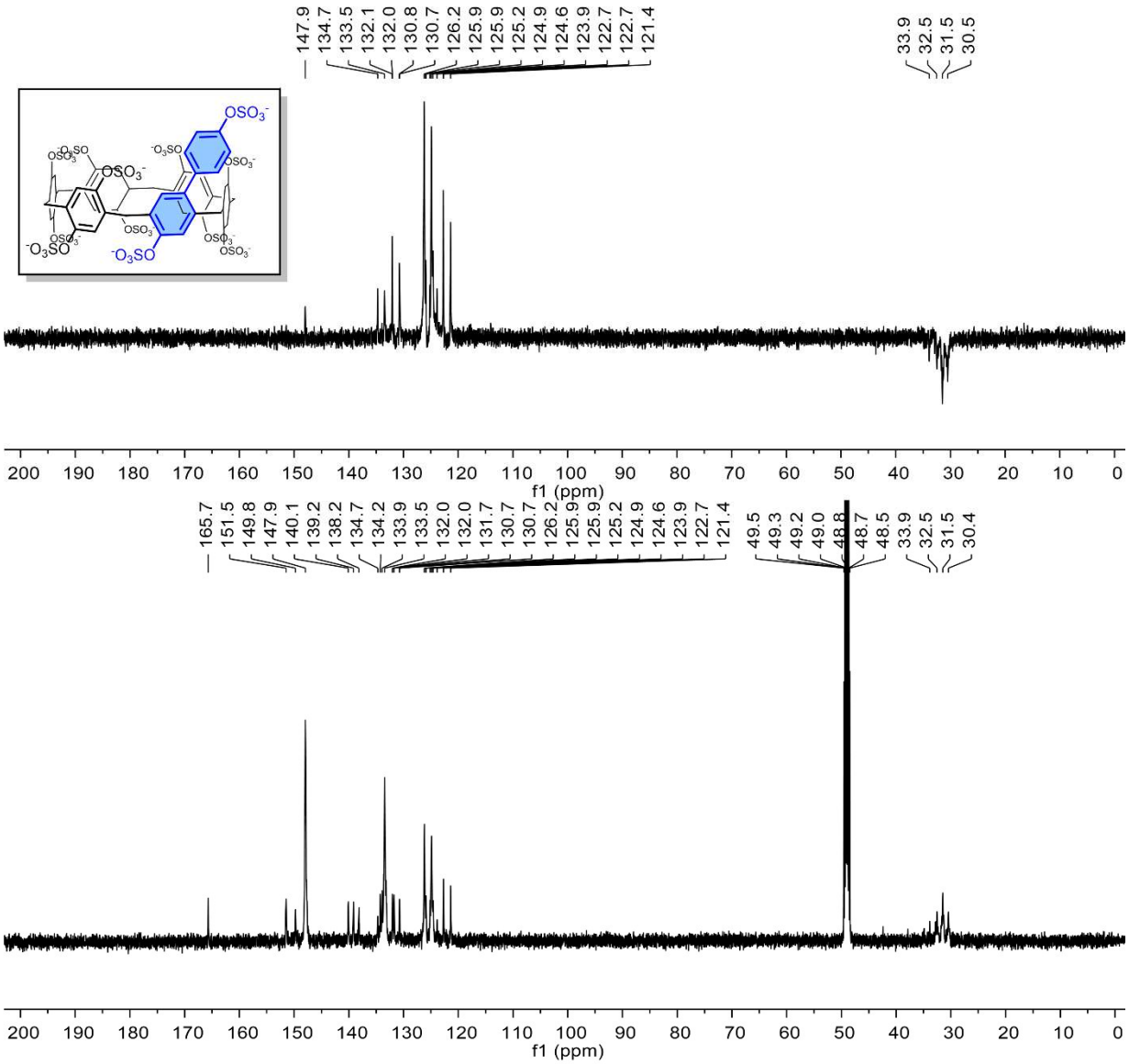

Figure S11: ^{13}C-NMR characterization of **A1sP6** (126 MHz, D_2O/CD_3OD, 298 K), DEPT-135 ^{13}C-NMR top panel.

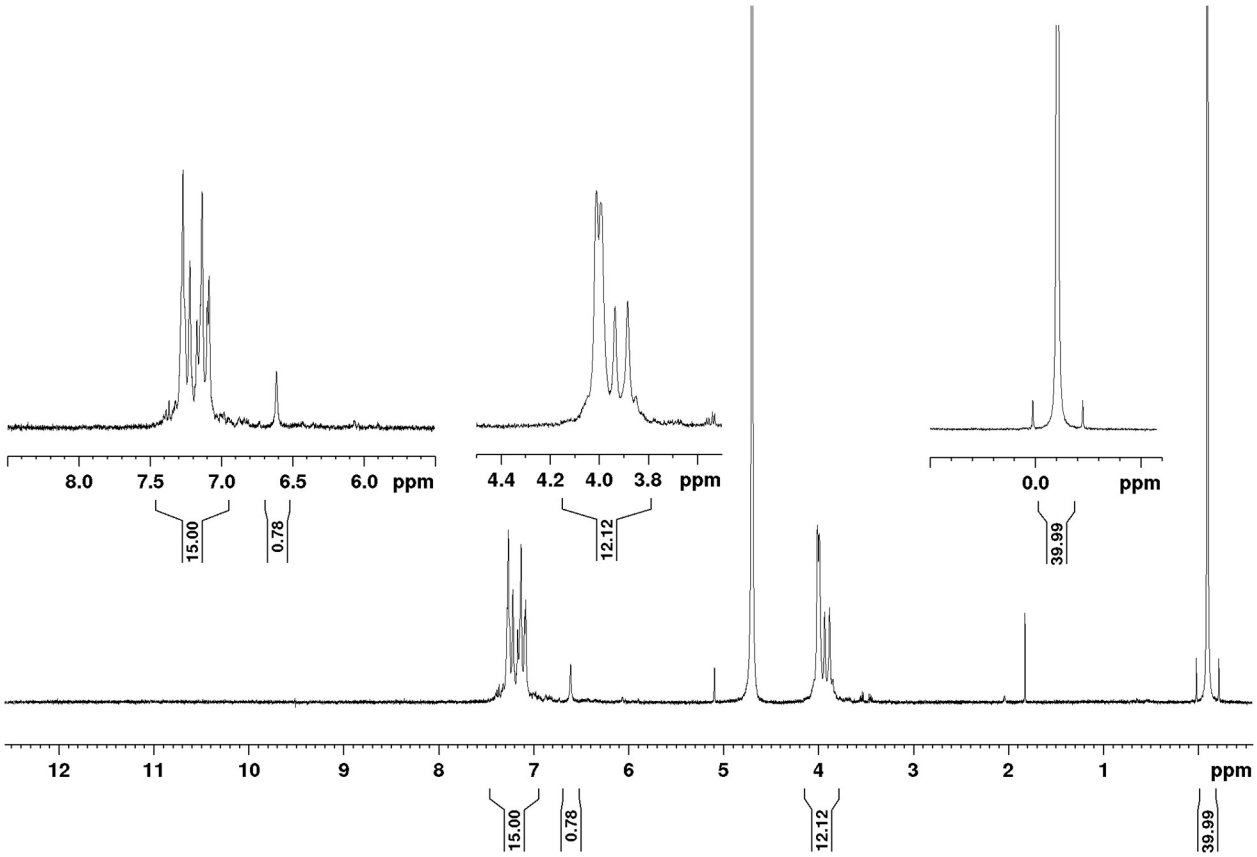

Figure S12: Quantitative NMR characterization of **A1sP6** (500 MHz, D_2O, 298 K). Acquired with 4.9 mg **A1sP6**, 1.3 mg of 2,2,3,3-d(4)-3-(trimethylsilyl)propionic acid sodium salt. Salt content calculated per region; methylene (30%) aromatics (31%), singlet aromatic (46%). Average salt content of **A1sP6** (36%).

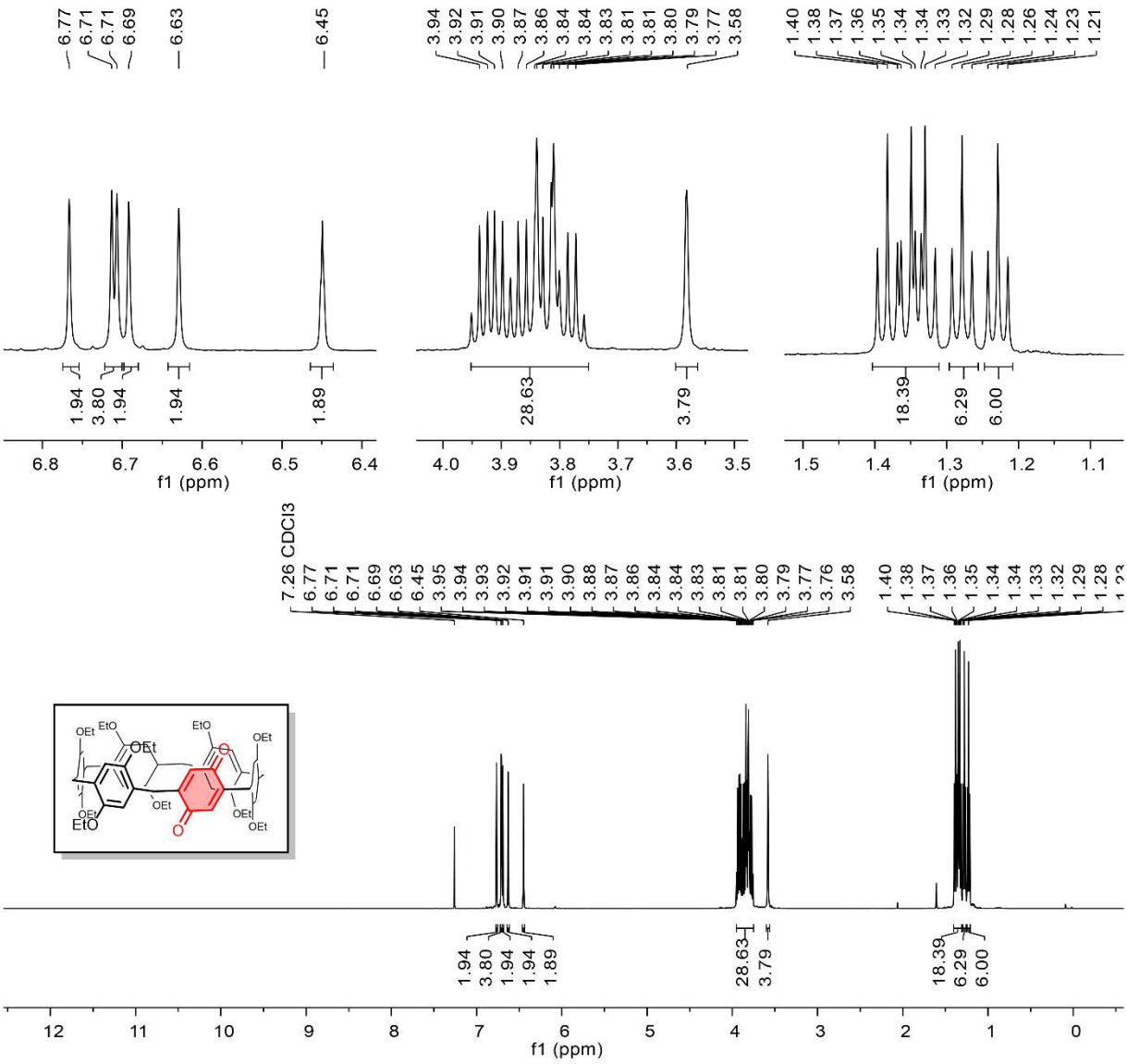

Figure S13: ^{1}H-NMR characterization of **5** (500 MHz, $CDCl_3$, 298 K), expansion in top panel.

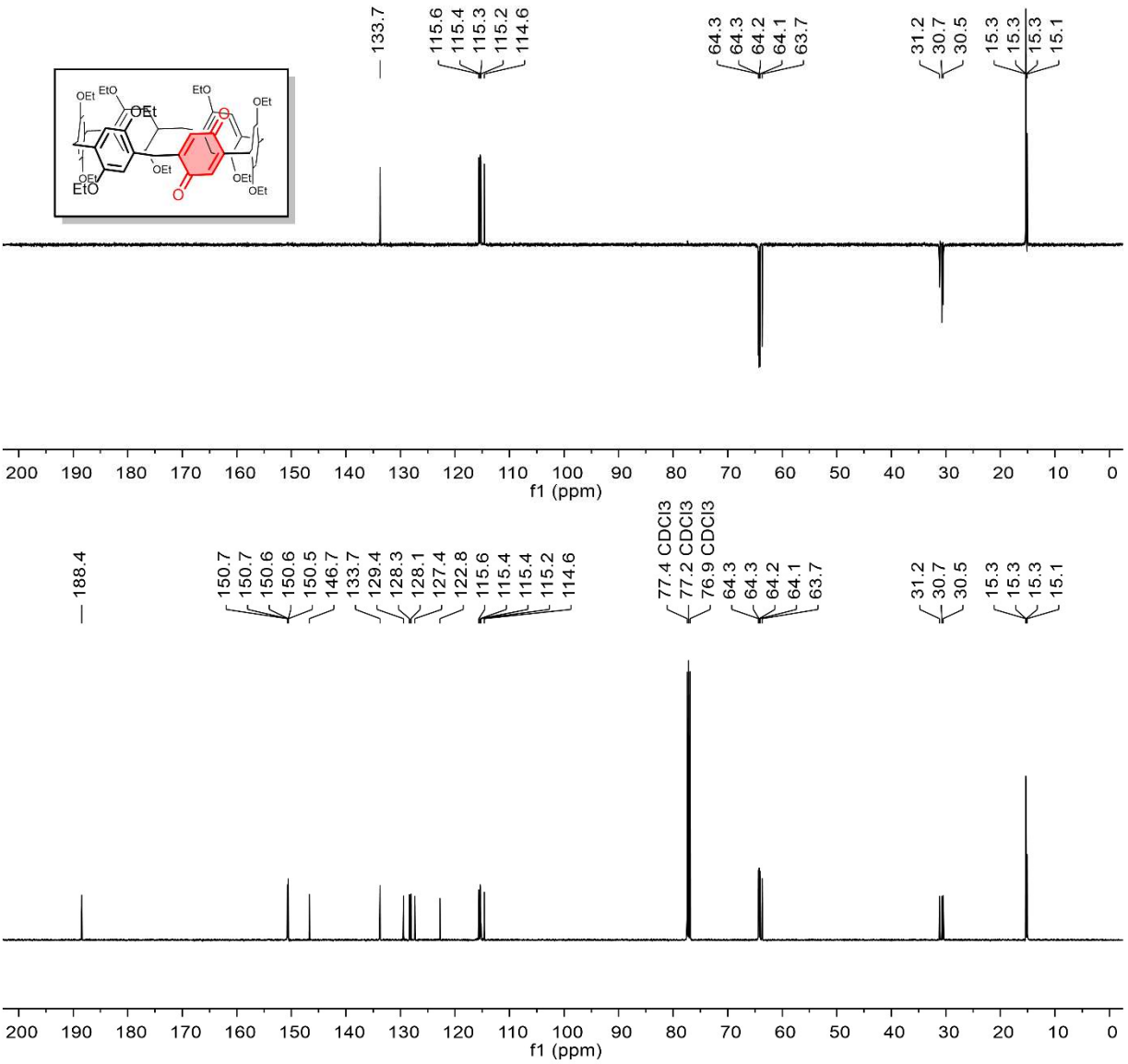

Figure S14: ^{13}C-NMR characterization of **5** (126 MHz, $CDCl_3$, 298 K), DEPT-135 ^{13}C-NMR top panel.

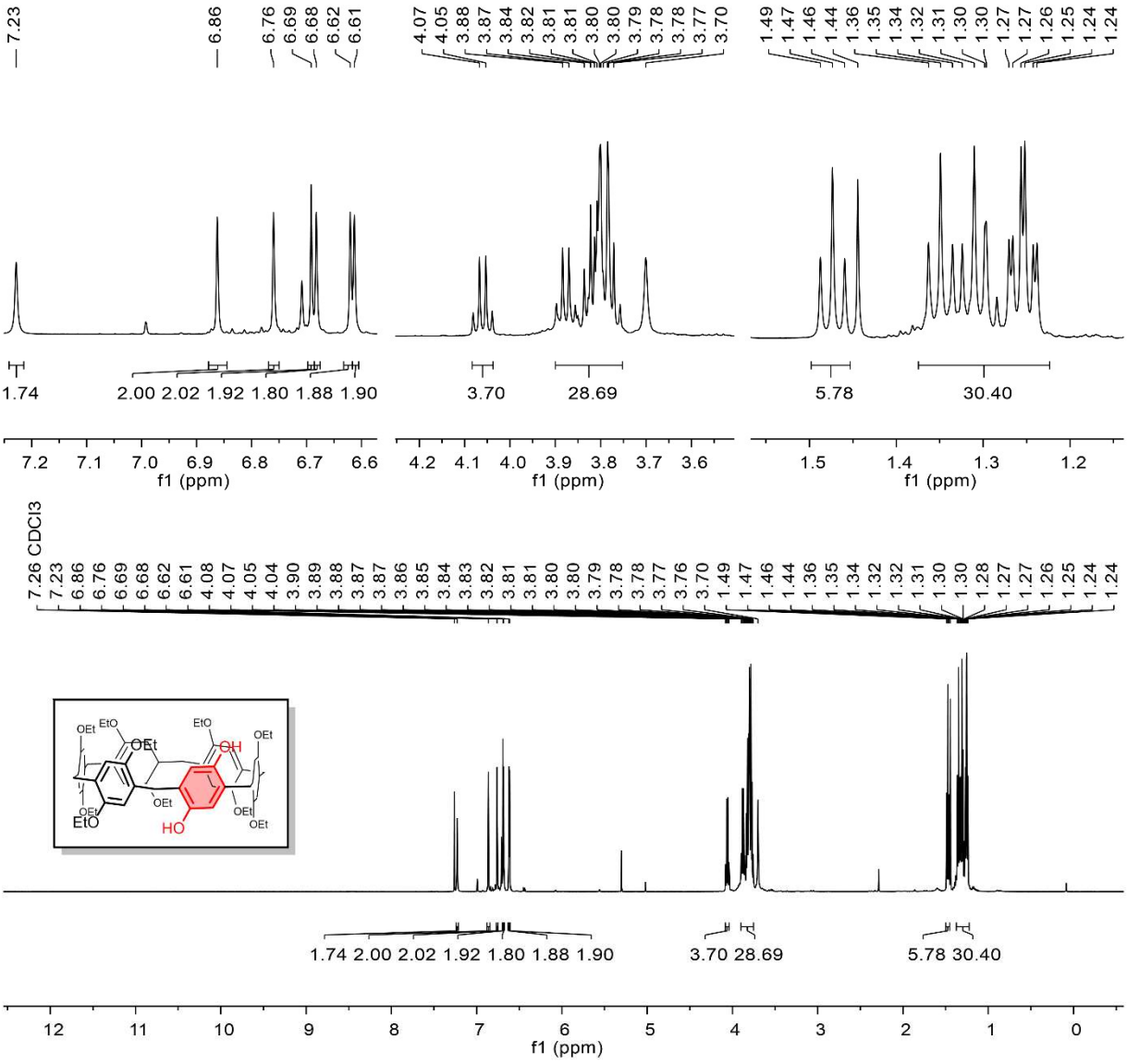

Figure S15: ^{1}H-NMR characterization of **6** (500 MHz, $CDCl_3$, 298 K), expansion in top panel.

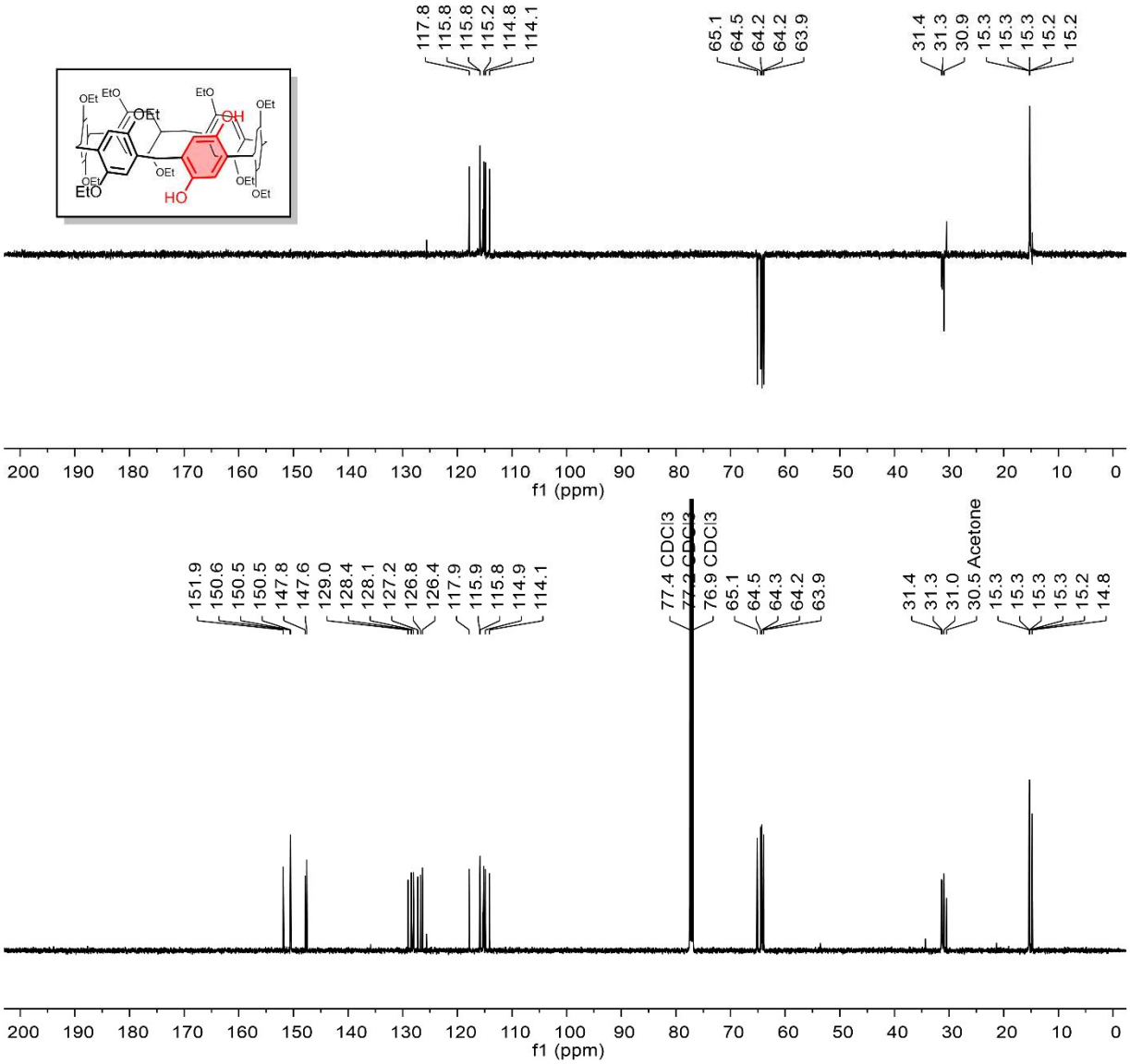

Figure S16: ^{13}C-NMR characterization of **6** (126 MHz, $CDCl_3$, 298 K), DEPT-135 ^{13}C-NMR top panel.

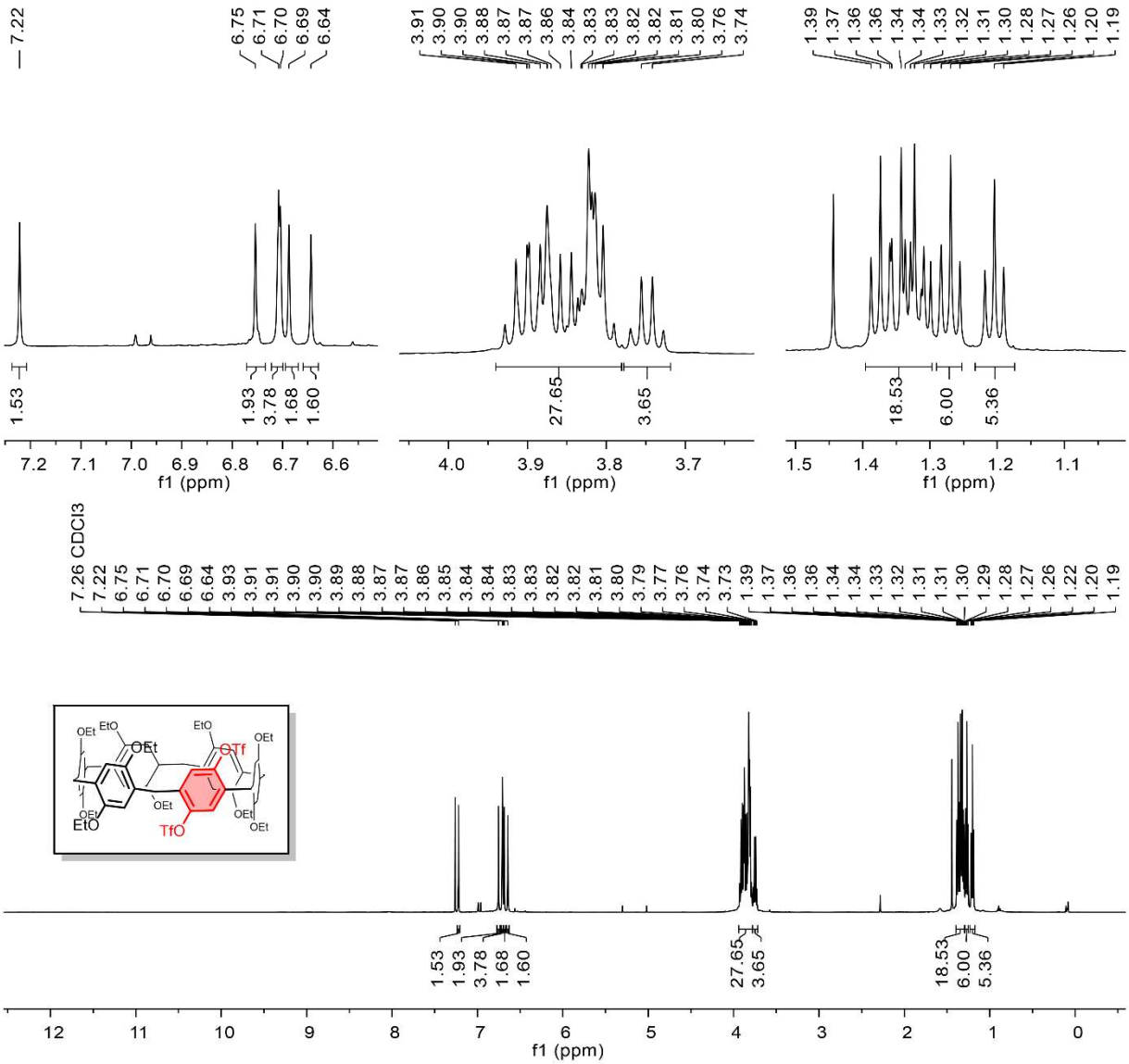

Figure S17: ^{1}H-NMR characterization of **7** (500 MHz, $CDCl_3$, 298 K), expansion in top panel.

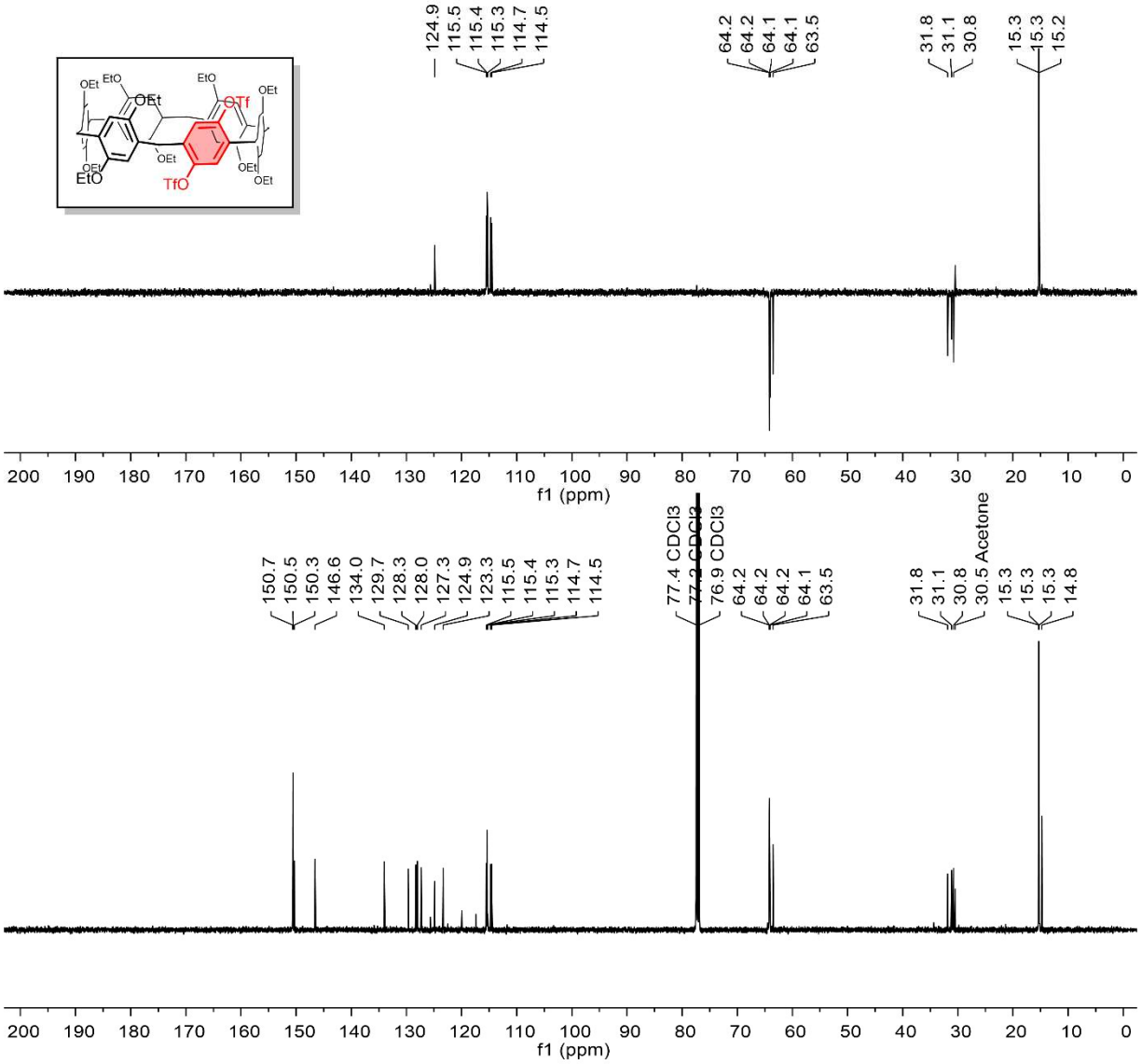

Figure S18: ^{13}C-NMR characterization of **7** (126 MHz, $CDCl_3$, 298 K), DEPT-135 ^{13}C-NMR top panel.

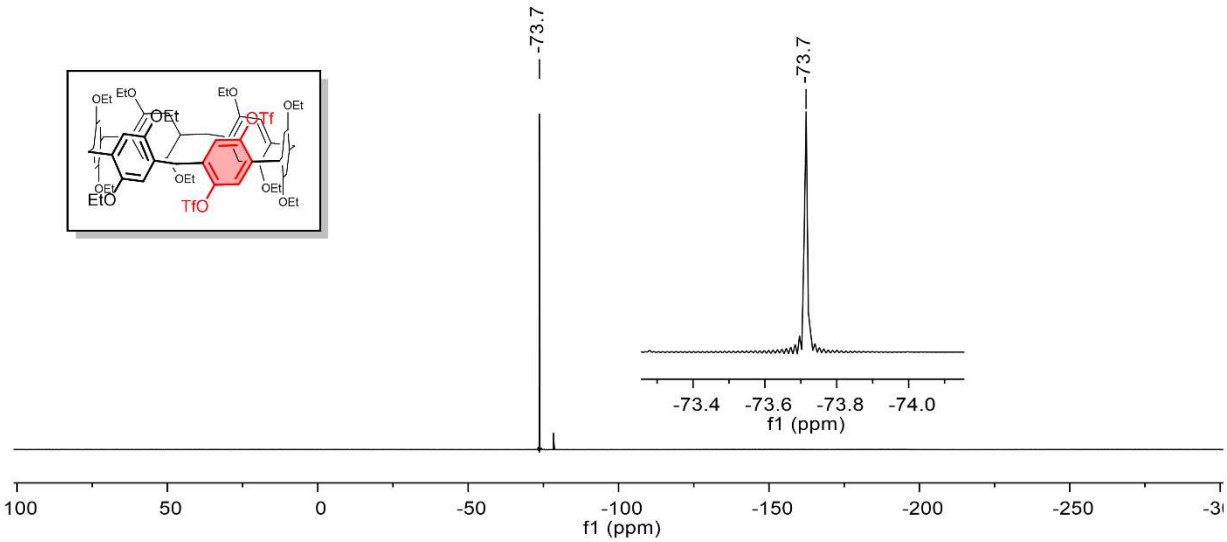

Figure S19: ^{19}F-NMR characterization of **7** (283 MHz, $CDCl_3$, 298 K).

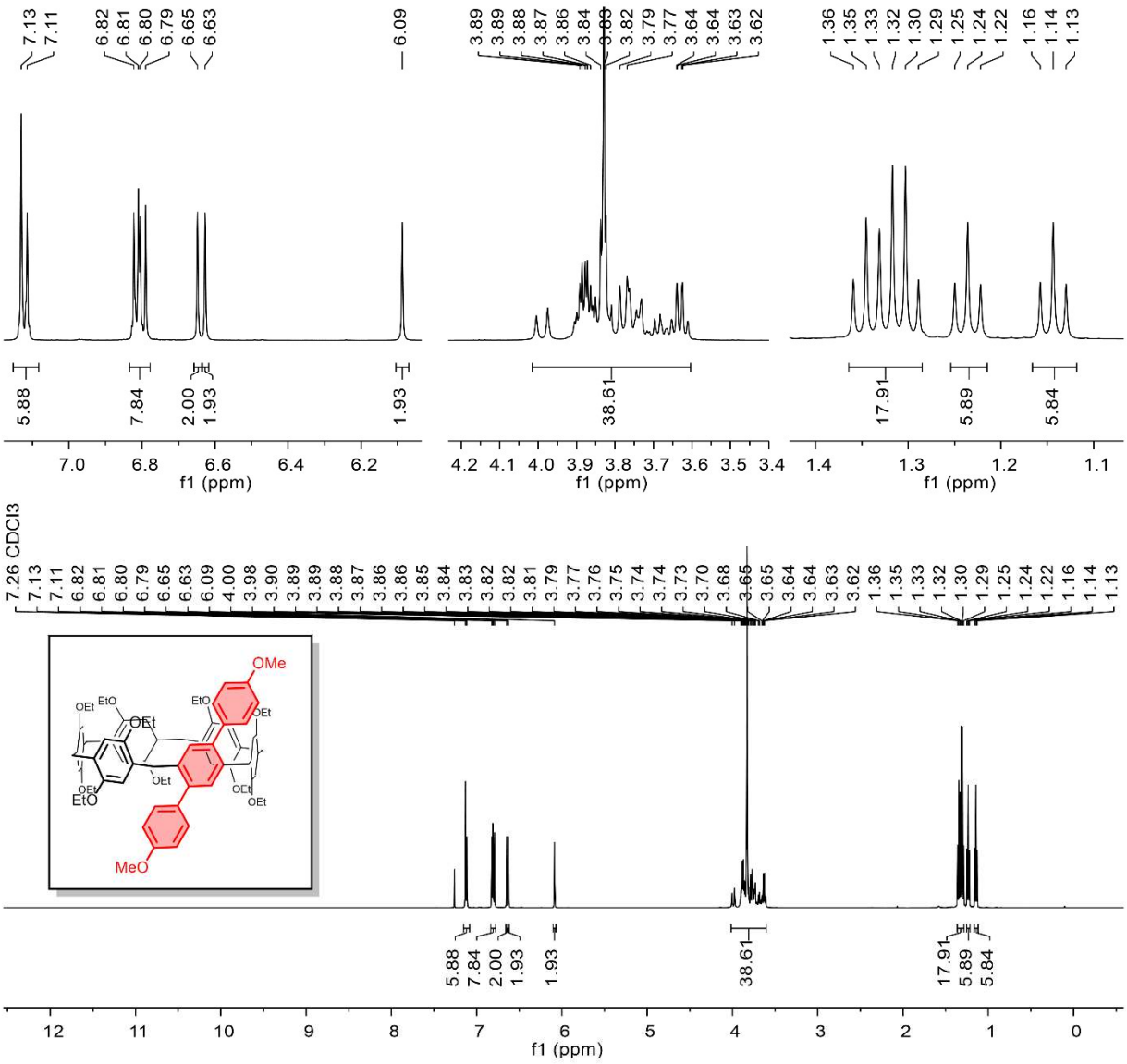

Figure S20: ^{1}H-NMR characterization of **8** (500 MHz, $CDCl_3$, 298 K), expansion in top panel.

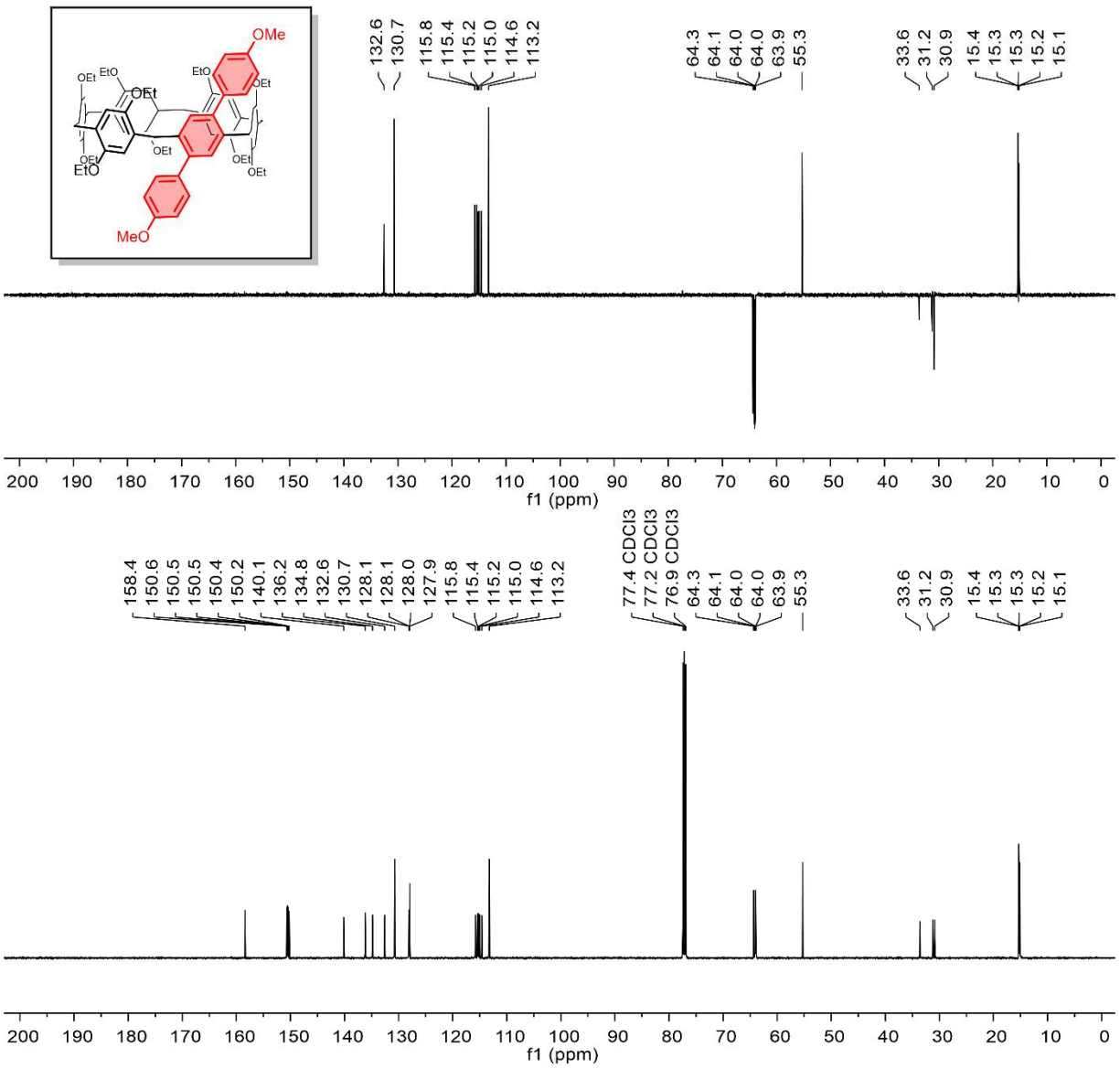

Figure S21: ^{13}C-NMR characterization of **8** (126 MHz, $CDCl_3$, 298 K), DEPT-135 ^{13}C-NMR top panel.

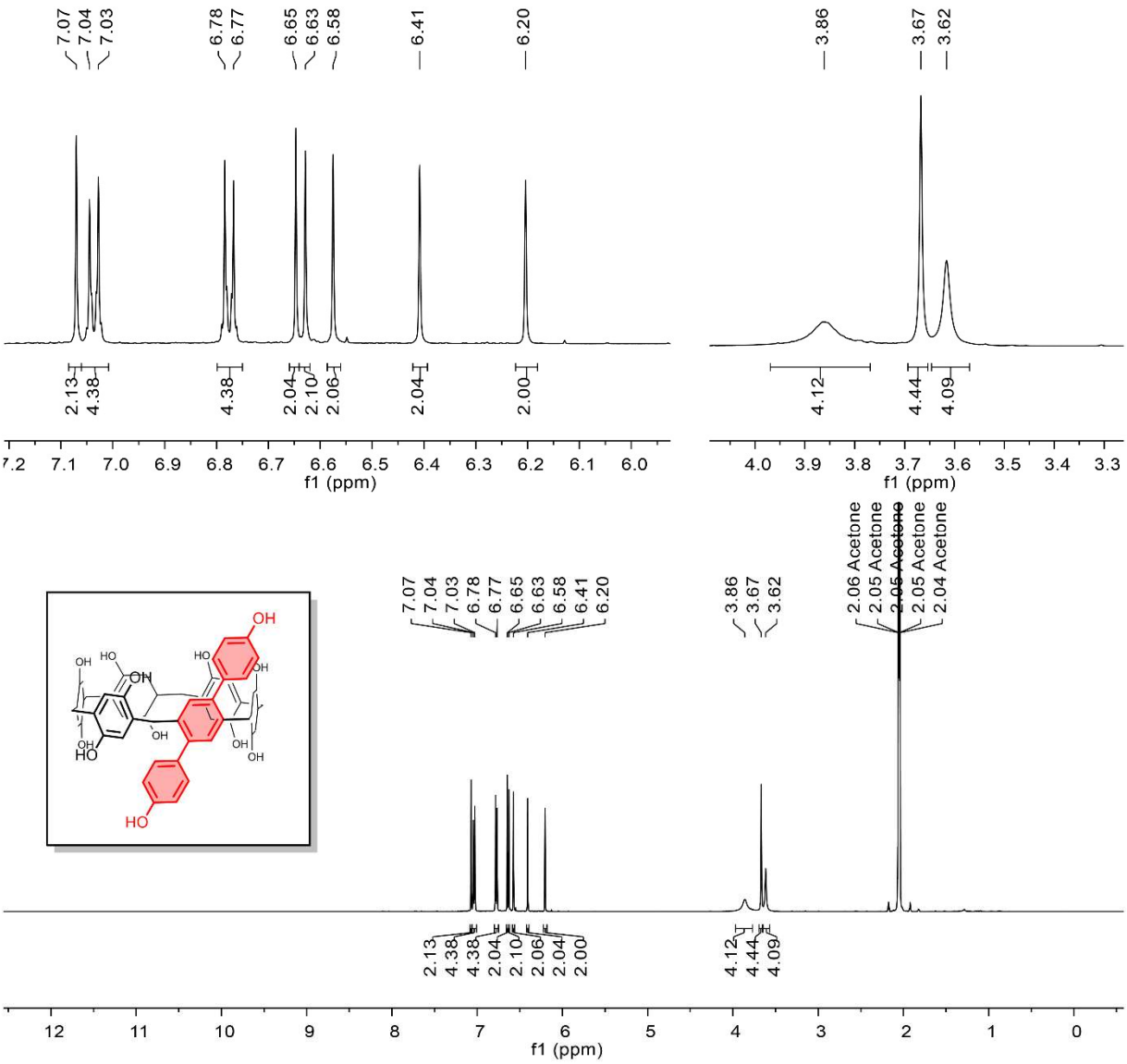

Figure S22: ^{1}H-NMR characterization of **9** (500 MHz, $(CD_3)_2CO$, 298 K), expansion in top panel.

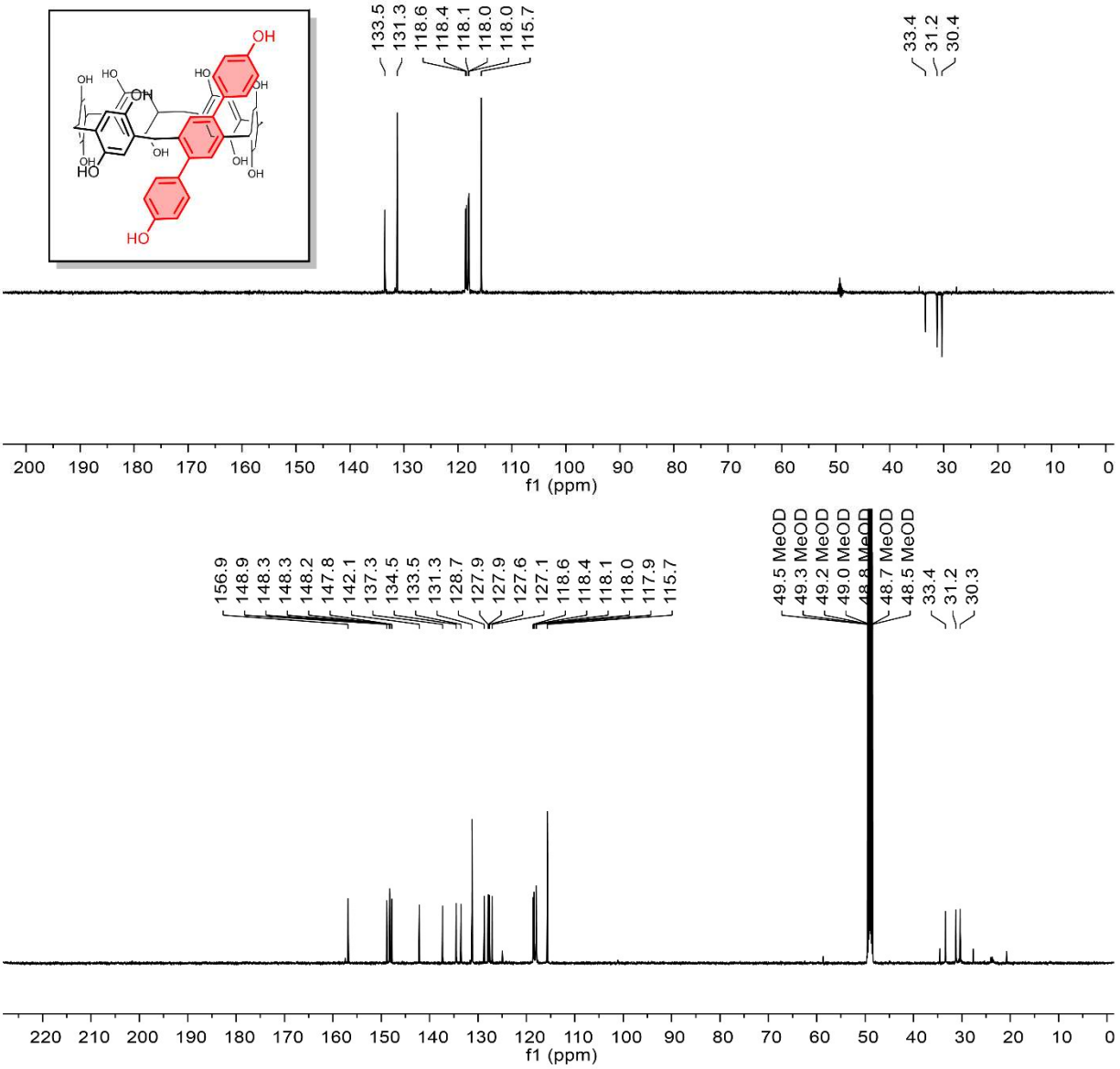

Figure S23: ^{13}C-NMR characterization of **9** (126 MHz, CD_3OD, 298 K), DEPT-135 ^{13}C-NMR top panel.

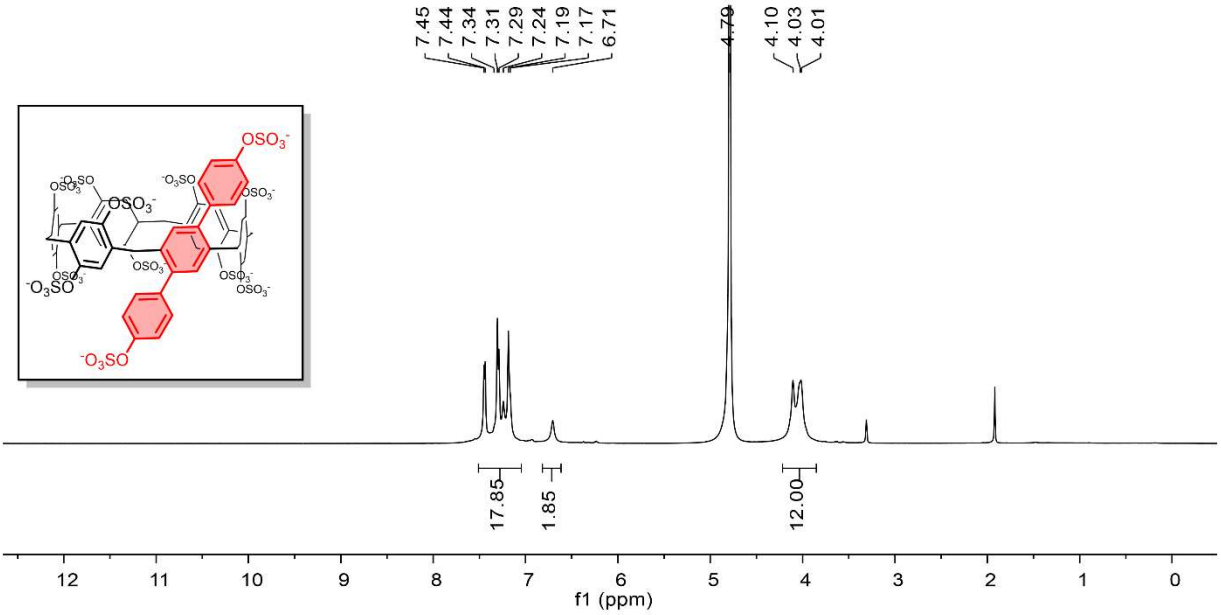

Figure S24: ^{1}H-NMR characterization of **A1A2sP6** (500 MHz, D_2O, 298 K).

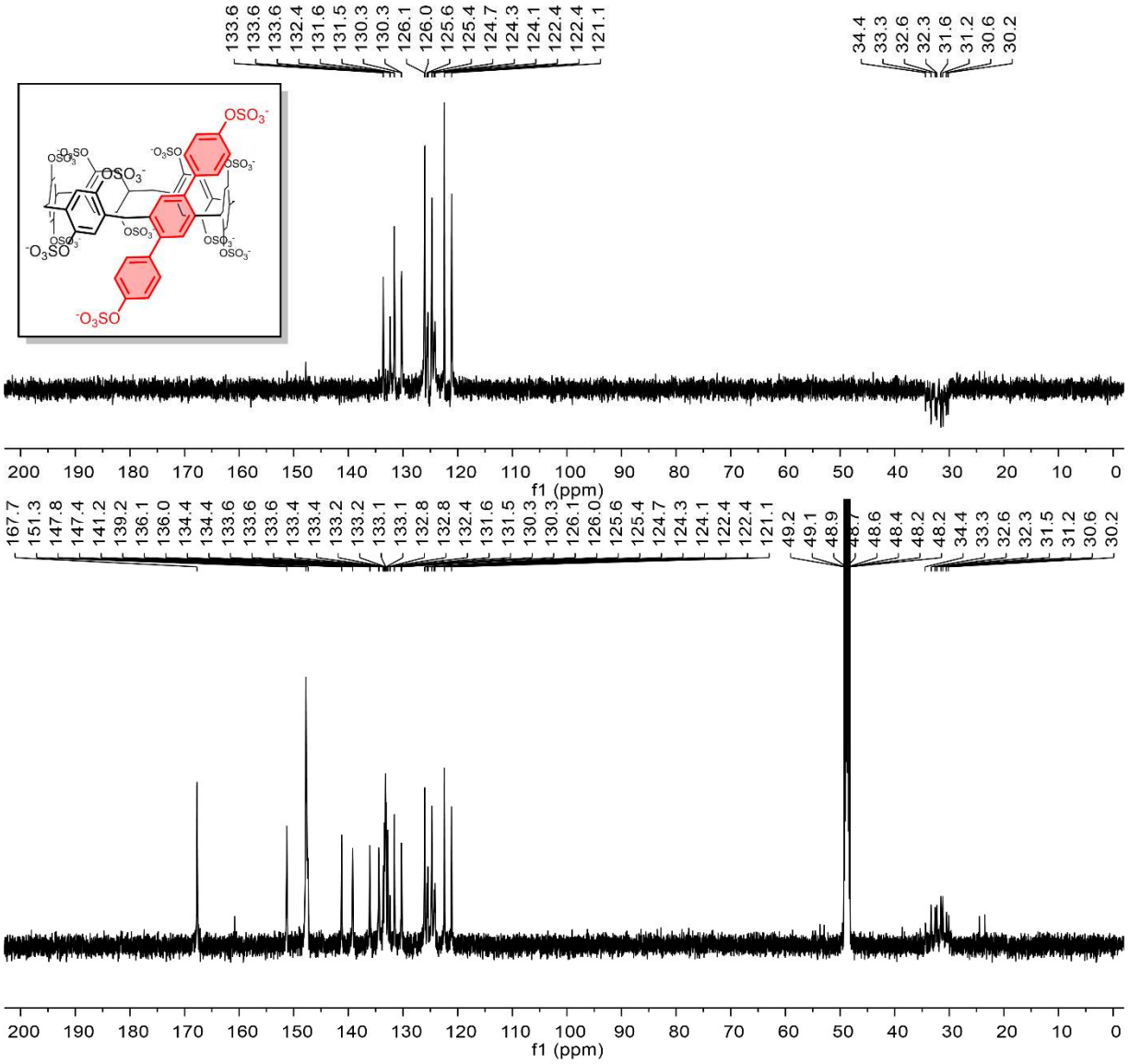

Figure S25: ^{13}C-NMR characterization of **A1A2sP6** (126 MHz, D_2O/CD_3OD, 298 K), DEPT-135 ^{13}C-NMR top panel.

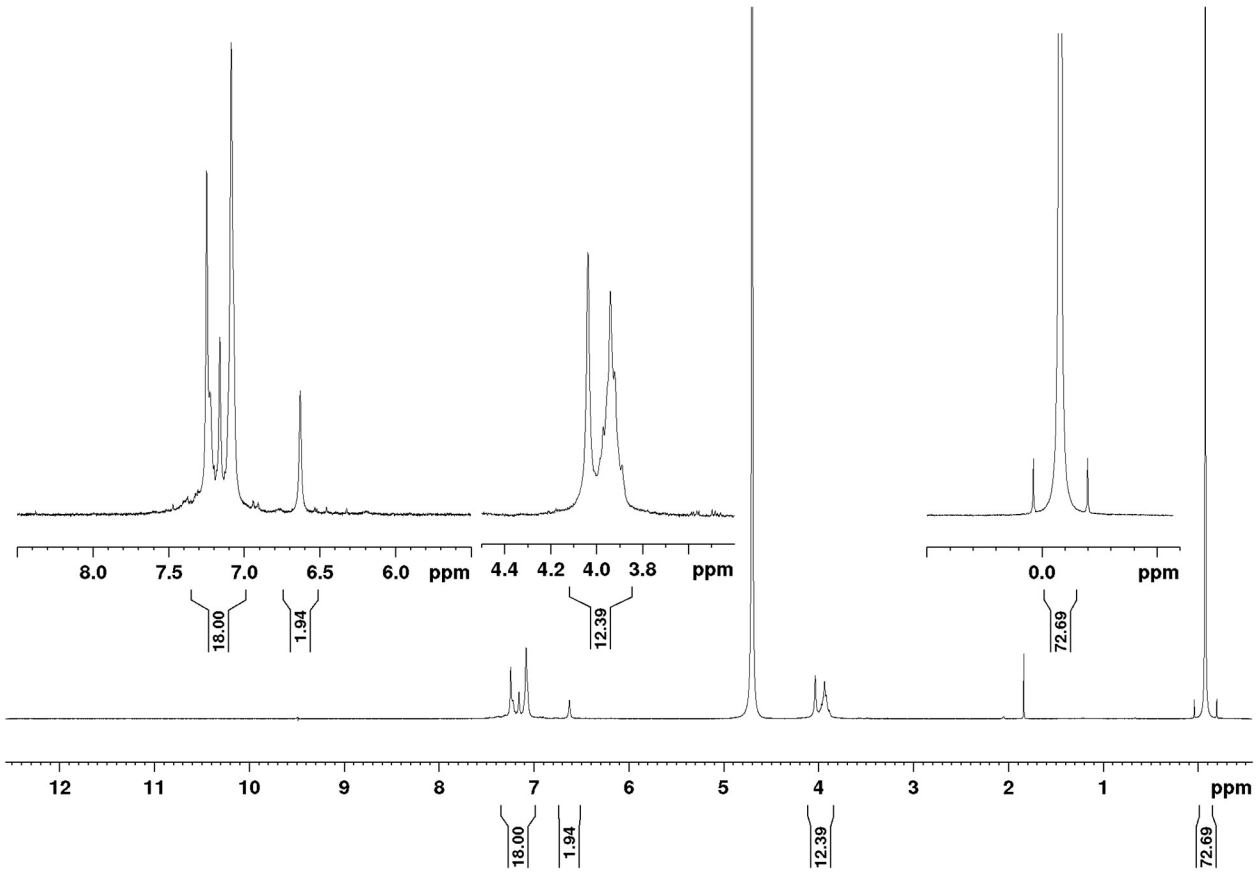

Figure S26: Quantitative NMR characterization of **A1A2sP6** (500 MHz, D_2O, 298 K). Acquired with 3.8 mg **A1A2sP6**, 1.3 mg of 2,2,3,3-d(4)-3-(trimethylsilyl)propionic acid sodium salt. Salt content calculated per region; methylene (48%) aromatics (49%), singlet aromatic (51%). Average salt content of **A1A2sP6** (49%).

2. Crystallography

2.1 General remarks

X-Ray quality crystals of **8** were obtained by slow evaporation. **8** was dissolved in $CDCl_3$ and a drop was added to ~ 1 mL of acetonitrile. The solution was left to evaporate and **8** crystallized as colorless block-like crystals. There are two molecules of the cyclododecaphane in the unit cell of the primitive, centrosymmetric, triclinic space group P-1. The structure of the hexa-benzocyclododecaphane is as expected (see Figure S27-28). The interior of the ring system is occupied by four pendant ethoxy and one pendant. methoxybenzene ring. One pair of ethoxy groups (bonded to ring C8-C13) is excluded from this orientation. The interior methoxy benzene ring (O1, C43-C49) is oriented to form a pi-stacking interaction with dodecaphane benzene ring C36-C41. Bond distances and angles within the molecule are as expected.

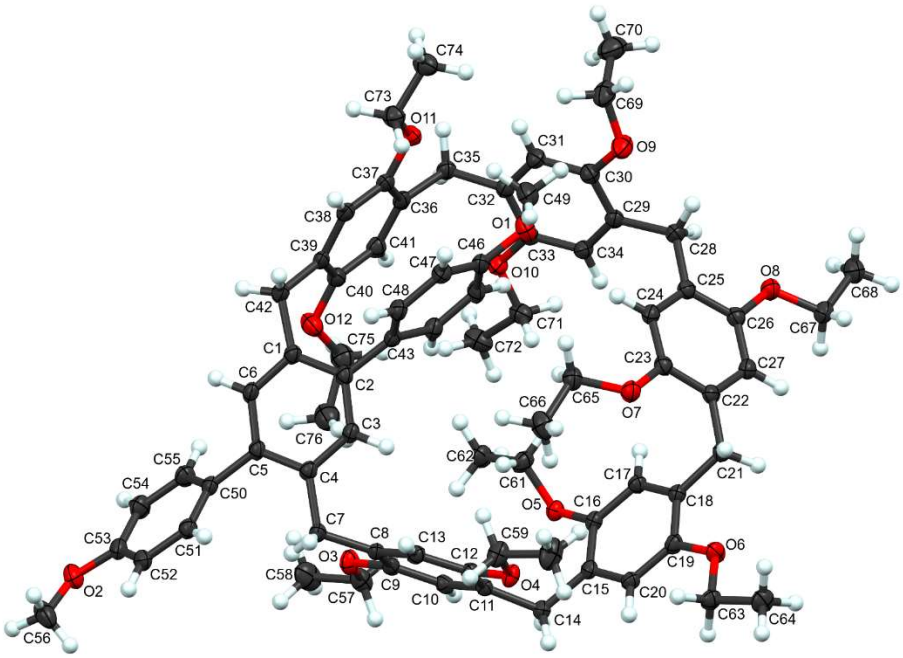

Figure S27: Thermal ellipsoid representation of crystal structure of compound **8**.

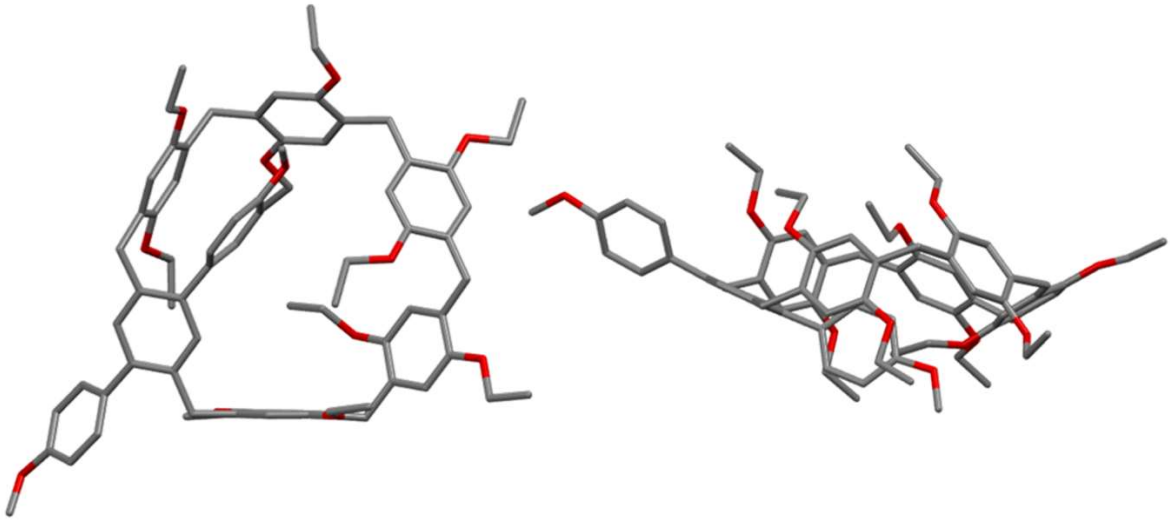

Figure S28: Wireframe representation of crystal structure of **8**.

2.2 Crystal Summary

An arbitrary sphere of data was collected on a colourless block-like crystal, having approximate dimensions of 0.177 × 0.119 × 0.106 mm, on a Bruker Venture diffractometer equipped with a Bruker PHOTON-III detector using a combination of ω- and φ-scans of 0.5°[7]. Data were corrected for absorption and polarization effects and analyzed for space group determination.[8] The structure was solved by dual-space methods and expanded routinely.[9] The model was refined by full-matrix least-squares analysis of F^2 against all reflections.[10] All non-hydrogen atoms were refined with anisotropic atomic displacement parameters. Unless otherwise noted, hydrogen atoms were included in calculated positions. Atomic displacement parameters for the hydrogens were tied to the equivalent isotropic displacement parameter of the atom to which they are bonded (U_{iso}(H) = 1.5U_{eq}(C) for methyl, 1.2U_{eq}(C) for all others).

Table 1. Crystal data and structure refinement for **8** (cwfh2301).

Identification code	cwfh2301
Empirical formula	$C_{76}H_{88}O_{12}$
Formula weight	1193.46
Temperature (K)	120(2)
Wavelength (Å)	1.54178
Crystal system	Triclinic
Space group	P-1
Unit cell dimensions	
a (Å)	11.2087(6)
b (Å)	12.9135(7)
c (Å)	23.4378(13)
α (°)	76.152(2)
β (°)	76.271(2)
γ (°)	84.017(3)
Volume (Å^3)	3195.7(3)
Z	2
Density (calculated, g.cm^{-3})	1.240
Absorption coefficient (μ, mm^{-1})	0.660
F(000)	1280
Crystal color, habit	colourless, block
Crystal size (mm^3)	0.177 × 0.119 × 0.106
θ range for data collection (°)	3.529 to 72.576
Index ranges	-13 ≤ h ≤ 13, -15 ≤ k ≤ 15, -28 ≤ l ≤ 28
Reflections collected	139083
Independent reflections	12606 [R_{int} = 0.0423]
Completeness to θ = 67.679°	99.9 %
Absorption correction	Numerical
Max. and min. transmission	0.8593 and 0.7683
Refinement method	Full-matrix least-squares on F^2
Data / restraints / parameters	12606 / 0 / 805
Goodness-of-fit on F^2	1.033
Final R indices [I>2σ(I)]	R_1 = 0.0411, wR_2 = 0.1089
R indices (all data)	R_1 = 0.0450, wR_2 = 0.1126
Extinction coefficient	n/a
Largest diff. peak and hole (e$^-$.Å^{-3})	0.606 and -0.348

3. Fluorescence experiments

3.1 General remarks for fluorescence experiments. All assays were performed in a Thermo Scientific™ Nunc MicroWell 96-Well Optical-Bottom, black-walled Plate (265031). Plates were read on a BioTek Cytation-5 cell imaging and multi-mode reader plate reader, plates were top-read with a read height of 7 mm. All solutions were made using Milli-Q® ultrapure water, 10 mM PBS buffer (137 mM NaCl, 2.7 mM KCl, 10 mM Na_2HPO_4, 1.8 mM KH_2PO_4) or 10 mM CBS buffer (137 mM NaCl, 2.7 mM KCl, 0.94 mM Sodium citrate dihydrate, 9.06 mM Citric acid). 4′,6-diamidino-2-phenylindole dihydrochloride (DAPI) was purchased from Sigma-Aldrich (D9542, ≥98%). Apixaban (A726700, 98%), betrixaban (B329500, 97%), dabigatran (D100090, 95%), edoxaban (E555520, 98%) and rivaroxaban (R538000, 98%) were purchased from Toronto Research Chemical. To aid in solubility DMSO (up to 2.5%) was added in the competitive titrations with betrixaban, edoxaban and apixaban.

3.2 Emission and excitation change of DAPI in the presence of host.

The emission and excitation of DAPI in the presence and absence of sulfo-pillar[6]arene host was determined at pH 3.0 (10 mM CBS) and pH 7.4 (10 mM PBS). For emission spectra the excitation was fixed to λ_{ex} = 360/10 nm and for excitation the emission was fixed to λ_{em} = 450/10 nm. The emission and excitation spectra of the buffer was subtracted from the respective spectrum.

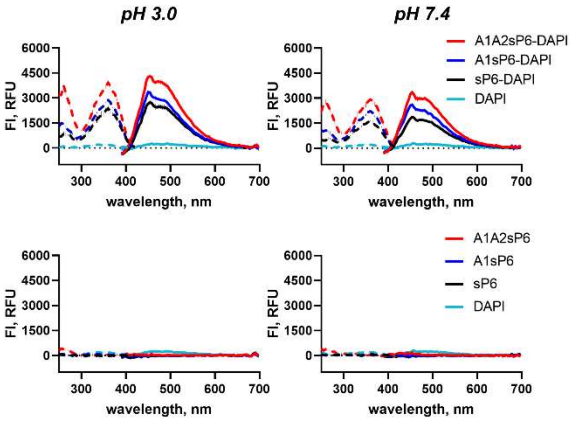

Figure S29. Top: emission (λ_{ex} = 360 nm, solid lines) and excitation (λ_{em} = 450 nm, dashed lines) of DAPI (100 nM), **sP6**-DAPI (1μM; 100 nM), **A1sP6**-DAPI (1μM; 100 nM) and **A1A2sP6**-DAPI (1μM; 100 nM) at pH 3.0 (10 mM CBS) and pH 7.4 (10 mM PBS). Bottom: emission (λ_{ex} = 360 nm, solid lines) and excitation (λ_{em} = 450 nm, dashed lines) of DAPI (100 nM), **sP6** (1μM), **A1sP6** (1μM) and **A1A2sP6** (1μM) at pH 3.0 (10 mM CBS) and pH 7.4 (10 mM PBS).

3.3 Direct fluorescence titration of host into DAPI. The direct binding of sulfo-pillararene host to DAPI was studied by fluorescence titrations. The method was adapted from our previous report.[11] In summary: a 96-well plate row 12 contained a 200 μL solution of DAPI (100 nM for **sP6** and **A1sP6**, 50 nM for **A1A2sP6**) and sulfo-pillararene host in 10 mM buffer. Row 1 – 11 contained DAPI (100 nM for **sP6** and **A1sP6**, 50 nM for **A1A2sP6**) in 10 mM buffer at a volume of 100 μL. The solution in row 12 was serially diluted across the plate to well 1, whereupon 100 μL was discarded after mixing. All wells (1 – 12) contained a final volume of 100 μL. In a separate column of the 96-well plate, three wells contained the buffer blank (10 mM buffer), three wells contained the host blank (host at highest concentration in 10 mM buffer), and three wells contained the dye blank (DAPI (100 nM for **sP6** and **A1sP6**, 50 nM for **A1A2sP6**), in 10 mM buffer), all at a volume of 100 μL. Following the serial dilution, the plates were centrifuged (1300 rpm, pulse approximately 10 seconds) and read with a λ_{ex} 360/20 nm and λ_{em} 450/20 nm.

The K_d of the host-DAPI complex was determined from two sets of technical triplicates, for a total of six replicates. Each triplicate was plotted in GraphPad Prism 9, the host blank (Fl_o) was subtracted, and the fluorescence response (Fl-Fl_o, RFU) was plotted as a function of host concentration with standard error. The binding curve was fitting using the direct one site binding equation (Equation 1) and was constrained to the concentration of DAPI. Each set of triplicates was plotted with standard error and residuals. From averaging the two sets of triplicates the K_d with the propagated standard error was determined.

Equation 1: Curve fit for direct titration.

$$Y = F_{min} + (F_{max} - F_{min})\left(\frac{(D + x + K_{d\ DAPI}) - \sqrt{(D + x + K_{d\ DAPI})^2 - (4xD)}}{2D}\right)$$

Where:
Y = Fitted data point
F_{max} = Maximum signal
F_{min} = Minimum signal
D = Concentration of DAPI in micromolar
x = Concentration of titrant in micromolar
$K_{d\ DAPI}$ = Dissociation constant of DAPI

5.4 Direct titration curves.

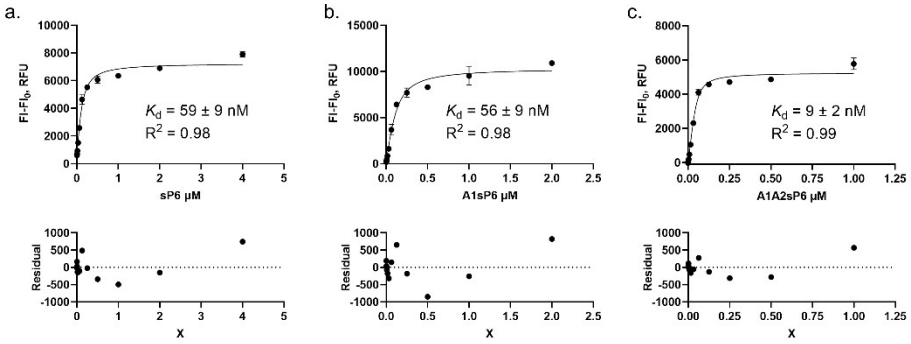

Figure S30. Exemplary data of direct titrations with residuals in 10 mM phosphate buffer saline, pH 7.4. Reported dissociation constants and R^2 are for the exemplary set of triplicates. a. Titration of **sP6** (4 µM) into DAPI (100 nM). b. Titration of **A1sP6** (2 µM) into DAPI (100 nM). c. Titration of **A1A2sP6** (1 µM) into DAPI (50 nM).

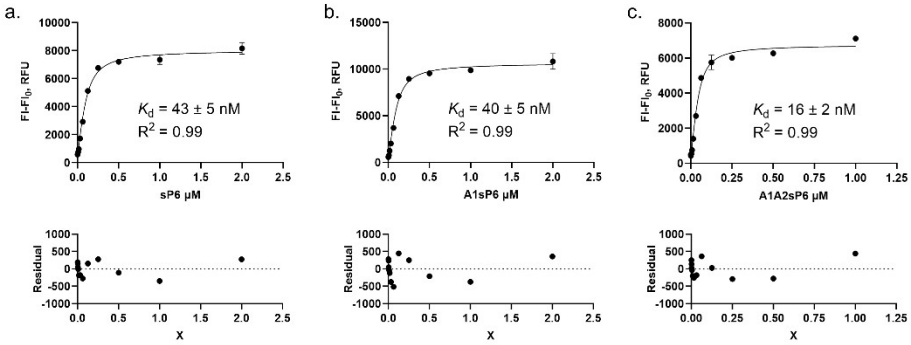

Figure S31. Exemplary data of direct titrations with residuals in 10 mM citrate buffer saline, pH 3.0. Reported dissociation constants and R^2 are for the exemplary set of triplicates. a. Titration of **sP6** (2 µM) into DAPI (100 nM). b. Titration of **A1sP6** (2 µM) into DAPI (100 nM). c. Titration of **A1A2sP6** (1 µM) into DAPI (50 nM).

3.4 Competitive titration of DOAC into host-DAPI complex.

The concentration of DAPI and host for the competitive assay was determined from the IC_{90} point of the direct titrations. This was determined to be 125 nM for **sP6** and **A1sP6** with 100 nM DAPI; and 62.5 nM for **A1A2sP6** with 50 nM DAPI. To perform the assay two solutions were used, solution A and solution B. Solution B contained host, DAPI, and the DOAC of interest (between 10 – 500 μM) in 10 mM CBS buffer. Solution A contained host and DAPI in 10 mM CBS buffer. Analogous to the direct titration, solution B was serially diluted across a 96 well plate into solution A. In summary row 12 contained 200 μL solution B, row 1 – 11 contained 100 μL solution A. B was diluted across to row 1, whereupon 100 μL was discarded after mixing, leaving the total volume of 100 μL in all wells. Additionally, three wells of the 96-well plate contained either a buffer blank (10 mM CBS), a host blank (125 nM **sP6**, 125 nM **sP6 A1sP6** or 62.5 nM for **A1A2sP6** in 10 mM CBS), a dye blank (100 nM or 50 nM DAPI in 10 mM CBS), guest blank (guest at highest concentration used in assay in 10 mM CBS buffer); and three wells contained solution A. For edoxaban, betrixaban and apixaban ≤2.5 % DMSO was used to aid in solubility, the % DMSO used was held constant through the dilution. All wells had a volume of 100 μL. Following titration, the plate was centrifuged (1300 rpm, pulse approximately 10 seconds) and read with a λ_{ex} 360/20 nm and λ_{em} 450/20 nm.

For each host-DAPI complex two sets of triplicates were performed a total of six replicates. To obtain the K_d value the host blank (Fl_o) was subtracted, and the logarithm of the fluorescence response (Fl-Fl_o, RFU) was plotted against the guest concentration for each triplicate measurement. In GraphPad Prism 9 a competitive one site binding equation (Equation 2) was used, and the data was plotted with standard error and x residuals. Note this model directly fits K_d assuming 1:1 stoichiometry, it does not report the EC_{50}. Each fit was constrained to the direct dissociation constant of DAPI, K_d = 40 nM for **sP6**, K_d = 35 nM for **A1sP6**, K_d = 15 nM for **A1A2sP6**. Additionally, the fits were constrained to the concentration of DAPI (100 nM for **sP6** and **A1sP6**, 50 nM for **A1A2sP6**). In some instances, the data representing the highest guest concentrations had to be excluded due to aggregation (0 – 1 points). For the two sets of triplicates an average K_d was determined with propagated standard error.

Equation 2: Curve fit for competitive titration.

$$Y = \frac{(F_{max} - F_{min})}{1 + 10^{(x - log\ \ _{50})}} + F_{min}$$

Where:
Y = Fitted data point
F_{max} = Maximum signal
F_{min} = Minimum signal
$logEC_{50}$ is solved by the equation below;

Equation 3: Curve fit for competitive titration.

$$logEC_{50} = log\left(10^{log\ \ _{d\ guest}\left(1+\frac{D}{K_{d\ DAPI}}\right)}\right)$$

Where:
$K_{d\ guest}$ = Dissociation constant for guest
D = Concentration of DAPI in nM
$K_{d\ DAPI}$ = Dissociation constant of the DAPI in nM

3.5 Competitive titration curves.

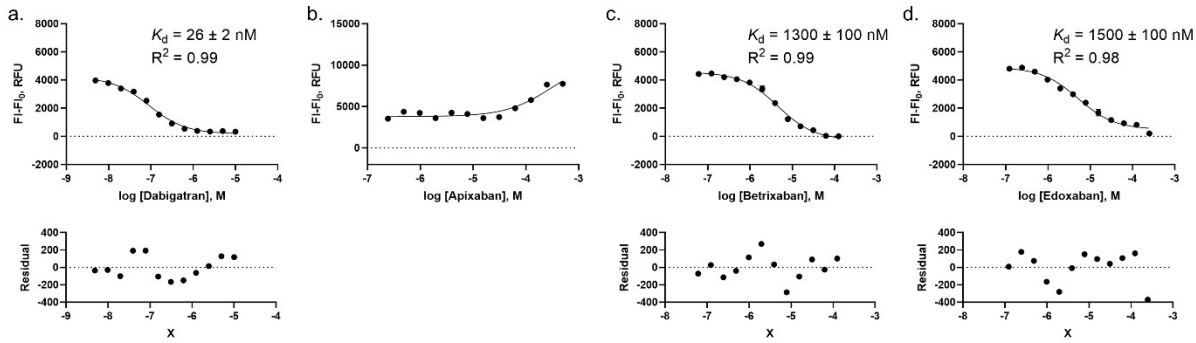

Figure S32. Exemplary data of competitive titrations with residuals of **sP6** in 10 mM citrate buffer saline, pH 3.0. Reported dissociation constants and R^2 are for the exemplary set of triplicates. a. Competitive titration of Dabigatran (10 µM) into **sP6** (125 nM) and DAPI (100 nM). b. Competitive titration of Apixaban (500 µM) into **sP6** (125 nM) and DAPI (100 nM), 2.5% DMSO. c. Competitive titration of Betrixaban (125 µM) into **sP6** (125 nM) and DAPI (100 nM), 1.25% DMSO. d. Competitive titration of Edoxaban (250 µM) into **sP6** (125 nM) and DAPI (100 nM), 2.5% DMSO.

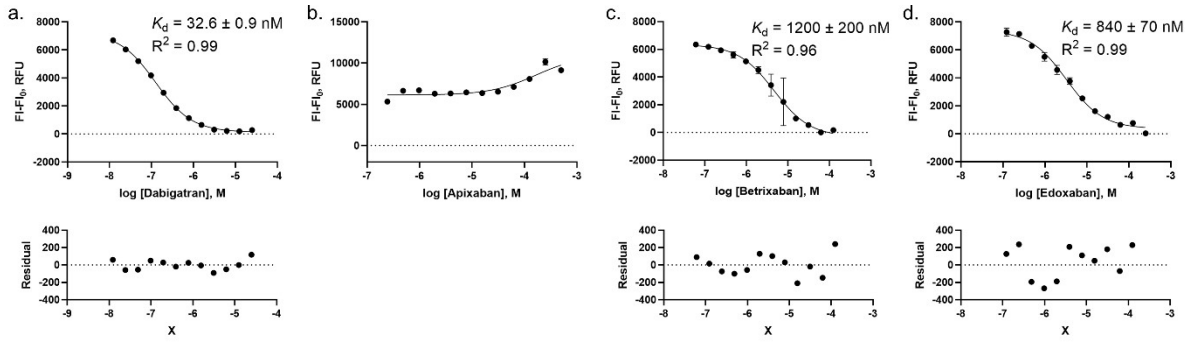

Figure S33. Exemplary data of competitive titrations with residuals of **A1sP6** in 10 mM citrate buffer saline, pH 3.0. Reported dissociation constants and R^2 are for the exemplary set of triplicates. a. Competitive titration of Dabigatran (25 µM) into **A1sP6** (125 nM) and DAPI (100 nM). b. Competitive titration of Apixaban (500 µM) into **A1sP6** (125 nM) and DAPI (100 nM), 2.5% DMSO. c. Competitive titration of Betrixaban (125 µM) into **A1sP6** (125 nM) and DAPI (100 nM), 1.25% DMSO. d. Competitive titration of Edoxaban (250 µM) into **A1sP6** (125 nM) and DAPI (100 nM), 2.5% DMSO.

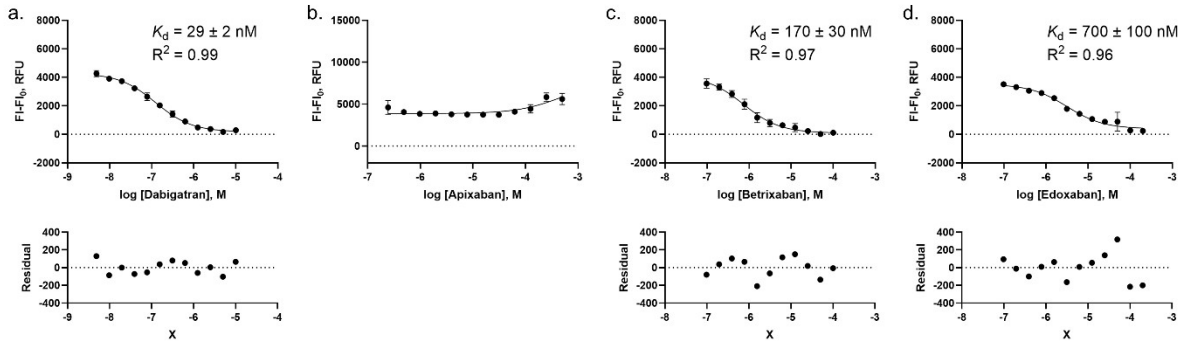

Figure S34. Exemplary data of competitive titrations with residuals of **A1A2sP6** in 10 mM citrate buffer saline, pH 3.0. Reported dissociation constants and R^2 are for the exemplary set of triplicates. a. Competitive titration of Dabigatran (10 µM) into **A1A2sP6** (62.5 nM) and DAPI (50 nM). b. Competitive titration of Apixaban (500 µM) into **A1A2sP6** (62.5 nM) and DAPI (50 nM), 2.5% DMSO. c. Competitive titration of Betrixaban (200 µM) into **A1A2sP6** (62.5 nM) and DAPI (50 nM), 1% DMSO. d. Competitive titration of Edoxaban (200 µM) into **A1A2sP6** (62.5 nM) and DAPI (50 nM), 2.5% DMSO.

4 Isothermal titration calorimetry

4.1 General remarks for ITC.

Isothermal titration calorimetry (ITC) was performed using a VP-ITC calorimeter (MicroCal, Northampton, MA). Host and guest samples were prepared in specified concentrations using the same stock of 10 mM CBS at pH 3.0. Titrations were performed at 30°C by 29 injections (10 µL aliquots) of host solution into the ITC sample cell (volume = 1.4217 mL) containing guest. To aid in solubility, edoxaban and betrixaban solutions contained 0.5% DMSO. To control for the DMSO a blank was run at 30°C by 29 injections (10 µL aliquots) of CBS buffer into the ITC sample cell (volume = 1.4217 mL) containing edoxaban or betrixaban (0.5% DMSO). All solutions were degassed immediately before use. The DMSO blank was subtracted from the edoxaban and betrixaban thermograph prior to analysis.

The thermodynamic parameters of the host-guest complexes were determined using a one set of sites model with the fitting parameters K_d, ΔH and N (number of sites). Data was analyzed in Origin 7.0 using the manufacturer's settings. Δ*S* was calculated from K_d and ΔH. All titration experiments were completed in duplicate, the K_d, ΔH, −TΔS, N are reported as an average with propagated standard error.

4.2 DMSO Blank.

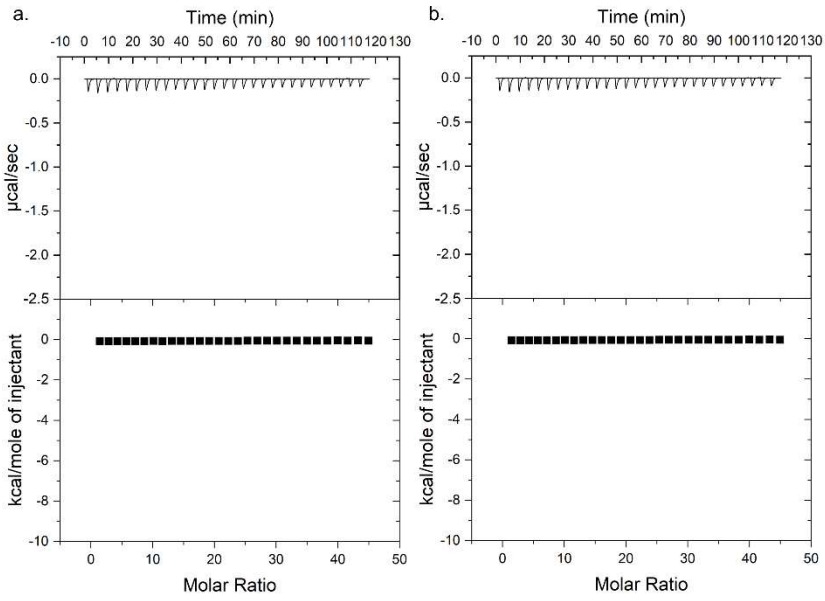

Figure S35. DMSO blank of a. Edoxaban (50 µM, 0.5% DMSO) in CBS (10 mM, pH 3.0) into CBS at 30°C. b. Betrixaban (50 µM, 0.5% DMSO) in CBS (10 mM, pH 3.0) into CBS at 30°C. Top panels shows the differential power between the reference and sample cell (µcal/sec) vs time, bottom panels show a plot of ΔH (kcal/mol) as a function of the molar ratio.

4.3 ITC curves.

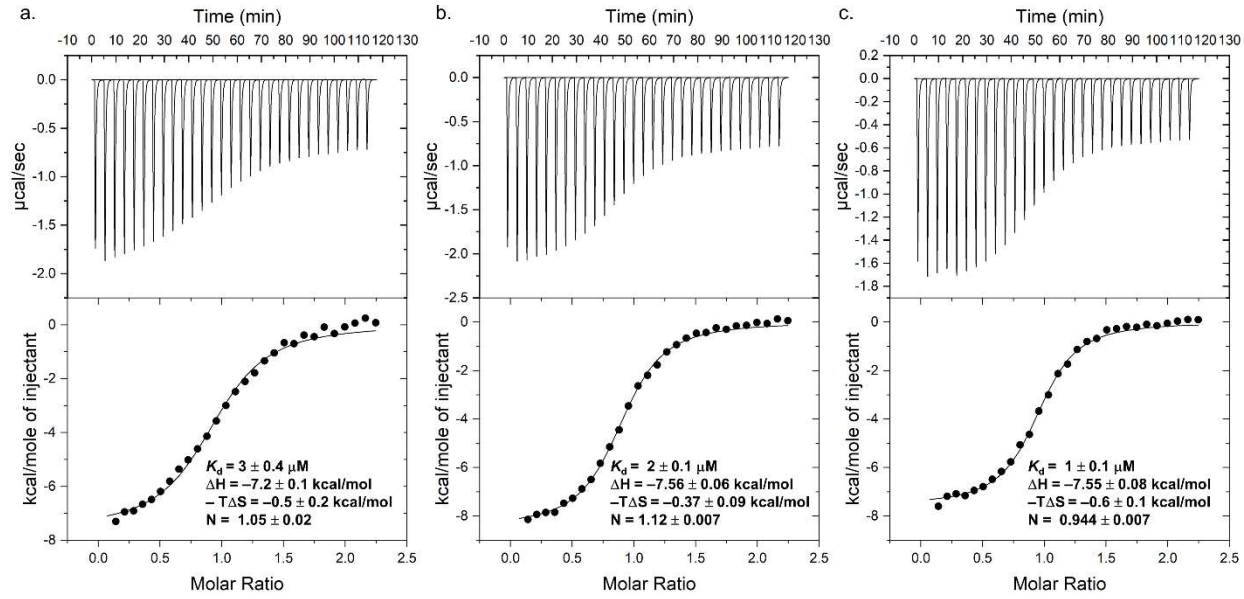

Figure S36. Exemplary ITC titrations of a. **sP6** (500 µM), b. **A1sP6** (500 µM) and c. **A1A2sP6** (500 µM), into betrixaban (50 µM) in CBS (10 mM, pH 3.0) at 30°C. Top panels shows the differential power between the reference and sample cell (µcal/sec) vs time, bottom panels show a plot of ΔH (kcal/mol) as a function of the molar ratio. Data was fit with a one set of sites binding model.

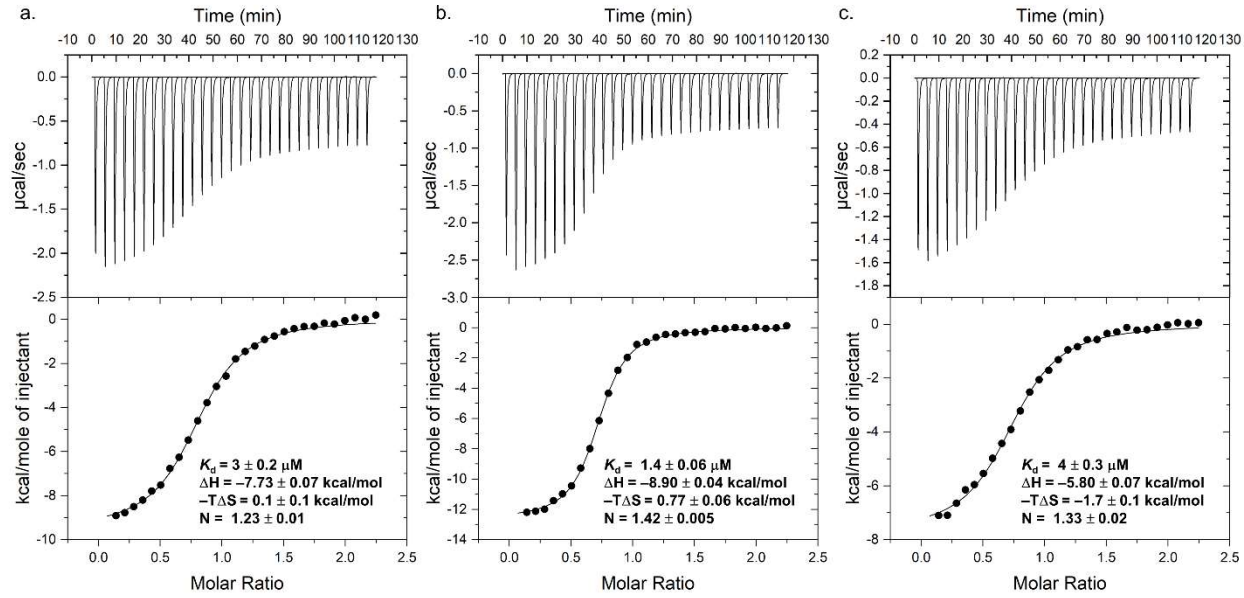

Figure S37. Exemplary ITC titrations of a. **sP6** (500 µM), b. **A1sP6** (500 µM) and c. **A1A2sP6** (500 µM), into edoxaban (50 µM) in CBS (10 mM, pH 3.0) at 30°C. Top panels shows the differential power between the reference and sample cell (µcal/sec) vs time, bottom panels show a plot of ΔH (kcal/mol) as a function of the molar ratio. Data was fit with a one set of sites binding model.

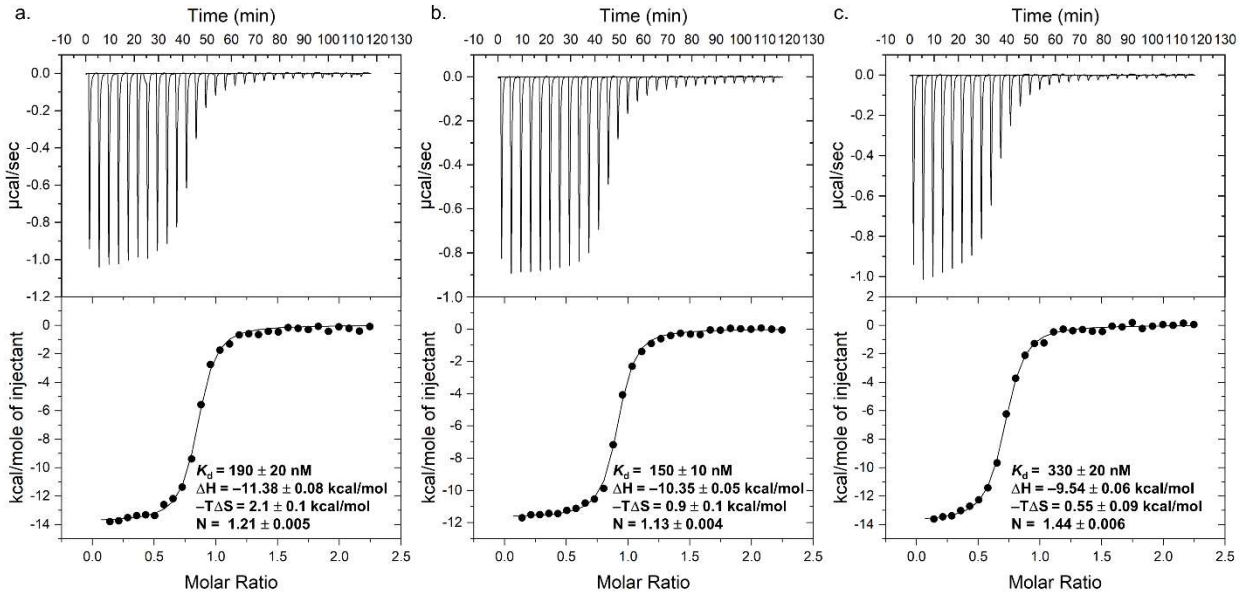

Figure S38. Exemplary ITC titrations of a. **sP6** (250 µM), b. **A1sP6** (250 µM) and c. **A1A2sP6** (250 µM) (right), into Dabigatran (25 µM) in CBS (10 mM, pH 3.0) at 30°C. Top panels shows the differential power between the reference and sample cell (µcal/sec) vs time, bottom panels show a plot of ΔH (kcal/mol) as a function of the molar ratio. Data was fit with a one set of sites binding model.

5. NMR titrations

5.1 General remarks

^{1}H-NMR titrations were performed on a Bruker Avance Neo 500 MHz spectrometer. Solutions were made in 20 mM deuterated CBS buffer (274 mM NaCl, 5.4 mM KCl, 1.88 mM Sodium citrate dihydrate, 18.12 mM Citric acid in D_2O) with 1% DMSO (solubility aid for betrixaban). All spectra were referenced to D_2O (δ 4.79). Spectra were processed using MestReNova by Mestrelab Research S.L.

5.2 NMR data

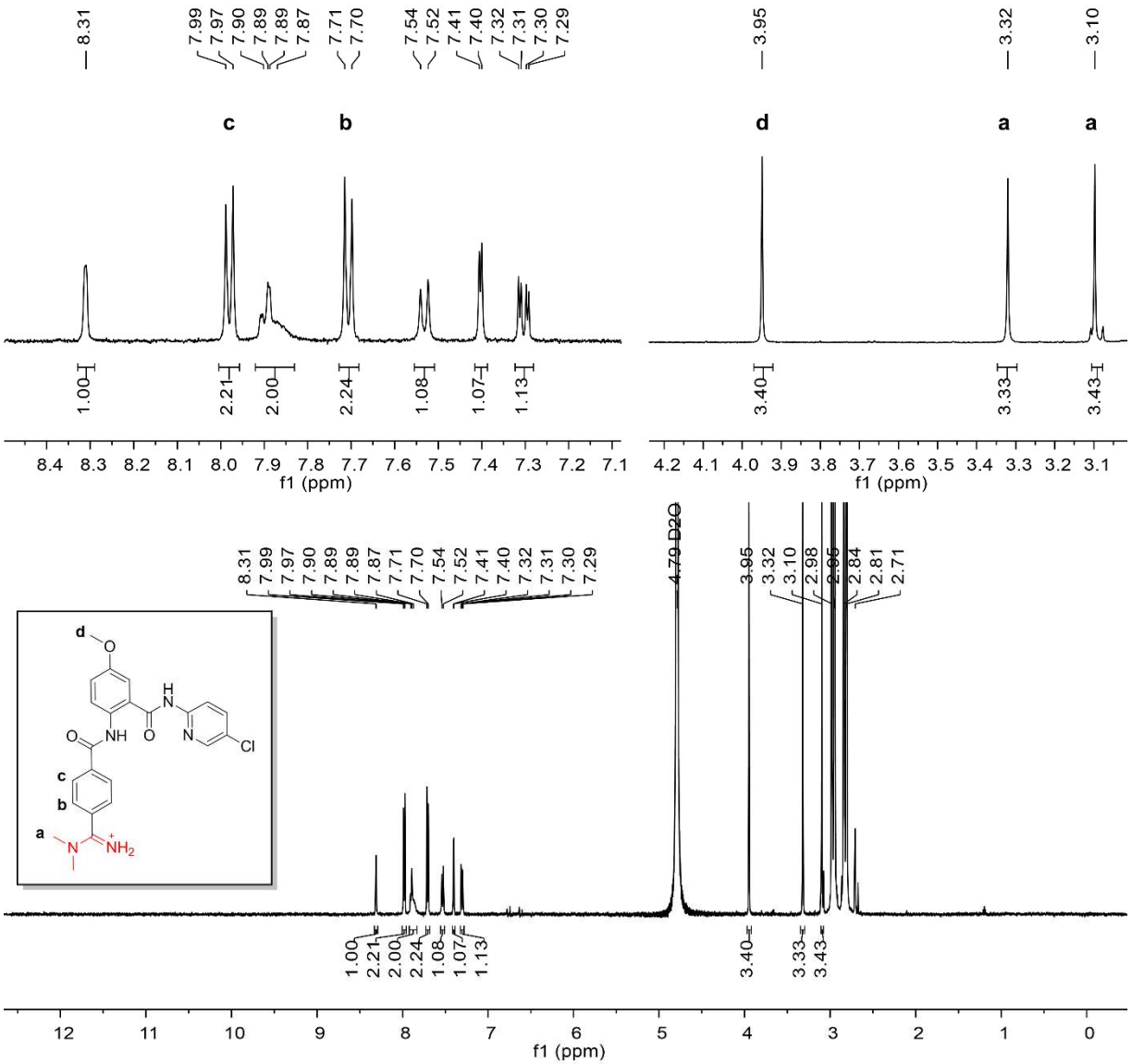

Figure S39: [1]H-NMR characterization of **Betrixaban** in 20 mM deuterated CBS with 1% DMSO (500 MHz, 298 K). Expansion in top panel. Peak assignment based off COSY correlations and chemical shifts (Figure S40).

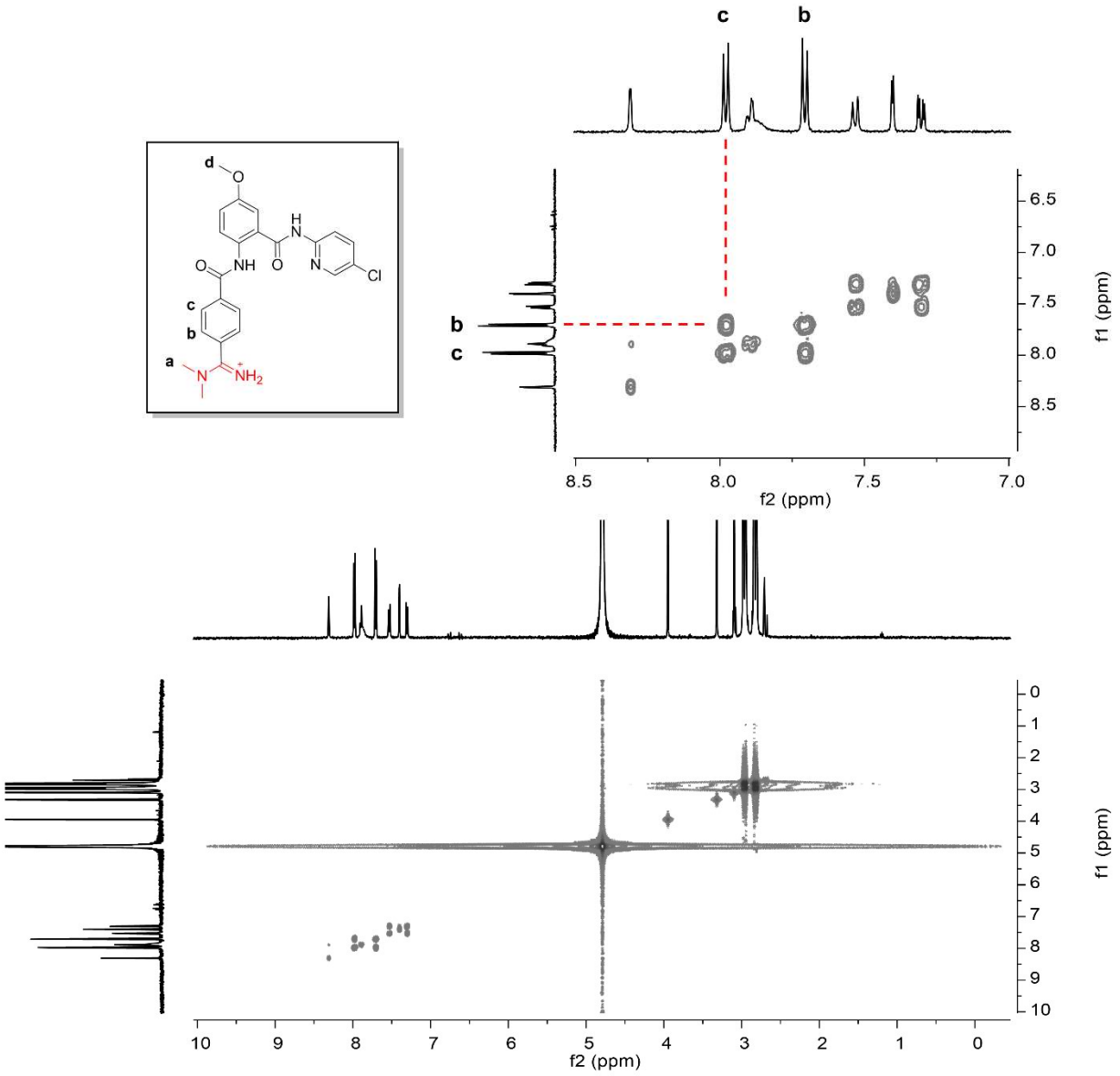

Figure S40: ^{1}H-NMR COSY characterization of 0.5 mM **Betrixaban** in 20 mM deuterated CBS with 1% DMSO (500 MHz, 298 K).

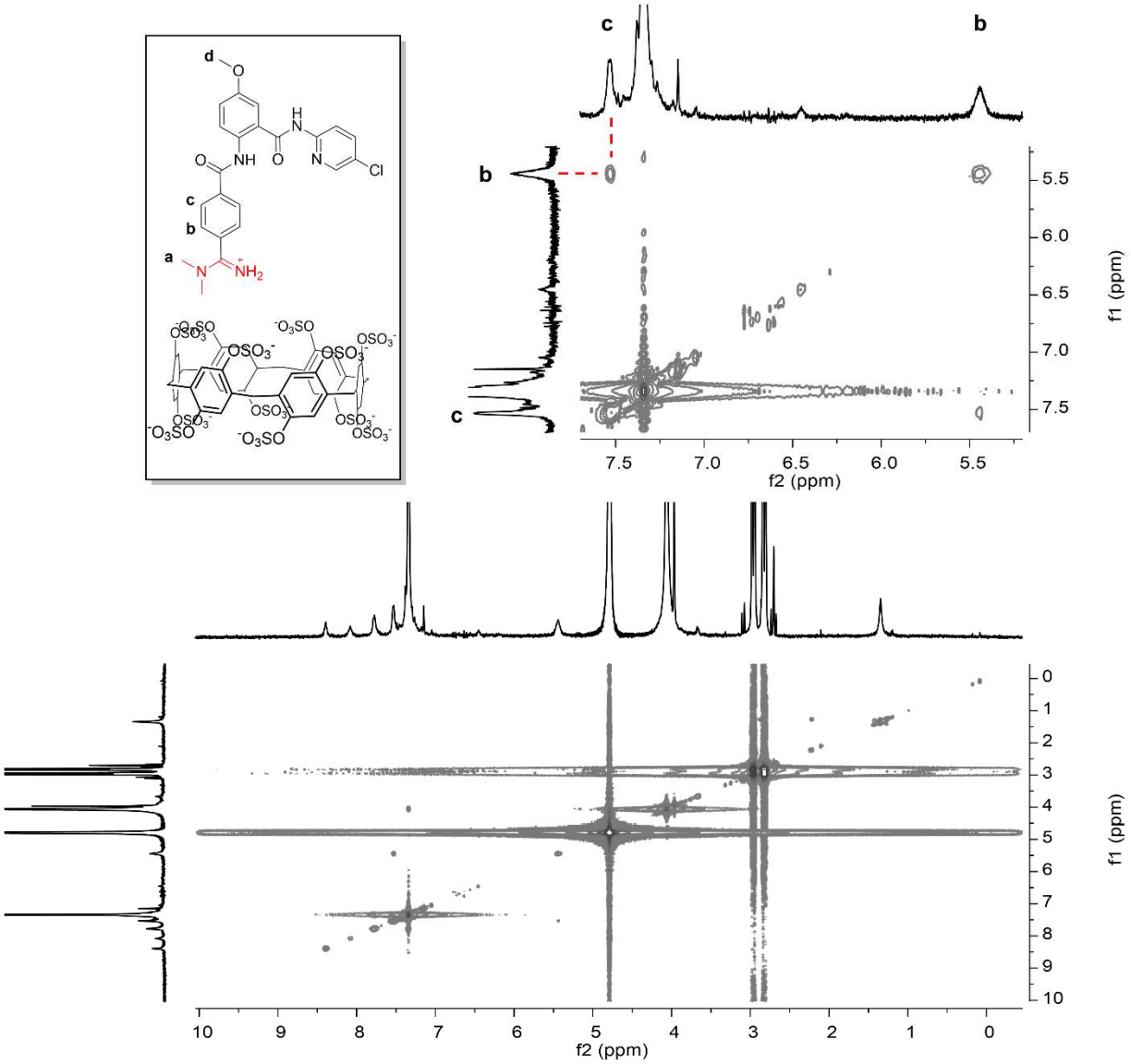

Figure S41: ^{1}H-NMR COSY characterization of 1 mM sP6 + 0.5 mM **Betrixaban** in in 20 mM deuterated CBS with 1% DMSO (500 MHz, 298 K).

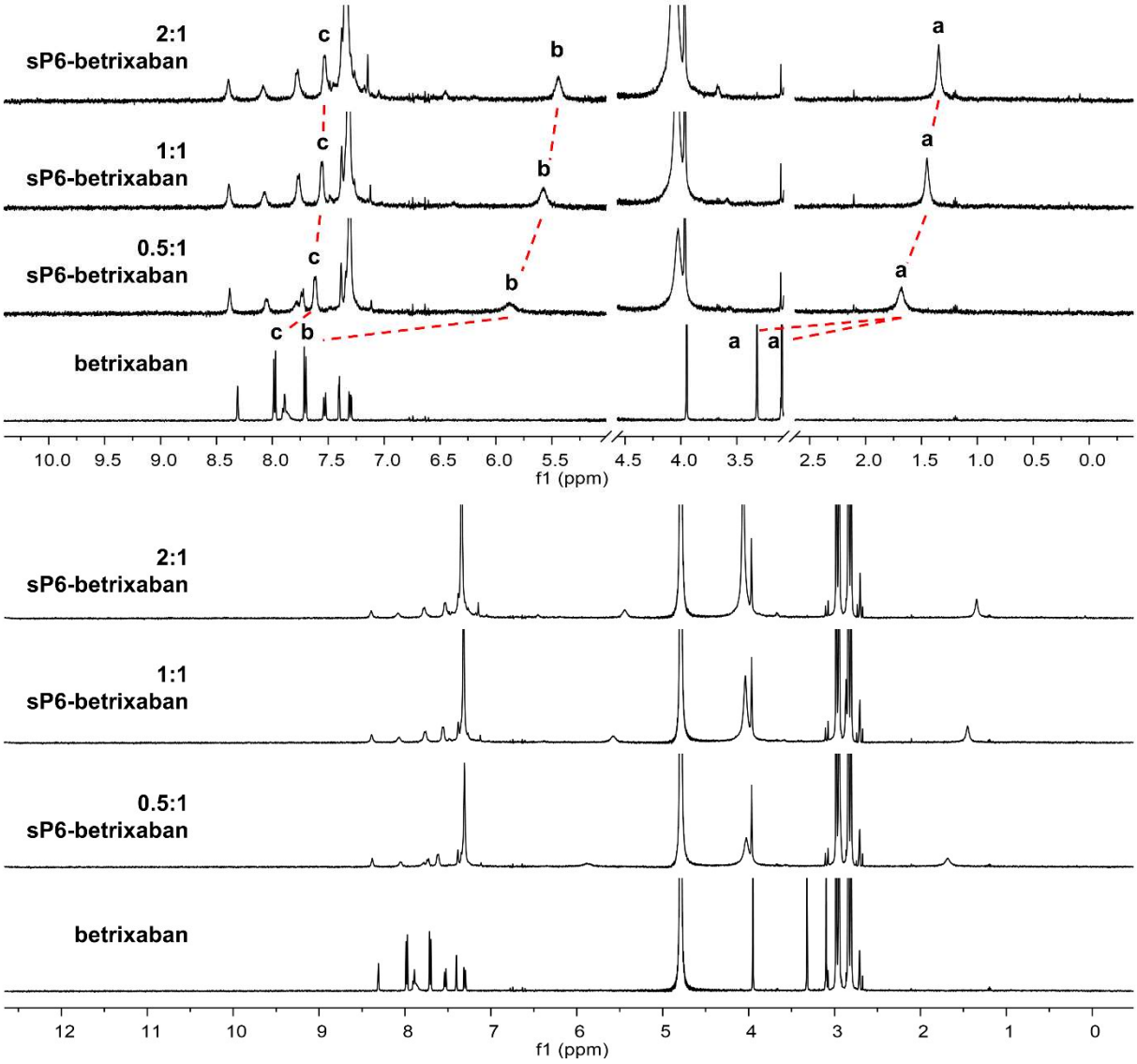

Figure S42: ^{1}H-NMR stacked plot of betrixaban (0.5 mM), **sP6** (0.25 mM) + betrixaban (0.5 mM), **sP6** (0.5 mM) + betrixaban (0.5 mM) and **sP6** (1 mM) + betrixaban (0.5 mM) in 20 mM deuterated CBS with 1% DMSO (500 MHz, 298 K). Top panel shows magnification of spectra with peak tracking of key signals. Citrate and D_2O signals removed for clarity.

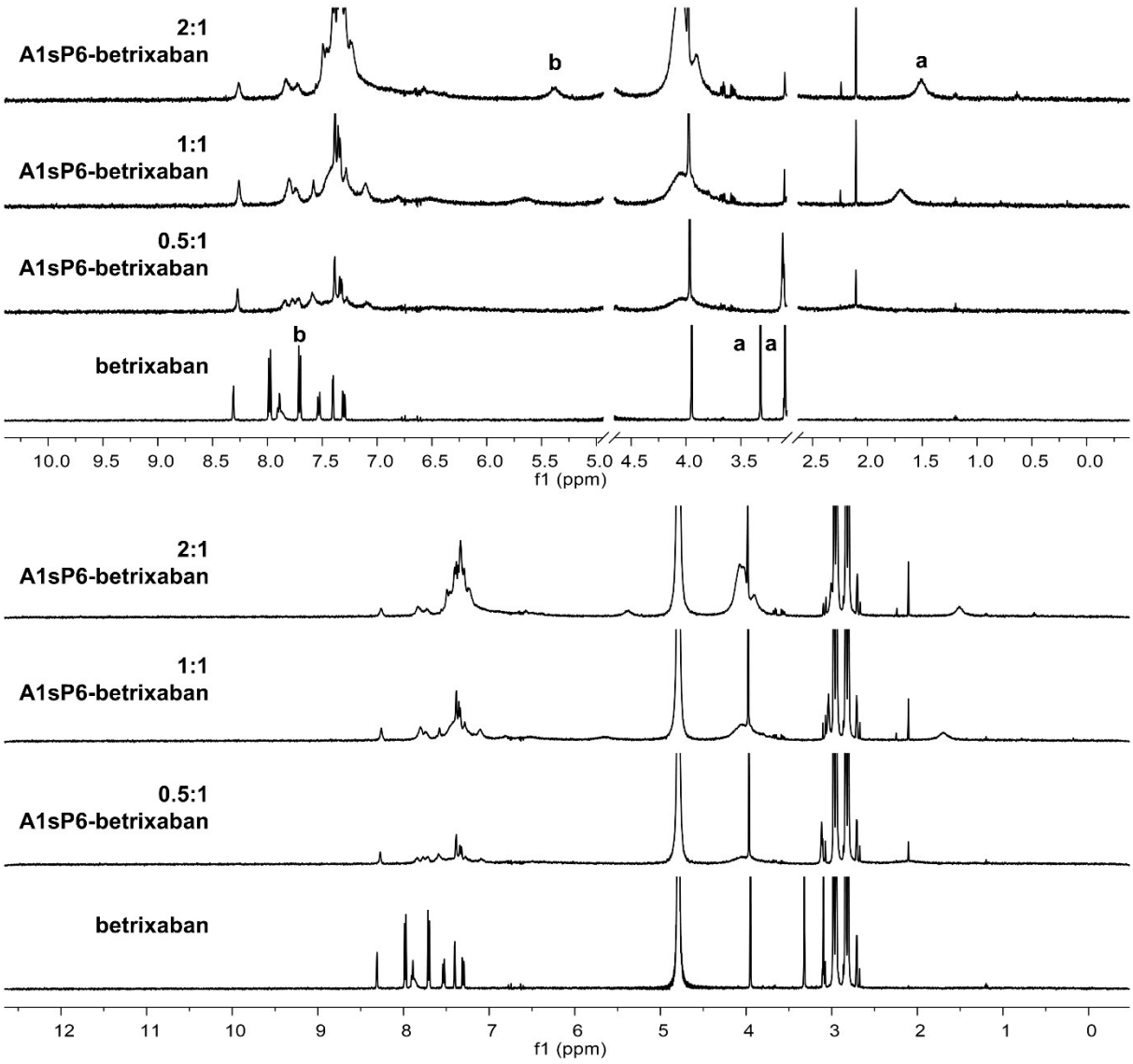

Figure S43: ^{1}H-NMR stacked plot of betrixaban (0.5 mM), **A1sP6** (0.25 mM) + betrixaban (0.5 mM), **A1sP6** (0.5 mM) + betrixaban (0.5 mM) and **A1sP6** (1 mM) + betrixaban (0.5 mM) in 20 mM deuterated CBS with 1% DMSO (500 MHz, 298 K). Top panel shows magnification of spectra with peak assignments of key signals. Citrate and D_2O signals removed for clarity.

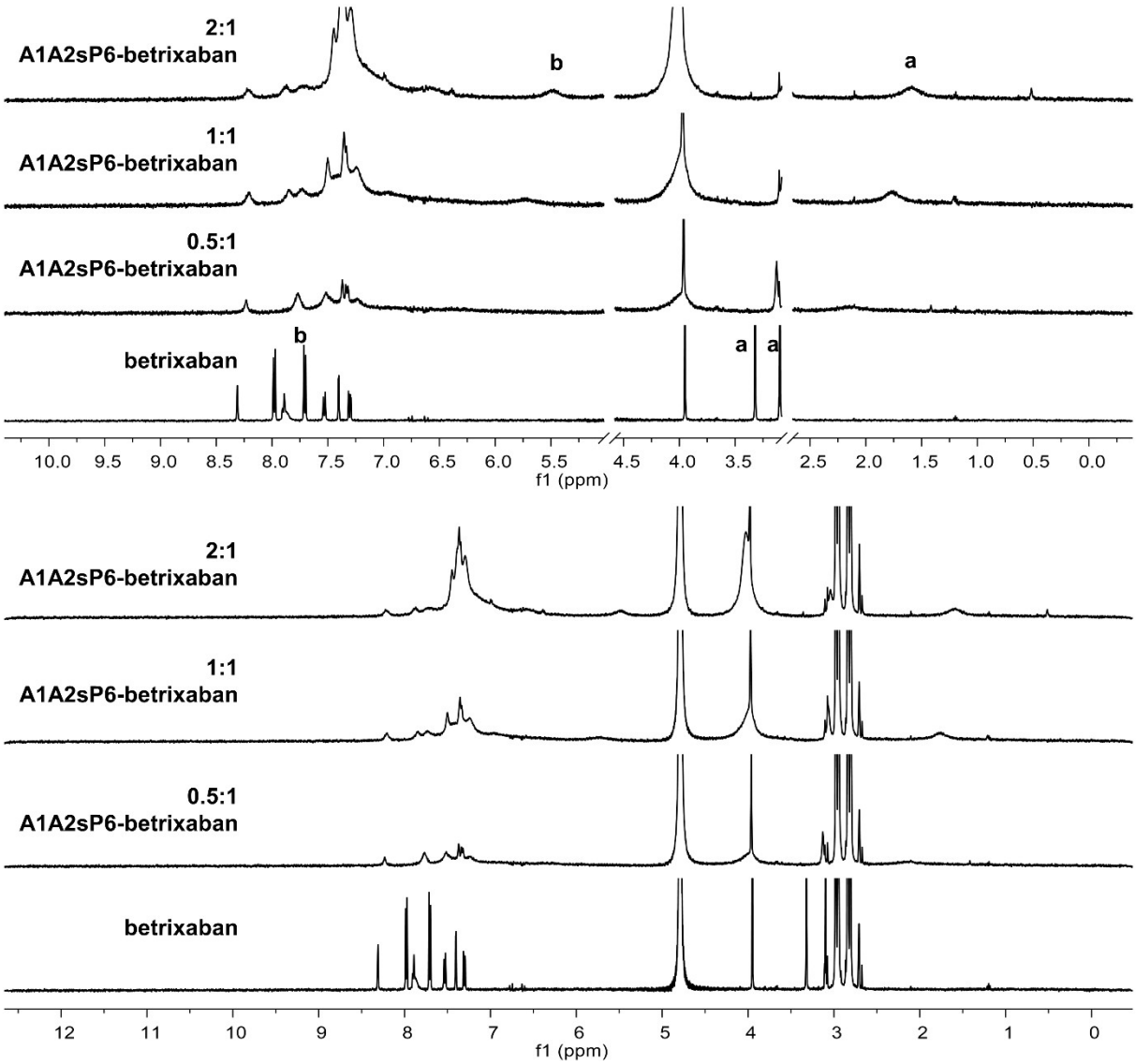

Figure S44: ^{1}H-NMR stacked plot of betrixaban (0.5 mM), **A1A2sP6** (0.25 mM) + betrixaban (0.5 mM), **A1A2sP6** (0.5 mM) + betrixaban (0.5 mM) and **A1A2sP6** (1 mM) + betrixaban (0.5 mM) in 20 mM deuterated CBS with 1% DMSO (500 MHz, 298 K). Top panel shows magnification of spectra with peak assignments of key signals. Citrate and D_2O signals removed for clarity.

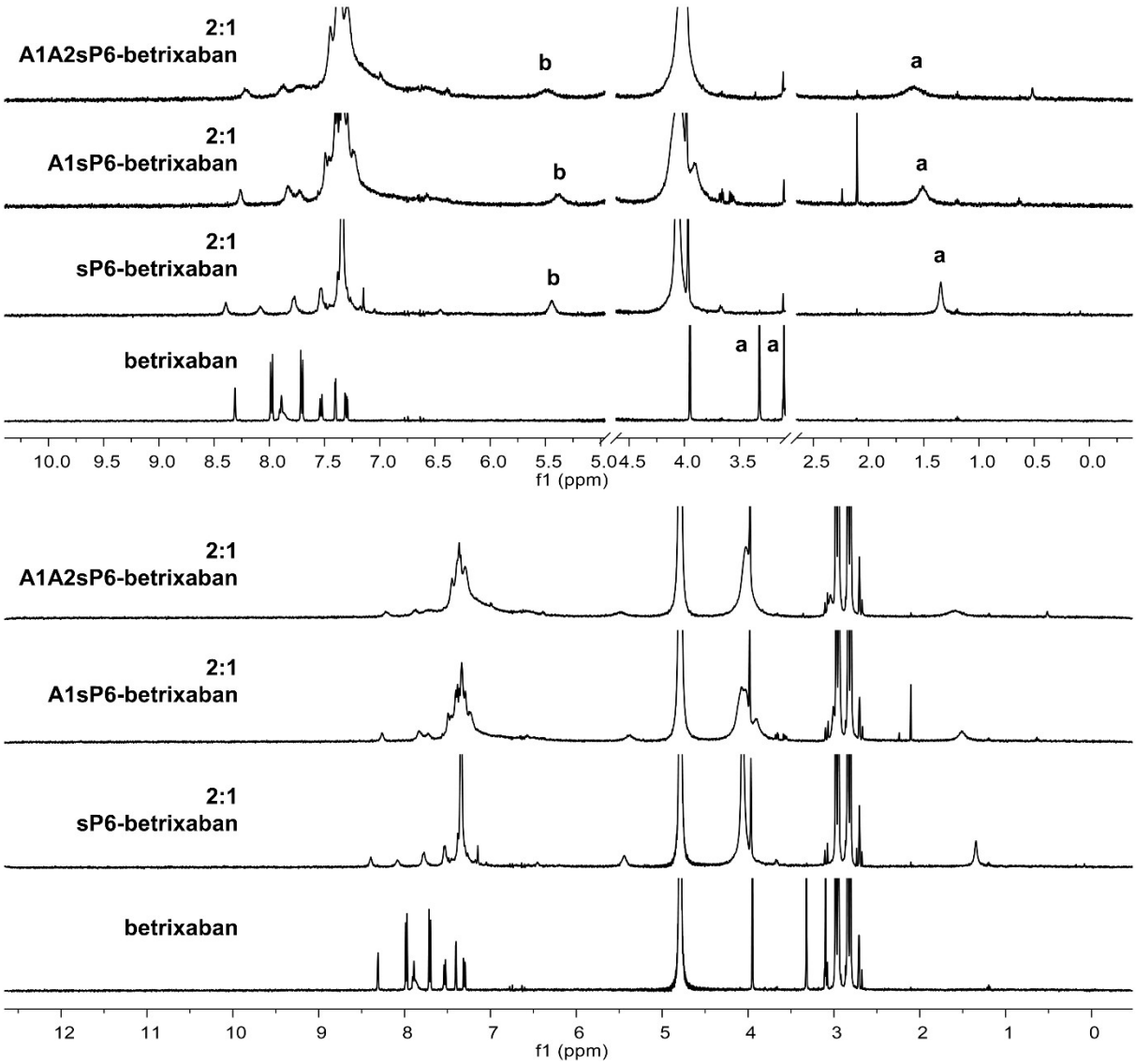

Figure S45: ^{1}H-NMR stacked plot of betrixaban (0.5 mM), **sP6** (1 mM) + betrixaban (0.5 mM), **A1sP6** (1 mM) + betrixaban (0.5 mM) and **A1A2sP6** (1 mM) + betrixaban (0.5 mM) in 20 mM deuterated CBS with 1% DMSO (500 MHz, 298 K). Top panel shows magnification of spectra with peak assignments of key signals. Citrate and D_2O signals removed for clarity.

6. Molecular modeling

Simple molecular models were produced in Maestro 13.8 for betrixaban and the sulfo-pillar[6]arene hosts. Based off the ^{1}H-NMR data, betrixaban was oriented in the host cavity with the amidinium in the cavity and the resulting structure was minimized with OPLS-2005. Note these models are to represent size complimentary and potential interactions between the host and guest.

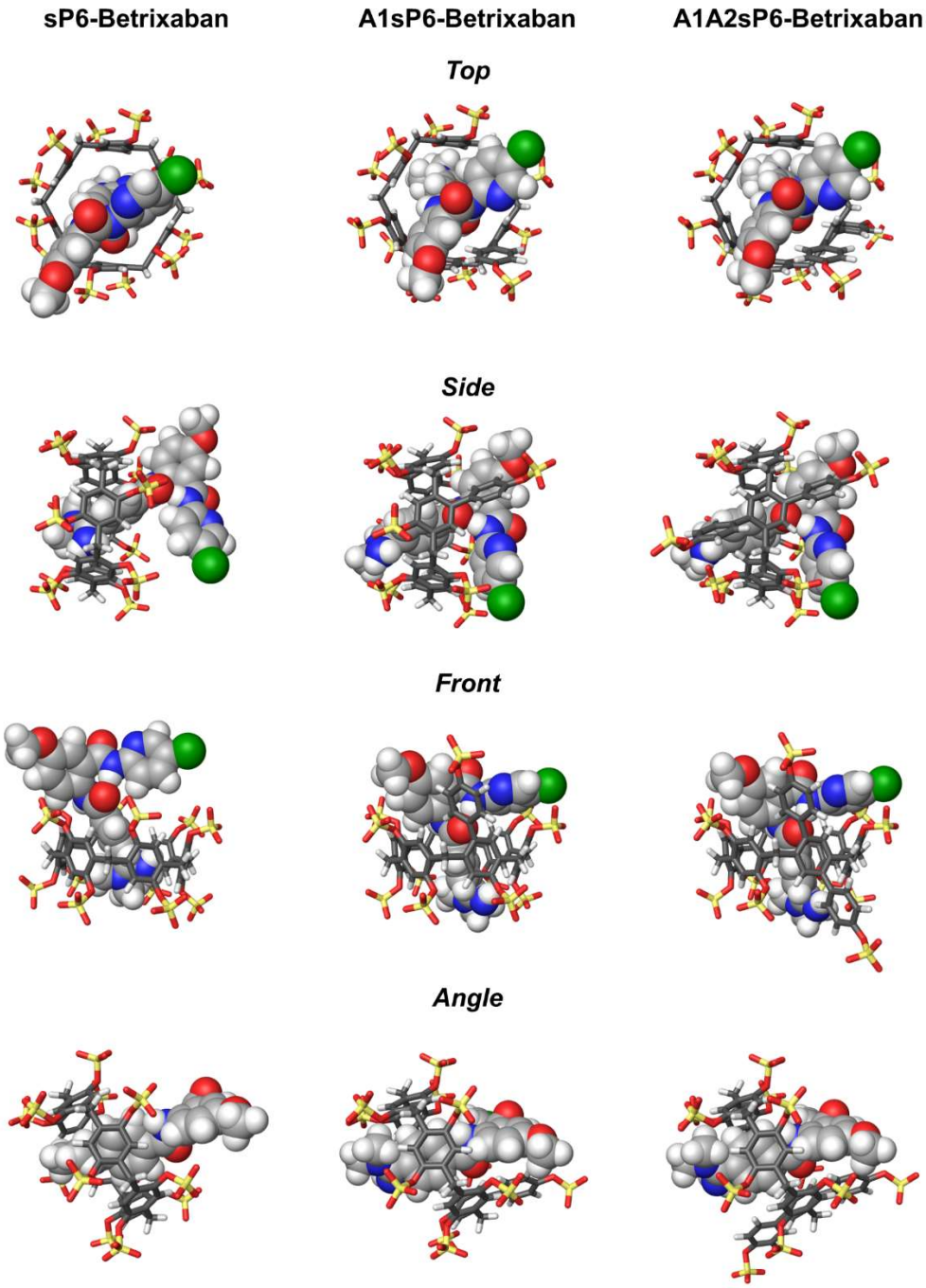

Figure S46. Molecular models of sulfo-pillar[6]arene analogs complexed with betrixaban.

8. References

(1) Wilson, C. R.; Chen, E. F. W.; Puckett, A. O.; Hof, F. Ethoxypillar[6]arene. *Org. Synth.* **2022**, *99*, 125-138. DOI: 10.15227/orgsyn.99.0125.
(2) Xue, W.; Zavalij, P. Y.; Isaacs, L. Pillar[*n*]MaxQ: A New High Affinity Host Family for Sequestration in Water. *Angew. Chem. Int. Ed.* **2020**, *59* (32), 13313-13319. DOI: 10.1002/anie.202005902.
(3) Ogoshi, T.; Kayama, H.; Yamafuji, D.; Aoki, T.; Yamagishi, T.-A. Supramolecular polymers with alternating pillar[5]arene and pillar[6]arene units from a highly selective multiple host–guest complexation system and monofunctionalized pillar[6]arene. *Chem. Sci.* **2012**, *3* (11), 3221. DOI: 10.1039/c2sc20982a.
(4) Rashvand Avei, M.; Etezadi, S.; Captain, B.; Kaifer, A. E. Visualization and quantitation of electronic communication pathways in a series of redox-active pillar[6]arene-based macrocycles. *Commun. Chem.* **2020**, *3* (1), 117. DOI: 10.1038/s42004-020-00363-4.
(5) Zhu, Y.; Escorihuela, J.; Wang, H.; Sue, A. C. H.; Zuilhof, H. Tunable Supramolecular Ag+-Host Interactions in Pillar[n]arene[m]quinones and Ensuing Specific Binding to 1-Alkynes. *Molecules* **2023**, *28* (20), 7009. DOI: 10.3390/molecules28207009.
(6) Ogoshi, T.; Yamafuji, D.; Kotera, D.; Aoki, T.; Fujinami, S.; Yamagishi, T. A. Clickable di- and tetrafunctionalized pillar[n]arenes (n = 5, 6) by oxidation-reduction of pillar[n]arene units. *J. Org. Chem.* **2012**, *77* (24), 11146-11152. DOI: 10.1021/jo302283n.
(7) APEX-4. Bruker AXS. Madison, Wisconsin, USA, 2021.
(8) Krause, L.; Herbst-Irmer, R.; Sheldrick, G. M.; Stalke, D. Comparison of silver and molybdenum microfocus X-ray sources for single-crystal structure determination. *J. Appl. Crystallogr.* **2015**, *48* (1), 3-10. DOI: 10.1107/s1600576714022985.
(9) Sheldrick, G. M. SHELXT - integrated space-group and crystal-structure determination. *Acta Crystallogr. A Found. Adv.* **2015**, *71* (1), 3-8. DOI: 10.1107/s2053273314026370.
(10) Sheldrick, G. M. Crystal structure refinement with SHELXL. *Acta Crystallogr. C Struct. Chem.* **2015**, *71* (1), 3-8. DOI: 10.1107/s2053229614024218.
(11) King, D.; Wilson, C. R.; Herron, L.; Deng, C.-L.; Mehdi, S.; Tiwary, P.; Hof, F.; Isaacs, L. Molecular recognition of methylated amino acids and peptides by Pillar[6]MaxQ. *Org. Biomol. Chem.* **2022**, *20* (37), 7429-7438. DOI: 10.1039/d2ob01487d.